

Levee morphology and evolution in the fluvial-tidal realm

Lonneke Roelofs



Utrecht University

Levee morphology and evolution in the fluvial-tidal realm

Lonneke Roelofs

In partial fulfilment of the degree of Master of Science
in the Earth Sciences

Department of Physical Geography
Utrecht University

Supervisors:
Prof. dr. M.G. Kleinhans
M. Boechat Albernaz MSc.
Dr. H.J. Pierik

March 6, 2019

Statement of originality

I declare that:

1. this is an original report, which is entirely my own work,
2. where I have made use of the ideas of other writers, I have acknowledged the source in all instances,
3. where I have used any diagram or visuals I have acknowledged the source in all instances,
4. this report has not and will not be submitted elsewhere for academic assessment in any other academic course.

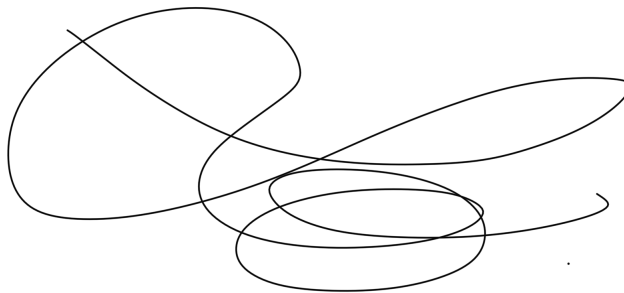
Student data:

Name: Lonneke Roelofs

Registration number: 4236297

Date: March 6, 2019

Signature:

A handwritten signature in black ink, consisting of several overlapping loops and curves, positioned below the 'Signature:' label.

Preface and Acknowledgements

This thesis on levee morphology and evolution in the fluvial-tidal realm has been written as part of the Master of Science degree in Earth Sciences, programme Earth Surface and Water, track Coastal Dynamics and Fluvial systems, at Utrecht University. The research was performed under the supervision of, and in close collaboration with Prof. dr. Maarten Kleinhans, Marcio Boechat Albernaz MSc. and dr. Harm Jan Pierik. In this report two complementary methods are combined to study levee morphology and evolution; numerical modelling in Delft3D and fieldwork. The fieldwork was conducted along the Old Rhine river between the cities of Utrecht and Leiden in The Netherlands, in the first weeks of September 2018. The field campaign was a joined effort for both this thesis as well as the thesis of Jelle Moree, who focussed on the development of crevasse systems along the Old Rhine.

First and foremost, I would like to thank my supervisors Maarten Kleinhans, Marcio Boechat Albernaz and Harm Jan Pierik, for their enthusiasm, great discussions and practical guidance during the research. I would like to express my special appreciation for dr. Wim Hoek for his help and guidance during numerous hours in the lab, processing and preparing C14 samples. I am also grateful to thank dr. Kim Cohen for providing Jelle and me with data from his *Moederbestand* in preparation for our field campaign. In addition, I must express my sincere appreciation to everyone that joined our field campaign and contributed their time and energy in unravelling the secrets of the Old Rhine. Therefore, thanks to Tim Winkels, Steven Weisscher, William McMahon, Bas Knaake, Jasper Candel, Joep Storms, Paul Veldhuijzen, Kaspar Sonnemans and Pascal Born. Not to forget the hospitality and generosity of the landowners who let us collect our data on their properties. The contribution of Arjan van Eijk to the preparation of the fieldwork is also greatly appreciated, as well as the company and help of all the other technicians in the deserted 'Zonneveldvleugel'. Special appreciation also goes to the archaeologists we met during our field campaign, whom let us use their trenches for our research and were always eager to discuss and combine findings.

Furthermore, I will never forget the always joyful and sometimes fruitful coffee- and lunch-breaks with my fellow master students. I think it is essential to thank Hugo, for being my greatest support and providing me with critical but constructive feedback, which always led to interesting discussions on the borders of scientific disciplines. Not only as a token of politeness, but also as a sign of my deepest appreciation and love, I would lastly like to thank my parents and my brother for always being there.

Abstract

Levees are geomorphological units consisting of sand, silt and/or mud that form along channels and slope towards the floodplain. They are common and pronounced features in river, delta and tidal landscapes in which they form elevated areas in further low-relief plains. Levees influence the hydraulics and distribution of sediment within river, delta and tidal systems, consequently influencing their evolution. Despite the relevance of levees for delta evolution and future delta management, research on levees is sparse and commonly limited to fluvial case-studies. Which causes a lack in general understanding and implications of levee evolution and morphology on a larger scale. Thereby, the limited amount of research on levees formed in tidal environments causes a gap in knowledge on the effects of tidal boundary conditions on levees. Hence, the objective of this study is to assess the influence of *boundary conditions* and *hydromorphological feedbacks* on the evolution, morphology and sedimentology of levees in the fluvial-tidal realm.

Two complementary methods were used to address the objective; numerical morphological modelling and field work. The set-up of the numerical model consisted of a shallow tidal basin (12.5 km x 10 km) partly closed by two barrier islands and a small relatively deeper oceanic basin (7.5 km x 10 km). In the tidal basin an initial straight river channel was present. Tides and fluvial discharge were forced into the basin. The tidal signal consisted of two components; the principal lunar semidiurnal (M2) and the shallow water overtides of the principal lunar (M4). Within the model six sediment fractions were used in transport calculations; four sand fractions, ranging from coarse to very fine and two mud fractions, one silt and one clay. The numerical model was used to study the effects of four boundary conditions; fluvial discharge magnitude, tidal amplitude, the concentration of fines and the variability of fluvial discharge. The field study was conducted along the Old Rhine river in the Netherlands that developed under changing fluvial and tidal boundary conditions over a period longer than 5000 years. The data in the field was used for comparing the effects of drivers and hydromorphological processes on real world levee complexes with those in the model.

The levees in the model consisted mainly of silt, had a height ranging from 1.1 to 2.5 m and were 1 to 3 km in width depending on the model settings and the method of width determination. The study showed that maximum levee height is bounded by the maximum water level if enough fine sediments are available. Levee width proved to be depended on the amount of sediment transport out of the channel and to be limited by large flow velocities in the floodplain, mainly caused by strong tidal flows. Overall, larger water level amplitudes, either caused by fluvial discharge fluctuations or tides, result in the formation of higher and wider levees with a more complex crevasse pattern due to larger volume of accommodation space and more sediment transport out of the channel. When water level fluctuations by tides dominate, levee sedimentology becomes more mixed, a finding underlined by both model results and field data. Furthermore, levee evolution in the model can be characterised by two distinct phases; 1) levee heightening and 2) levee widening. The transition from levee heightening and levee widening happens as accommodation space and transport gradients decrease over time. Accommodation space can both be created by high water levels, as in the model, or by thick peat layers, as in the field. The rate of levee evolution is proportional to the concentration of fines; higher concentrations cause faster evolution.

The findings presented in this thesis add to our understanding of the evolution of river, delta and

tidal systems under changing boundary conditions and hydromorphological feedback mechanisms. Furthermore, the results provide a first step towards the development of a sustainable management strategy for building new land in sinking deltas. The results of this thesis have shown that levee-crevasse complexes become larger if more sediment is transported out of the main channel, that their width is negatively affected by large flow velocities in the floodplain and that especially a low concentration of fine sediment can limit their growth. These conclusions have implications for the implementation of natural land-building projects in delta areas. In fluvial-sediment starved deltas as the Rhine-Meuse delta in The Netherlands, the fine sediments will have to come from a marine source (tidal import), which implies allowing the sea to influence the land; a sensitive topic in the country that battled against the water for centuries.

Key words; levee, morphology, river, tides, fine sediments, boundary conditions, internal processes, crevasse

Contents

Statement of originality	i
Preface and Acknowledgments	ii
Abstract	iii
1 Introduction	2
1.1 Problem definition	2
1.2 Relevance	3
1.3 Thesis outline	4
2 Literature review	5
2.1 Fluvial, deltaic and estuarine systems - an overview	5
2.2 Levee – a (lack of) generic definition	8
2.3 Levee formation	9
2.4 Levee morphology and sedimentology based on examples	11
2.5 Old Rhine - river and estuarine system	13
2.5.1 Geographical setting Rhine-Meuse delta	13
2.5.2 Holocene boundary conditions	14
2.5.3 Delta and coastal development focussing on the Old Rhine	15
2.6 Knowledge gaps	18
2.7 Hypotheses	19
2.7.1 Boundary conditions	19
2.7.2 Hydromorphological feedback mechanisms	19
3 Methods	20
3.1 Numerical modelling	20
3.1.1 Hydrodynamic and morphological model	20
3.1.2 Modelling scenarios	24
3.1.3 Analysis of model results	26
3.2 Field research	27
3.2.1 Stratigraphy and lithology	27
3.2.2 Dating the deposits	29
3.3 Comparison between model and field data	29
4 Results	30
4.1 General morphological and sedimentological development	30
4.1.1 Planform development	30
4.1.2 Cross-sectional development	32
4.2 Levee and crevasse morphology	36
4.2.1 Levee height	36
4.2.2 Maximum water level and maximum levee height	38
4.2.3 Levee width	39
4.2.4 Crevasse dimensions	43

4.3	Role of levee evolution on hydrodynamics & basin infilling	45
4.4	Levee stratigraphy and sedimentology	48
4.5	Field results - Cross-sections and grain size analysis	53
4.5.1	Old Rhine levee cross-sections	53
4.5.2	Comparison of the three levee phases along the Old Rhine	58
4.5.3	Detailed grain size analysis	59
5	Discussion	61
5.1	The effects of fluvial and tidal boundary conditions on levee evolution and properties	61
5.1.1	General morphological development	61
5.1.2	Levee dimensions	62
5.1.3	Levee sedimentology	64
5.2	The effects of hydromorphological feedbacks on levee evolution and properties	66
5.3	Effects of model simplifications	68
5.4	Recommendations and future research	69
5.5	Contribution to society	70
6	Conclusions	71
6.1	The effects of boundary conditions	71
6.2	The effects of hydromorphological feedbacks	71
	Appendices	78
A	Reconstruction Old Rhine - Limes	78
B	Delft3D input files	79
C	Classification of Bakker and Schelling (1966)	87
D	Final bathymetries	88
E	Levee width based on three methods for different fluvial discharge magnitudes	91
F	Grain size analysis tidal models	93
G	Sensitivity analysis of the critical shear stress for erosion	95
G.1	Results sensitivity analysis of the critical shear stress for erosion	95
G.2	Discussion sensitivity analysis of the critical shear stress of erosion	99
H	Core logs	100
I	Statistics of grain size analysis field samples	112

1 | Introduction

1.1 Problem definition

Natural levees are common landforms in river, delta and tidal systems that occupy the margins of channels (Adams et al., 2004). They consist of sand, silt and/or mud and are built up along the sides of channels where they slope towards the floodplain. Furthermore, levees are pronounced geomorphological features in river and delta landscapes in which they form elevated areas in further low-relief floodplains. The along channel position of levees and their morphologic characteristics influences the hydraulics and the distribution of water and sediment within river systems during flood periods (Brierley et al., 1997). Consequently, levees influence the development of delta systems.

Research on levee occurrence, evolution and the processes that control levee dimensions has focussed mostly on fluvial case-studies from the field. An extensive general understanding of levee evolution in different environments, fluvial as well as tidal, therefore does not exist. Pierik et al. (2017) were the first that studied levee dimensions on a delta scale. Using coring data, they found that levee dimensions varied throughout the delta spatially and over time, driven by changes in hydraulic and sedimentary processes. However, as their method focused on borehole data the identification and isolation of certain levee-forming processes remained limited.

To bridge the gap between case study-scale knowledge on levees and a more general understanding of the controls of levee morphology and sedimentology in the fluvial and tidal domain, a combination of two complementary methods is used; numerical modelling and field research. Numerical modelling enables the quantification of the effects of boundary conditions (e.g. river discharge and tidal amplitude) on levee morphology, sedimentology and evolution. Field studies are used to validate modelled trends and to study the evolution of levees under changing boundary conditions and internal feedbacks in nature. From this the aim of this thesis follows:

- To gain generic and quantitative understanding of the drivers of levee evolution and morphology in both fluvial and tidal environments.

To achieve the aim of this thesis two objectives were defined:

- Assessing the influence of *boundary conditions* on levee evolution, morphology and sedimentology in the fluvial-tidal realm.
- Assessing the influence of *internal processes* on levee evolution, morphology and sedimentology in the fluvial-tidal realm.

For studying the influence and relative importance of fluvial and tidal boundary conditions on levee evolution, morphology and sedimentology numerical models were used for systematically varying the boundary conditions. Based on literature (see Chapter 2), four boundary conditions were chosen as the core of the modelling study; 1) discharge magnitude, 2) tidal amplitude, 3) concentration of fines and 4) discharge variability. To further study the effects of fluvial versus tidal forcings, levees along the Old Rhine in the Netherlands were studied at three different locations representing the fluvial to tidal transition.

1.2 Relevance

Deltas and estuaries are of vital importance for present day societies (see Figure 1.1 for the world's major deltas). Deltas have become highly populated and productive areas due to their fertile soils, the abundant amount of accessible land and the easy access they provide, often via estuaries, to the ocean (Edmonds et al., 2017). The population in deltaic areas has grown from 237 million in 2000 to projected values of 322 million in 2020, growing at rates 60% larger than global average (Edmonds et al., 2017). In addition, estuaries are the home of an extensive amount of harbours, functioning as distribution points for goods around the world. Apart from the importance of deltas and estuaries for human purposes they are vital for nature. Deltas and estuaries are high in species density and diversity and form the birthing grounds of many marine species. Sustainable use and exploitation of delta and estuaries is, however, continuously threatened. Both due to accelerating sea-level rise, changing river discharge and sediment supply as well as anthropogenic subsidence and human interference with ecosystems. The importance of delta and estuarine systems and their vulnerability to changing boundary conditions creates the need for a detailed understanding of the formation and evolution of these systems. Especially under increasing anthropogenic influences.

Natural levees affect floodplain hydraulics and overbank sedimentation and form key elements in the formation of channels and fluvial sedimentary records (Brierley et al., 1997; Törnqvist and Bridge, 2002; Filgueira-Rivera et al., 2007; Pierik et al., 2017). They consequently influence the evolution of deltas and estuaries by distributing sediments and connecting channels to floodplains. In addition, natural levees are the main areas of human occupation in wet delta landscapes since the beginning of human settlements. Influencing agriculture and the residence of people in large alluvial regions (Allen, 1965; Saucier, 1969; Adams et al., 2004). As such, levees are important for understanding the interaction between the natural delta landscape and human occupation (Pierik et al., 2017; Van Dinter, 2013).

A deeper knowledge on levee morphology and evolution will help answering questions related to sediment transport and deposition in deltas, river floods and (anthropogenic) subsidence. With as ultimate goal; utilising the knowledge on natural sedimentation processes along rivers and estuaries, including levee formation, for sustainable delta-management.

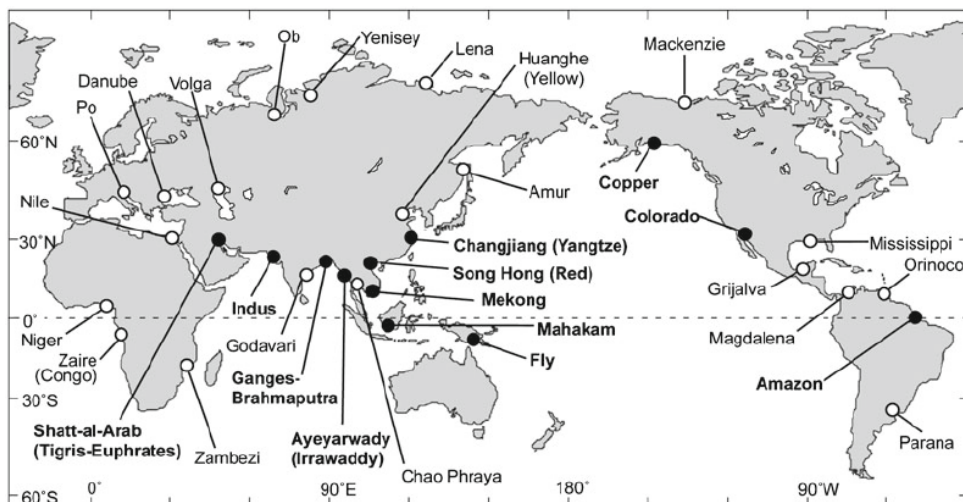


Figure 1.1: Map indicating the world's major river deltas, with tide-dominated deltas indicated by •. Source: Davis and Dalrymple (2010).

1.3 Thesis outline

The structure of this thesis follows the steps of scientific research. First, a theoretical framework is presented (Chapter 2). Within this framework, the morphodynamics of and controls on fluvial and estuarine systems are discussed, and literature on fluvial and tidal levees is reviewed. Based on this framework, hypotheses on the effects of boundary conditions and hydromorphological feedbacks are formulated. Second, the set-up of the numerical model and the details of the field study are explained (Chapter 3). Third, the results from the modelling study and the field campaign are presented separately (Chapter 4). Fourth, the results of the modelling study and the field will be combined to discuss the effects of boundary conditions and hydromorphological feedbacks on levee evolution, morphology and sedimentology (Chapter 5). Finally, the conclusions following from the research will be presented (Chapter 6).

2 | Literature review

This literature review starts with a short introduction on river, delta and estuarine systems. The purpose of this introduction is to create a conceptual framework with dominant processes and necessary terminology in which the rest of the thesis is embedded. Second, the focus will be on what a levee exactly is and how levees are formed. Third, levee morphology will be discussed with examples around the globe. At last the development of the Old Rhine river and estuary will be summarized as this system is used as a case study in this thesis.

2.1 Fluvial, deltaic and estuarine systems - an overview

Rivers are natural flowing watercourses that can be found all over the world in different forms for which many classifications exist (e.g. Leopold and Wolman, 1957; Ferguson, 1987). When rivers discharge in the ocean or in lakes, and sediment supply and accommodation space are sufficient, the transported sediment can build up extensive deltaic areas. Within these deltas the rivers build up and alter the land by depositing their sediment in different fluvial landforms, bifurcating their streams and changing their course by avulsion (e.g. Nichols, 2009; Stouthamer et al., 2015). In the coastal zone of deltas also waves and tides affect and rework the sediments resulting in a complex interplay between various processes, deposits and landforms.

Fluvial and deltaic systems

Within the depositional zone of fluvial systems a distinction can be made between different depositional environments. In the channels itself relatively coarse sediment is deposited as channel lag deposits (Figure 2.1-A). Relatively coarser sediment is also deposited in the accreting inner bends of meandering rivers in scroll bars, that together form point bar complexes (Figure 2.1-A). Due to meander migration, point bars show a fining upward sequence with relatively coarse deposits on the base (Nichols, 2009). Sediment accumulation outside of the channel is as important as sediment accumulation within the channel. When river discharge exceeds bank full discharge, finer sediment is transported out of the channel and is deposited in the floodplains (Figure 2.1) (Nichols, 2009). As a result of repeated deposition and differential settling due to changes in flow velocity, relatively coarser sediment is able to build levees and fine sediment is able to build up floodplain area (Figure 2.1). For further details on levee forming processes see section 2.2. When levees breach, crevasse splays form (Figure 2.1-A). Crevasse splays are often fan-shaped structures that silt up. They can, however, have a more elongated shape and be the start of a river bifurcation or avulsion. Although crevasses are not often the objective of studies, it is known from recent experiments that their channel width scales with the discharge in the main channel (Michelazzo et al., 2018). When rivers reach the coast, flow velocity drops causing the deposition of sediment in front of the river mouth which evolves into a mouth bar system (Figure 2.1). Mouthbars can transform into levees as the river mouth develops further under continuous deposition and evolution of new channel splits.

Estuarine systems

Moving downstream into the coastal zone of the delta, the interplay between fluvial and marine processes creates complex systems and landforms. Examples of these systems are barrier coasts with tidal inlets and estuaries.

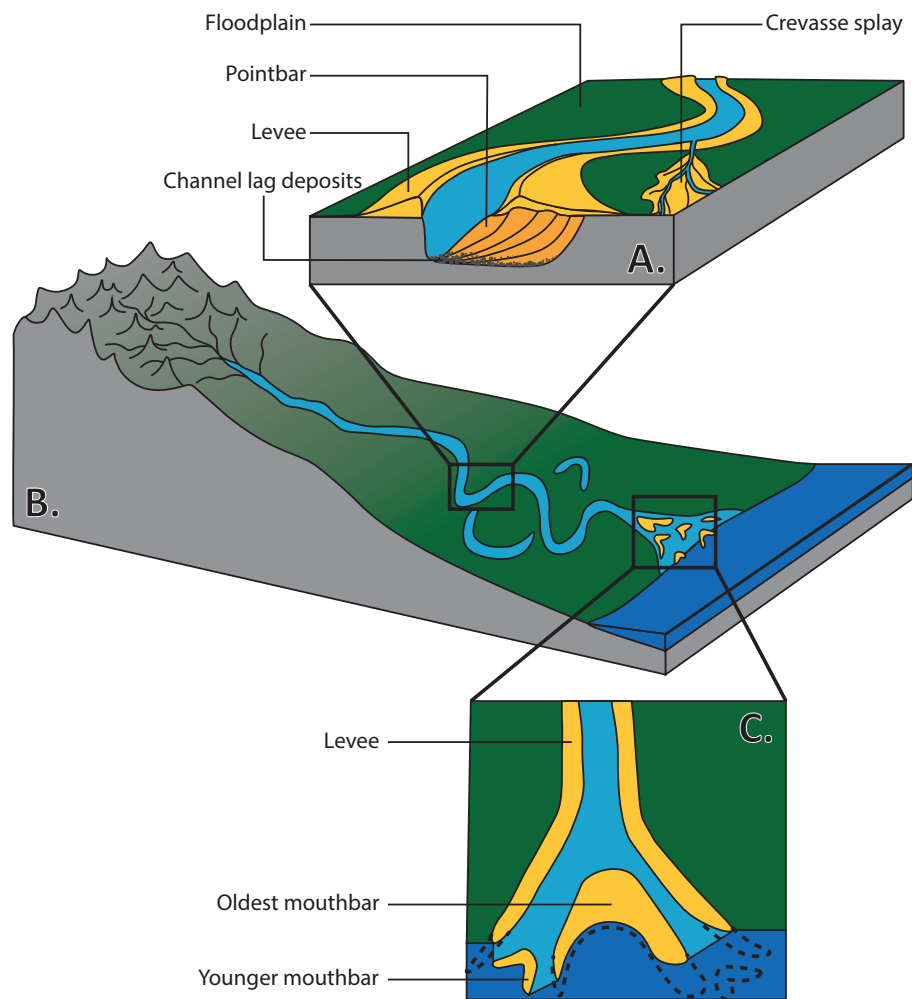


Figure 2.1: Illustration the fluvial landforms and deposits on different scales that are of importance for this thesis. A. Principal channel belt configuration with morphological units and deposits, adjusted from Allen (1964). B. Block diagram following a schematic river from source to sink, adjusted from Marshak (2011). C. Mouthbar configuration, based on Olariu and Bhattacharya (2006)

According to Perillo (1995) an estuary is a semi-enclosed coastal body of water that extends to the effective limit of tidal influence, within which sea water entering from a connection with the open sea is significantly diluted with fresh water derived from land drainage. Two end members of estuaries exist; wave-dominated estuaries and tide-dominated estuaries (Dalrymple et al., 1992; Nichols, 2009). A wave-dominated estuary (Figure 2.2-A) comprises of three distinct depositional environments; the bay-head delta, a central lagoon and the beach barriers (Dalrymple et al., 1992; Nichols, 2009). The bay-head delta is the zone where fluvial processes dominate and is similar in form to a river dominated delta. In bay-head deltas, a progradational succession can be observed with channel and overbank facies overlying mouth bar deposits which in turn overly fine-grained deposits of the central lagoon (Nichols, 2009). The central lagoon is an area of small river and wave influence. Therefore, deposition of fine-grained often organic rich material occurs (Nichols, 2009). Around the beach barrier, wave action reworks sediment into the barrier. Tide-dominated estuaries are characterised by tidal channels, tidal flats and tidal bars (see Figure 2.2-B). The coarsest sediment in estuaries can be found in the channels, the bay-head delta and the beach barriers, whereas the finer sediments dominate the tidal flats, bars and lagoonal zone.

According to Dalrymple et al. (1992) an estuary can be further distinguished into three zones, based on the dominant energy source, and the resulting morphology and sediment characteristics: 1. inner, river dominated zone, 2. central, mixed zone, 3. outer, marine dominated zone. In these zones the balance between fluvial processes (discharge) and marine processes (tides and waves) drives the morphology and sedimentology of the system.

A. Wave dominated estuary

B. Tide dominated estuary

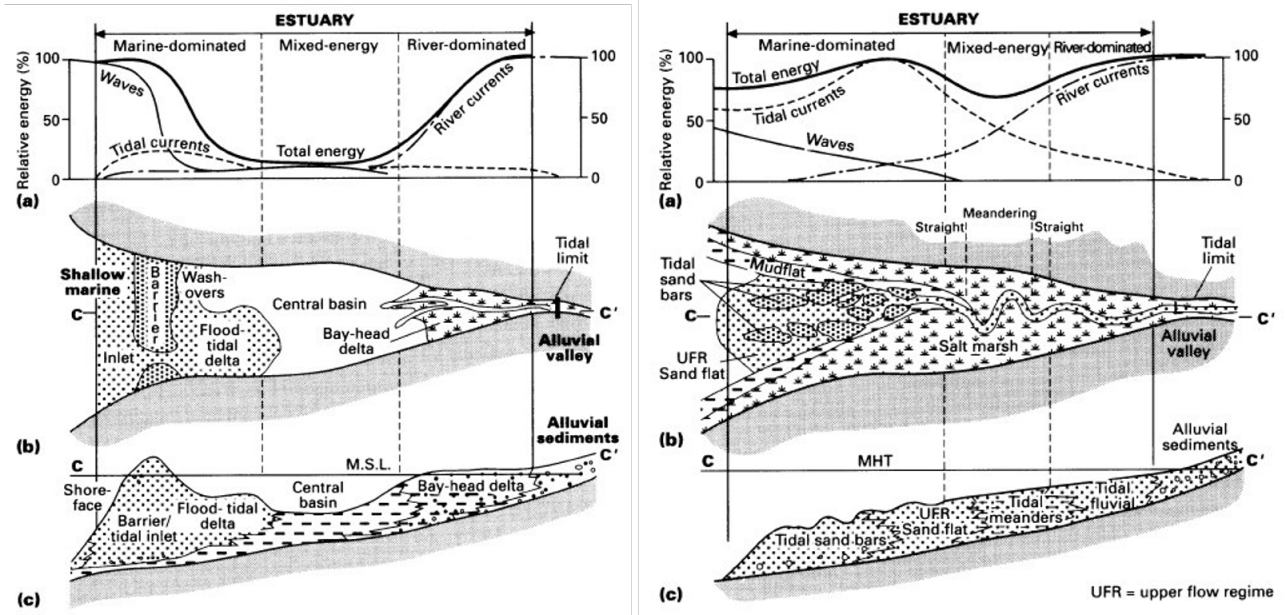


Figure 2.2: Schematic overview of a wave dominated (A.) and tide dominated estuary (B.). (a) Relative energy of waves tides and river. (b) Top view morphology. (c) cross-sectional sedimentology and morphology. Source: Dalrymple et al. (1992)

Dominant boundary conditions in fluvial and estuarine systems

Natural rivers on plains and deltas show a wide variety in planforms (Kleinhans, 2010). Trying to understand the cause of these patterns many qualitative classifications were developed based on the main river characteristics. These classifications give a first insight in the boundary conditions that dominate fluvial systems. The most well-known river pattern classification separates rivers in braided, meandering and straight (Leopold and Wolman, 1957). Further elaboration on this classification by Schumm (1985) and Ferguson (1987) showed that a combination of stream power, amount and size of bedload, width-depth ratios and channel stability all influence the channel pattern (Figure 2.3). Furthermore, the supply of mud has proven to largely influence fluvial systems by influencing bank strength and the cohesiveness of the floodplain. The latter has proven, by means of experiments, to be a necessary condition for a meandering river pattern (Van Dijk et al., 2013).

In estuaries the factors and processes that determine the morphology are more diverse than in rivers. The hydrodynamics in estuaries are driven by four components; wave action, tidal currents, river currents and density currents driven by gradients in salinity (e.g. Dalrymple et al., 1992; Nichols, 2009). All components influence the morphology of the estuary. Friedrichs (2010) showed that for generic estuarine geometry the cross-sectional integrated equation for the conservation of mass in the case of barotropic tides follows:

$$b \frac{\partial \eta}{\partial t} = - \frac{\partial}{\partial x} u w h \quad (2.1)$$

with b as the estuary width (m), η the tidal elevation (m), t time (s), x the along-channel distance (m), u the cross-sectionally averaged tidal velocity (m/s), w the width portion within all along-estuary transport of mass and momentum is assumed (m) and h the water depth of the channelized portion of the estuary (m). The left-hand side represents the time rate of change in the wetted cross-sectional area of the estuary, while the right-hand side represents the along-channel convergence in volume flux within the channel alone. The equation thereby shows us that generic estuarine morphology depends on tidal amplitude and average flow velocity, which is in part determined by tidal asymmetry and fluvial discharge.

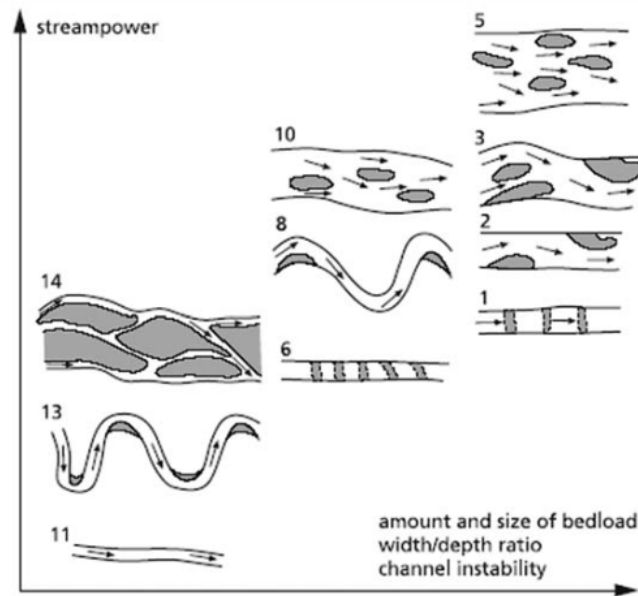


Figure 2.3: Classification of channel patterns (Ferguson, 1987)

The hydrodynamic characteristics are not the only factors influencing estuarine morphology. Despite consisting largely of sand, estuaries are flanked by mudflats and salt marshes (Dalrymple et al., 1992). As model studies have showed, mud is able to create narrower estuaries with reduced channel and bar dynamics (Braat et al., 2017). If mud concentrations are even higher, the estuary is able to narrow and fill until becoming a tidal delta (Braat et al., 2017).

Based on the summary above four boundary conditions can be selected that highly influence the morphodynamics of fluvial and estuarine systems; 1) fluvial discharge magnitude, 2) tidal amplitude, 3) concentration of fines and 4) fluvial discharge variability. Discharge magnitude influences flow strength in fluvial settings and averaged tidal velocity in estuarine systems. It therefore influences sediment transport and possibly levee evolution and morphology. Tidal amplitude largely determines estuarine morphology and water levels. Therefore, it could be hypothesised that tidal amplitude also influences levee morphology. The concentration of fines highly affects bank strength both in fluvial and estuarine systems and influences sedimentation rates outside of the channel, therefore influencing levee evolution. Lastly, the variability of fluvial discharge is hypothesised to influence overbank sedimentation and therefore the deposition of levees and floodplain fines.

2.2 Levee – a (lack of) generic definition

To be able to study the controls on levee forming processes and the influence of levees on larger scale delta development in the present (in models and in the field) as well as in the past (in the geologic record), an integrated process-based understanding of a levee is needed. An integrated approach is necessary to bridge the definition gap between geomorphologists and geologists. Thereby, a process-based understanding is required to be able to translate observations in the present-day field, the geological record as well as in models to physical correct interpretations.

Until now, the small amount of research focusing on levees has resulted in ambiguous and case study based definitions of levees that particularly vary in meaning between geological and geomorphological sites. Brierley et al. (1997) tried to bridge the gap between the geological and geomorphological definitions of levees. However, due to the limited number of detailed geomorphological and sedimentological studies at that time from modern depositional environments and the lack of a process-based approach, the question of what a levee is remained partly open. The different available definitions of a levee will be summarized below.

In geological studies a levee is often defined as the body of sediment between the 'identifiable' floodplain sediments and the 'identifiable' channel body (Brierley et al., 1997). This definition is limited as the transition between levee and floodplain is gradual. The definition therefore neglects the lateral connectivity between the two units. Brierley et al. (1997) reviewed seventeen geological studies of which two of the studies, Horne (1979) and Fielding et al. (1993), presented a non-ambiguous definition of a levee and in which the lateral connectivity between levee deposits and overbank facies were demonstrated. Another shortcoming of the 'geological' definition is the fact that it excludes levees in tidally dominated environments in which floodplain sediments are often non-existent or harder to distinguish.

Geomorphologists define levees based on four observable characteristics summarized by Brierley et al. (1997); 1) proximity to the channel margin, as a continuation of the channel bank, 2) prismatic bodies of triangular cross-section, mostly ridge or wedge-shaped features that are raised above the floodplain, 3) ribbon-like, elongated features parallel to the channel, 4) elevation is greatest at or close to the edge of the channel, where the levees commonly form steep banks and slope gently away into the flood basins. Numerous variations of these characteristics can be found in literature (e.g. Cazanagli and Smith, 1998; Törnqvist and Bridge, 2002; Adams et al., 2004; Filgueira-Rivera et al., 2007; Pierik et al., 2017). The small differences in the geomorphological definitions of a levee in these case studies inhibit the direct quantification of the effects of boundary conditions and processes that influence levee formation and dimensions. Therefore, it inhibits the general understanding of levees and their formative processes. It also makes it more complicated to make quantitative predictions on levee behaviour based on general rules.

The existence of various levee definitions has consequences. Due to the shape and location-based definition of a levee of the geomorphologists it is harder for the geologist to recognize levees in the geological record and to couple levees in the geological record to certain physical processes. This can lead to an underestimation of the preservation potential of levees and a misinterpretation of past river style, landscape configuration and source/sink conditions (an observation also made by van der Vegt (2018) in her PhD thesis, chapter 1, section 1.3.2). The difference between definitions can also cause translation problems between geologist and geomorphologist which may inhibit cooperation on larger scale scientific questions.

To overcome some of these problems, in this thesis a combination of formational, sedimentological and morphological characteristics is combined for defining and identifying a levee. These characteristics are needed for comparing modelled levee evolution, morphology and sedimentology with levee evolution, morphology and sedimentology from the field. The used definition is as follows:

- A levee is a sloping deposit of clay, silt and fine sand that is raised in elevation above the floodplain and is formed alongside a channel when sediment is transported out of the channel and deposited in proximity to this channel.

2.3 Levee formation

Having reviewed the geological and geomorphological definition of a levee it is needed to assess how levees are formed. In general, natural levees form when fluctuating water levels cause water and sediment to flow over the edges of the channel (Wolman and Leopold, 1957; Allen, 1965). As flow velocities drop rapidly when the water flows out of the channel a large part of the sediment is deposited in proximity of the channel, forming the basis of the levee. Differential deposition of sediment falling out of suspension, as flood waters lose carrying capacity, causes the levees to grow (Wolman and Leopold, 1957; Allen, 1965; Adams et al., 2004). The coarsest sediment with the highest settling velocity is deposited closest to the channel and the finer fractions are transported further away to the floodplain. Consequently, sediment grain sizes decrease abruptly or gradually from the main channel with the largest grainsizes in the levee and the smallest in the floodplain (examples can be found in Cazanagli and Smith, 1998; Adams et al., 2004; Filgueira-Rivera et al., 2007; Smith and

Pérez-Arlucea, 2008).

The above given general description of levee formation illustrates that it is hard to draw a strict line between the levee and the floodplain purely based on formation. Levees and floodplains are both members in the continuous spectrum of overbank deposits. Although, in general levees contain coarser grained sediments than floodplains due to differential settling and are higher in elevation. This leads to the conclusion that the best way to generally separate a levee from the floodplain, in the present-day field and in the rock record, is by a combination of lithological composition and levee height or sediment thickness.

In the past it has been observed in the field that two end-member levee morphologies can be recognised; wide and gently sloped levees, and narrow and steep levees (Adams et al., 2004). Wide and gently sloped levees were observed in unconfined floodplains whereas narrow and steep levees were found in confined floodplain settings (Figure 2.4). Adams et al. (2004) suggested, based on these findings, that the two end-member morphologies were coupled to two distinct levee forming processes: advection and turbulent diffusion. In addition, it was suggested that the relative dominance of one of these processes could explain the wide variety in levee morphology along rivers. Advection would cause relatively wide and gently sloped levees to form and turbulent diffusion would cause relatively narrow and steep levees to form. According to Adams et al. (2004) levee formation by advection occurs when a water surface slope causes water to flow orthogonal to the direction of the main channel flow. Hereby, sediment is transported into the flood basin, as flow velocity drops rapidly sediment is deposited adjacent to the channel. This process is similar to the general levee forming process described above. Turbulent diffusion describes the process in which turbulent eddies develop along the free shear boundary between channel and flood basin because of the interaction between the faster flowing channel waters and the nearly stagnant water in the floodplain. This process should dominate levee formation in very confined floodplains, in which the water level rises as quickly as in the main channel. As the free shear eddies move across the floodplain their turbulence decreases and sediment is being deposited preferentially adjacent to the channel forming levees. Although this process has been reproduced and verified in laboratory studies (Sellin, 1964), the process has never been observed to transport sediment in the field (e.g. Filgueira-Rivera et al., 2007). Therefore, alternative mechanisms controlling levee morphology need to be explored.

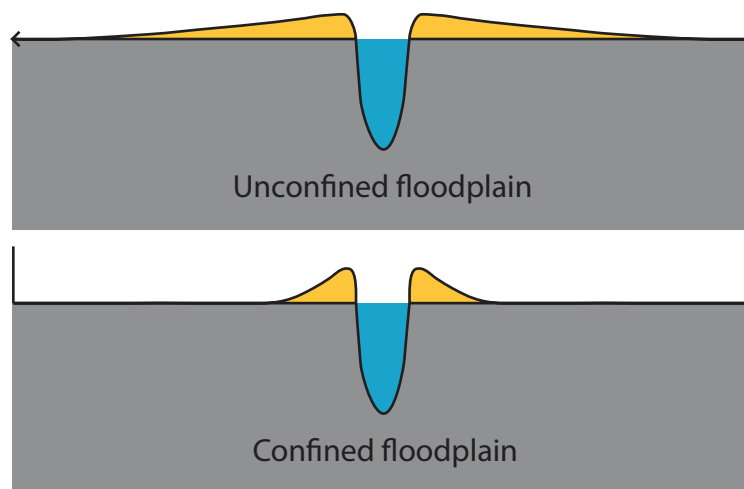


Figure 2.4: Levee morphology end-members according to Adams et al. (2004).

2.4 Levee morphology and sedimentology based on examples

From the paragraph above it became evident that water flow out of channels is essential for the formation of levees. Water level fluctuations that cause this overflow can be found in different environments. In rivers, discharge fluctuations cause channel overflow. In tidal basins and estuaries also tides can cause channel overflow. Even in peat landscapes located in proximity of the coast, fluctuating water levels can push water and sediment out of the peat drainage systems to form levees Van Dinter (2013). Below, examples of levee morphology and sedimentology around the world will be discussed, together with processes and factors that have found to be important for their morphology and sedimentology.

Natural fluvial levees can be found all over the world along lowland rivers. However, currently active levees become scarcer as an increasing number of lowland rivers are being embanked. Examples of present day active fluvial levees can be found, among others, along the Columbia River in south-east British Columbia in Canada (Filgueira-Rivera et al., 2007; Adams et al., 2004) (see 2.5-A), in the Cumberland Marshes region of the Saskatchewan River in east-central Saskatchewan in Canada (Cazanacli and Smith, 1998; Smith and Pérez-Arlucea, 2008), along the River Culm in the county of Devon in England (Nicholas and Walling, 1997), along the Mississippi river in the USA (Fisk et al., 1953; Saucier, 1969; Farrell, 1987; Kim et al., 2009; Nienhuis et al., 2018), and in the fluvial belt of the Amazon River in Brazil (Latrubesse and Franzinelli, 2002). The morphology, lithology and dimensions of the levees differ significantly along the different rivers as well as along one single river, see Table 2.1. In general, fluvial levees have heights varying from tens of centimetres to several meters, and widths in the order of meters to several kilometres. The lithology of fluvial levees is often silt dominated. However, significant amounts of coarser and finer fractions are present as well.

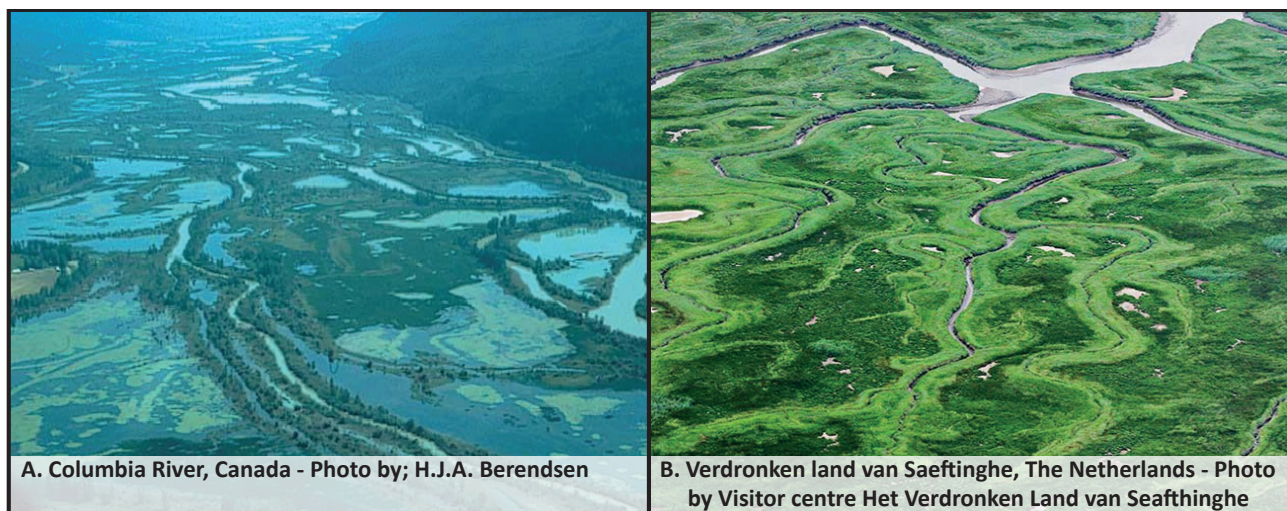


Figure 2.5: Examples of levees in fluvial (A.) and tidal (B.) environments. A. Levees along the Columbia River, Canada - Photo by; H.J.A. Berendsen. B. Levees along the tidal creeks in the Verdronken Land van Saeftinghe, The Netherlands - Photo by; Visitor centre Het Verdronken Land van Saeftinghe.

A couple of explanations exist for the wide variety in levee morphology. Filgueira-Rivera et al. (2007) found that levee shape primarily results from two factors: 1) maximum water elevation during flooding, which limits levee height, and 2) flood basin hydraulics, which determines sediment transport capacity and controls levee width. The observation that flood basin hydraulics affect the lateral extent of levees was underlined by a modelling study of Kleinhans et al. (2018) on the effects of muddy and vegetated floodplains on fluvial patterns in an incised river. They found that vegetation can cause mud to deposit close to a channel causing the formation of relatively narrow levees. Earlier field studies, summarized by Adams et al. (2004), indicated that levee shape and lateral textural trends may vary with channel area (or discharge), mean particle size and distribution, and the hydraulics in the flood basin. Adams et al. (2004) however only found a weak correlation between levee morphology

and channel cross-sectional area and concluded that levee morphology appeared to be independent of channel size. He also did not find a clear correlation between levee morphology and mean grain size in his own data set. Suggesting that levee morphology is not simply a function of mean grain size or sorting of the sediment during transport. On the other hand, Hudson and Heitmuller (2003) found that natural levee width along the Moctezuma and Pànucó alluvial valleys in Mexico is a function of the bankfull channel width. Thereby, they found that the radius of the meander bend influences levee width as well; the smaller the radius, the wider the levees are. Pierik et al. (2017) found that levee width varies along individual channel belts, regardless of their longitudinal position, age or channel-belt width. They found that levee width along alluvial ridges can be asymmetric as a result of the delta plain slope, with widths of 500-1500 m on one side of the river and widths of only a few hundreds of metres on the other. The asymmetry caused by the overall delta plain slope indicates again that levee width is controlled by flow patterns. Pierik et al. (2017) also found that increasing flood frequency and an increase in fines resulted in relatively higher levees in the Rhine-Meuse delta in the period 300-800 CE.

In tidal environments levees bound the tidal channels in intertidal and supratidal environments, e.g. on salt marshes (see 2.5-B). Due their abundance tidal levees are mentioned and studied in numerous studies (e.g. Syvitski and Farrow, 1983; Cloyd et al., 1990; Temmerman et al., 2004, 2005; Torres and Styles, 2007). The controlling factors and processes on their morphology are however rarely the subject of study. An exception is the study by Temmerman et al. (2004). They found, through a modelling study, that an equilibrium exists between levee height and basin elevation. Levees can grow to 20 to 30 cm above basin elevation before negative feedbacks decrease sedimentation rate on top of the levees. When levees obtained this equilibrium height, levees and basins accumulated at the same rate. The equilibrium elevation difference between the levees and basins is controlled by the rate of mean sea-level rise and the incoming sediment concentration (Temmerman et al., 2004). The relief between tidal levees and the creek beds principally varies with tidal range but according to field observations planform relief is often less than 0.3-0.5 m (Torres and Styles, 2007). Furthermore, tidal levees are often high in biomass as the higher elevation allows the establishment of plants (Belliard et al., 2016).

Table 2.1: Characteristics of fluvial levees around the world

River	Levee height (m)	Levee width (m)	Grainsize levee (mm)	Peak Q (m ³ /s)	Reference
Columbia	0.92 – 2.28	6.0 – 81.0	0.15 – 0.014	351	Filgueira-Rivera et al. (2007)
Columbia	0.20 – 3.70	7.6 – 954.1	0.13 – 0.01	320	Adams et al. (2004)
Saskatchewan	0.59 – 1.69	23 – 260	0.25 – <0.016	450-500	Cazanacli and Smith (1998)
Saskatchewan	-	20 – 49	0.11 – 0.01	2960	Smith and Pérez-Arlucea (2008)
Culm	Up to 1.5	-	>0.063 – 0.008	-	Nicholas and Walling (1997)
Mississippi	1.5 – 1.8	~300	0.5 – 0.005	24300	Fisk et al. (1953)
Mississippi	4.5 – 6.1	~4800	Clay – Silt	-	Saucier (1969)
Mississippi	Up to 9.1	-	Clay – Sand	-	Farrell (1987)
Amazon	1 – 10	~4000	-	1300000	Latrubesse and Franzinelli (2002)

2.5 Old Rhine - river and estuarine system

In this section the Holocene evolution of the Dutch delta will be given with an emphasis on the Old Rhine river and estuarine system. First, the geographical setting of the Rhine-Meuse delta will be described. Second, the Holocene boundary conditions in the Rhine-Meuse delta will be discussed, focussing on the Old Rhine system. Third, a summary will be given on the development of the Old Rhine system during the Holocene with as base the development of the Rhine-Meuse delta and Dutch coast.

2.5.1 Geographical setting Rhine-Meuse delta

The Rhine-Meuse delta extends from its apex at the Dutch-German border towards the Holland barrier coast located on the southeastern edge of the North Sea (Pierik et al., 2017) (see Figure 2.6). The delta is approximately 140 km in length and has a maximum width around 80 km, covering an area of approximately 120 km² (Stouthamer, 2001). The floodplain of the Rhine differs in width along its reach. Near the apex the floodplain has a width up to 20 km, after which it narrows to 10 km, before widening to 50 km in the central and lower parts of the delta (Pierik et al., 2017). At present, the Rhine bifurcates just after the apex into the Waal and the Nederrijn, branches that both bifurcate further when moving downstream (see Figure 2.6). At the barrier coast only a few inlets remain that form the connection between river and sea. From these inlets the Rhine-Meuse outlet just west of the city of Rotterdam is the most dominant, and the only one still carrying significant river discharge. Older branches of the Rhine system, such as the Hollandse IJssel and the Old Rhine were abandoned due to upstream avulsions.

The Holocene deposits in the delta have a thickness of a few meters in the upper delta and increase in thickness up to 20 m in the lower delta near the coast (Pierik et al., 2017). The sedimentary architecture of the delta is built up from peat and flood basin clays, sand bodies related to multiple generations of channel belts, and their flanking levee and crevasse complexes (Pierik et al., 2017; Törnqvist, 1993; Stouthamer, 2001).

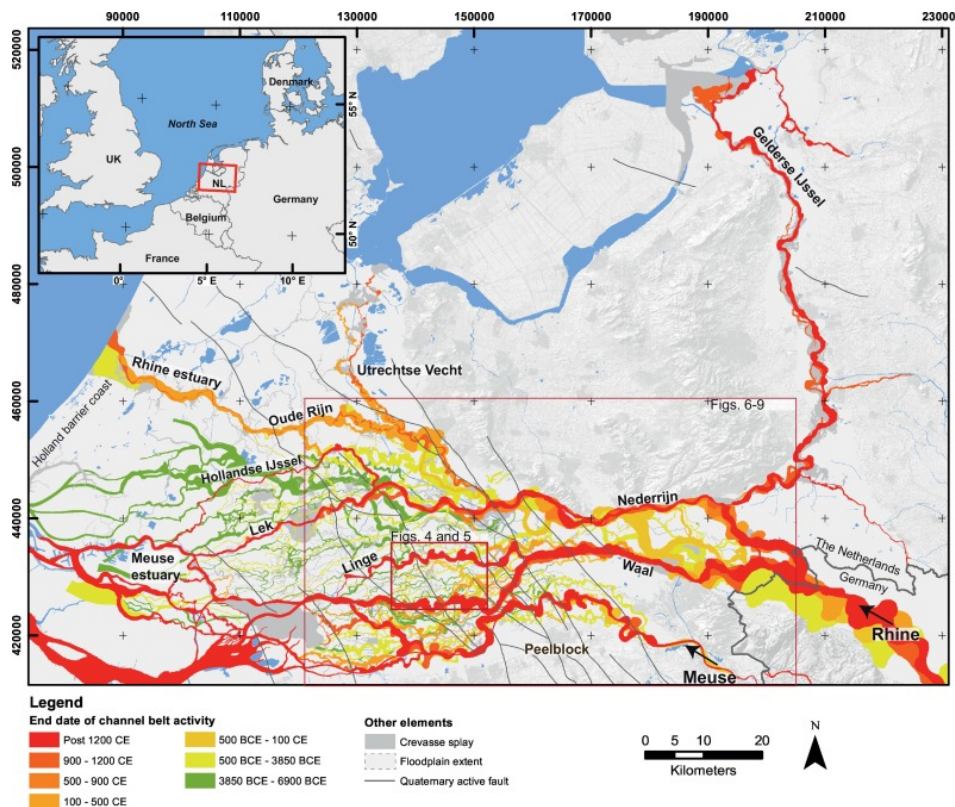


Figure 2.6: Location of the Rhine-Meuse delta. Source: Pierik et al. (2017).

2.5.2 Holocene boundary conditions

Sea-level rise during the Holocene created accommodation space for the delta to form. In the Early and Middle Holocene sea level rose fast (see Figure 2.7) due to a combination of absolute sea-level rise, caused by the melting of the ice caps, and subsidence of the area due to the collapse of the forebulge (De Haas et al., 2018b; Vink et al., 2007; Hijma and Cohen, 2010). During this period of accelerating sea level rise (8.45 - 8.25 ka BP) the former surface partly drowned causing estuaries and large tidally influenced areas to form.

The increase in sea-level changed the hydrodynamics in the North Sea. Resulting in an increase in tidal amplitude as well as an increase in the significant wave height (Figure 2.7). Despite the changes, tides have dominated the net sediment transport in this region for almost the entire Holocene by a strong flood-dominated tidal asymmetry (De Haas et al., 2018b; Van der Molen, 2002).

During the Holocene large volumes of sediment were transported by the Rhine and Meuse rivers. However, the amount of sediment transported by the rivers was not constant over time (Figure 2.7-d). Surprisingly, the difference in transport over time is not caused by changes in discharge, as the discharge of the Rhine only fluctuated within 10% (Stouthamer et al., 2011). Erkens (2009) found that the suspended sediment in the Rhine however fluctuated up to 50%. With more sediment trapping in the Early and Late Holocene than in the Middle Holocene. The enhanced sediment load in the Late Holocene is linked by Erkens (2009) to human-induced land use change in the hinterland. Deforestation in the period 3000-1000 yr. BP has increased the fine sediment supply to the Rhine river by 60% (Erkens, 2009).

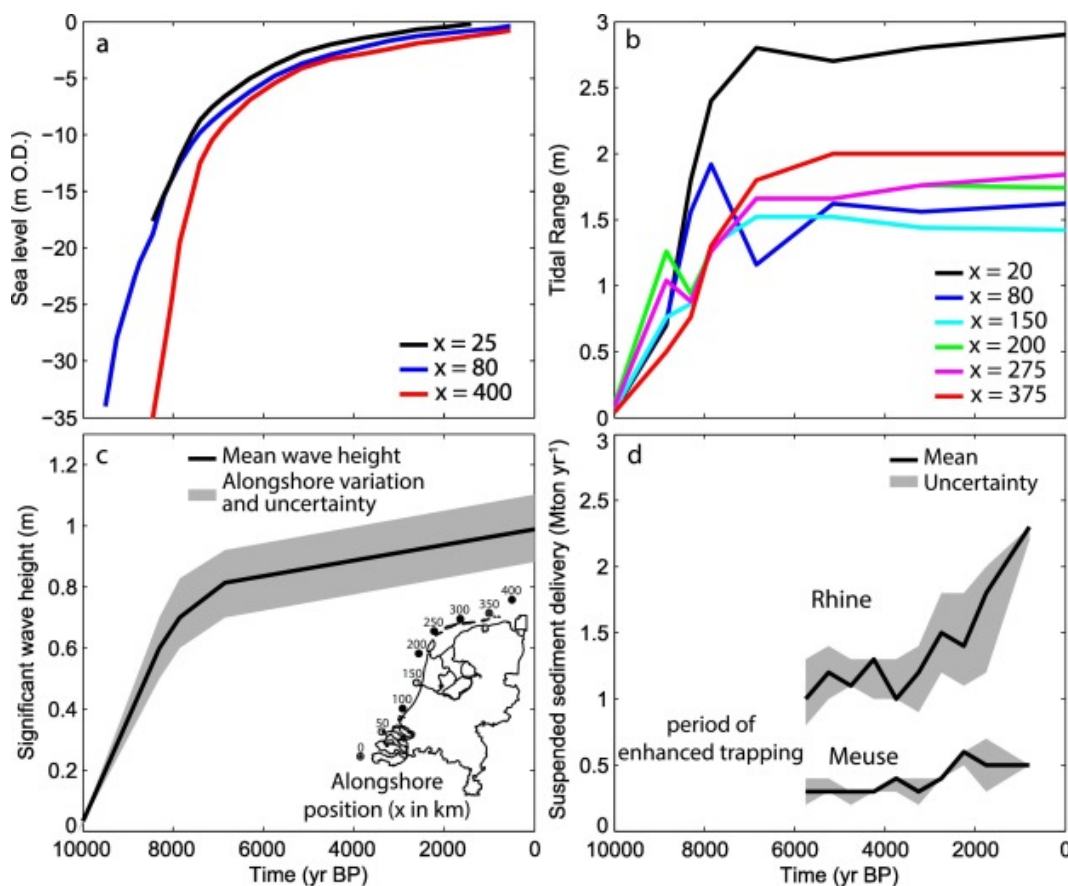


Figure 2.7: Holocene environmental boundary conditions after. (a) Relative sea level. (b) Tidal range. (c) Mean significant wave height. (d) Trapped part of suspended sediment supplied to fluvial area of Rhine-Meuse delta. Source: De Haas et al. (2018b). See De Haas et al. (2018b) for further references to data.

2.5.3 Delta and coastal development focussing on the Old Rhine

Due to sea-level rise in the early Holocene extensive tidal areas formed along the Dutch coast (7500 BP). With estuaries and tidal basins in former paleo valleys from the Pleistocene. A combination of sea-level rise and changes in discharge, sediment composition and vegetation caused the braiding rivers upstream in the paleo valleys to transform into meandering rivers (Berendsen et al., 1995; Stouthamer et al., 2015; Vos, 2015; De Haas et al., 2018b). Sea-level rise also created accommodation space which enabled the infilling of the former paleo valleys. Hence, rivers were no longer bounded by inherited topography and started to avulse. Causing the development of a complex fluvial architecture (Weerts and Bierkens, 1993), see Figure 2.6.

During the same time, beach barriers developed along the Holland coast due to the extensive availability of sand on the North Sea floor and the reworking of these sediments by tides and waves. The process of beach barrier formation was not exclusive to the Dutch coast but happened all around the world after flooding of the continental shelves after the last glaciation (De Swart and Zimmerman, 2009). Examples can be found on the east coast of the United States, the coast of the Adriatic Sea and the south coast of Portugal (De Swart and Zimmerman, 2009). Around 6000 yr. BP the Dutch barriers started migrating inland (Hijma et al., 2010).

As sea level rise slowed down later in the Holocene, marine and fluvial sediments were able to fill the back-barrier basin around 6000 yr. BP. Around the same time as the barriers started moving towards the coast. Together the developments resulted in the closing off the western part of the Dutch coast (e.g. Stouthamer et al., 2015; Beets et al., 1992; De Haas et al., 2018b; Vos, 2015).

Due to the infilling of the Pleistocene paleo valleys the Rhine started to avulse northwards, which happened simultaneously with the formation of the beach barriers. As a result of two successive avulsions of the Rhine around 7300 and 6300 yr. BP the river reached its current location near Leiden (Berendsen and Stouthamer, 2000; Hijma and Cohen, 2011; Cohen et al., 2012). Around 7300 yr. BP the first Rhine distributary began to flow into the tidal basin near Leiden (Berendsen and Stouthamer, 2000; Hijma and Cohen, 2011). The avulsion around 6300 yr. BP eventually formed the Old Rhine River branch as we now know it (Berendsen and Stouthamer, 2000; Hijma and Cohen, 2011). The Old Rhine grew to convey the vast majority of the Rhine discharge around 6100 yr. BP (Berendsen and Stouthamer, 2000). At the moment the Rhine fully avulsed northwards the fluvial channel connected with a former tidal channel in an extensive tidal basin, forming the Old Rhine estuary (De Haas et al., 2018b; Vos, 2015).

Due to the decreasing rate of sea-level rise and an increase in discharge of the Old Rhine, a well-developed river channel established through the former back barrier basin around 5700 yr. BP (De Haas et al., 2018b) (Figure 2.8). Along the Old Rhine channel and estuary levees developed that laterally confined the main water flow (De Haas et al., 2018b). The levees connected themselves to the landward migrating beach barriers resulting in a sheltering effect that facilitated the development of peat and clastic infilling (Figure 2.8), 5700 yr. BP).

Between 5000-3500 yr. BP the beach barriers started to close and the mouth of the Old Rhine estuary shifted northwards around 3800 yr. BP (De Haas et al., 2018b,a) (Figure 2.8). Both developments caused a decrease in marine influence and thus the effect of tidal boundary conditions on the river. Back water effects however still reached around 30 km inland (Van Dinter, 2013). Blocking of river discharge during storm surges caused the water level in the lower river reach to rise, causing perimarine crevasse splays to form and expand into the peat lands as the fluvial-tidal levees became more mature (Van Dinter, 2013). The perimarine crevasse systems are mainly directed landwards, following the hydrodynamic gradients (De Haas et al., 2018a). Ages of these perimarine crevasses are estimated between 4000-3500 BP onward according to Cohen et al. (2012) and Van Dinter (2013). Besides the changing direction of the crevasses, the number of crevasses seem to decrease going upstream (Van Dinter, 2013), see Appendix A for reconstruction. The location at which the amount of

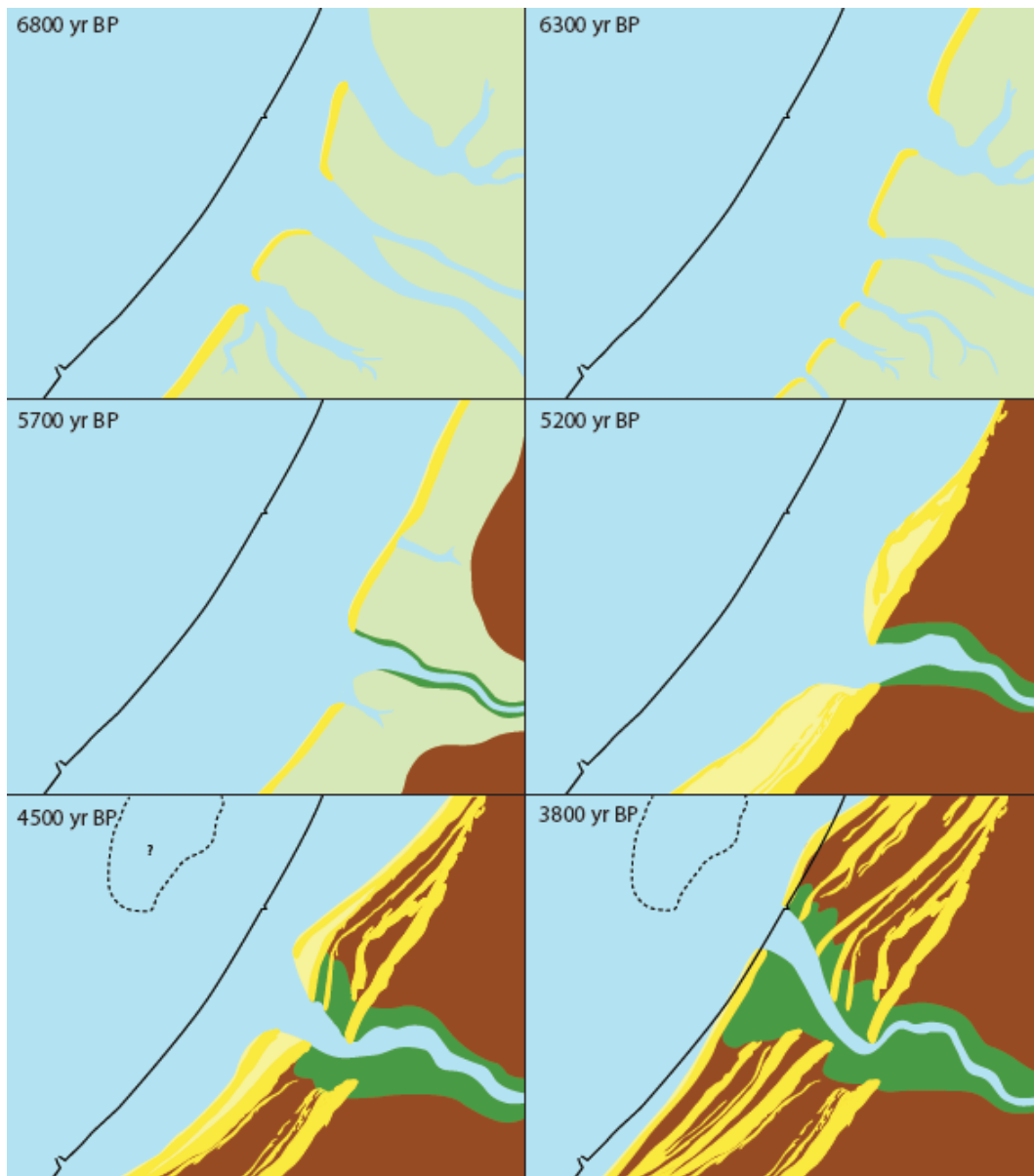


Figure 2.8: Paleogeographical maps of the Holocene development of the downstream reach of Old Rhine. Source: De Haas et al. (2018a)

crevasse decreases drastically corresponds with the characteristic backwater length of the estuary and therefore the tidal influence (De Haas et al., 2018a). Around 3000 yr. BP the Rhine partly avulsed into the Oer-IJ, which was the beginning of a decreasing discharge in the Old Rhine estuary (De Haas et al., 2018b; Van Dinter, 2013). The reduction in fluvial discharge triggered a period of enhanced estuarine overbank sedimentation mainly consisting of clay (De Haas et al., 2018a). Explained by the decrease in discharge that possibly enabled tides and storm surges to propagate further inland (De Haas et al., 2018a).

Old Rhine overbank deposits

During the time the Old Rhine was active it deposited large amounts of sediment in the form of channel belt deposits, levees, crevasses and floodplains. Due to the thick peat layers surrounding the Old Rhine river, meander migration was hampered (De Haas et al., 2018a) and the position of the river remained relatively stable (Van Asselen, 2011). Furthermore, the peat layers enabled the formation of thick natural levees due to high compaction rates of the peat below them (Van Asselen, 2011). The levee and floodplain deposits occur in multiple phases separated by peat layers (Stouthamer, 2005), see Figure 2.9. Stouthamer (2005) couples the occurrence of these phases to different active channel

belts upstream and the reoccupation of older channel belts which creates a new impulse of sediment input (Figure 2.10). The oldest overbank deposits, at a depth between 5.80 and 5.50 m -NAP (Figure 2.9-A), have an undetermined age but are coupled to the Werkhoven system upstream (Figure 2.10). The presence of these oldest overbank deposit is rare, which Stouthamer (2005) attributed to later reworking of the sediments. At a depth between 5 m and 2 m -NAP, a second phase of deposits can be recognised (Figure 2.9). In this phase the deposits increase their lateral extent between 4 and 2.5 m -NAP. The deposits have an age between 4000 yr. BP till 2800 year BP and are coupled to the Houten system upstream (Figure 2.10-B). From 1.70 m- NAP up to the surface an extensive layer of overbank deposits occurs (Figure 2.9). Correlated by Stouthamer (2005) to fluvial sedimentation of the youngest phase of the Old Rhine, when the Kromme Rijn was active upstream (Figure 2.10-C). The hypothesis by Stouthamer (2005) can explain the existence of different levee phases along the Old Rhine. However, as described above the morphology of the levees of the different phases differs. Even within one levee phase the morphology can shift significantly. Therefore, alternative hypothesis for the different levee morphology must be examined. Possibly the changing boundary conditions, as described above, influenced morphology. Or it could be hypothesised that other feedbacks between morphology, hydrodynamics and peat compaction also influence levee morphology and phasing. To temporarily remove the morphogenetic interpretation by Stouthamer (2005) the phases are renamed in Figure 2.9 based on their stratigraphical position.

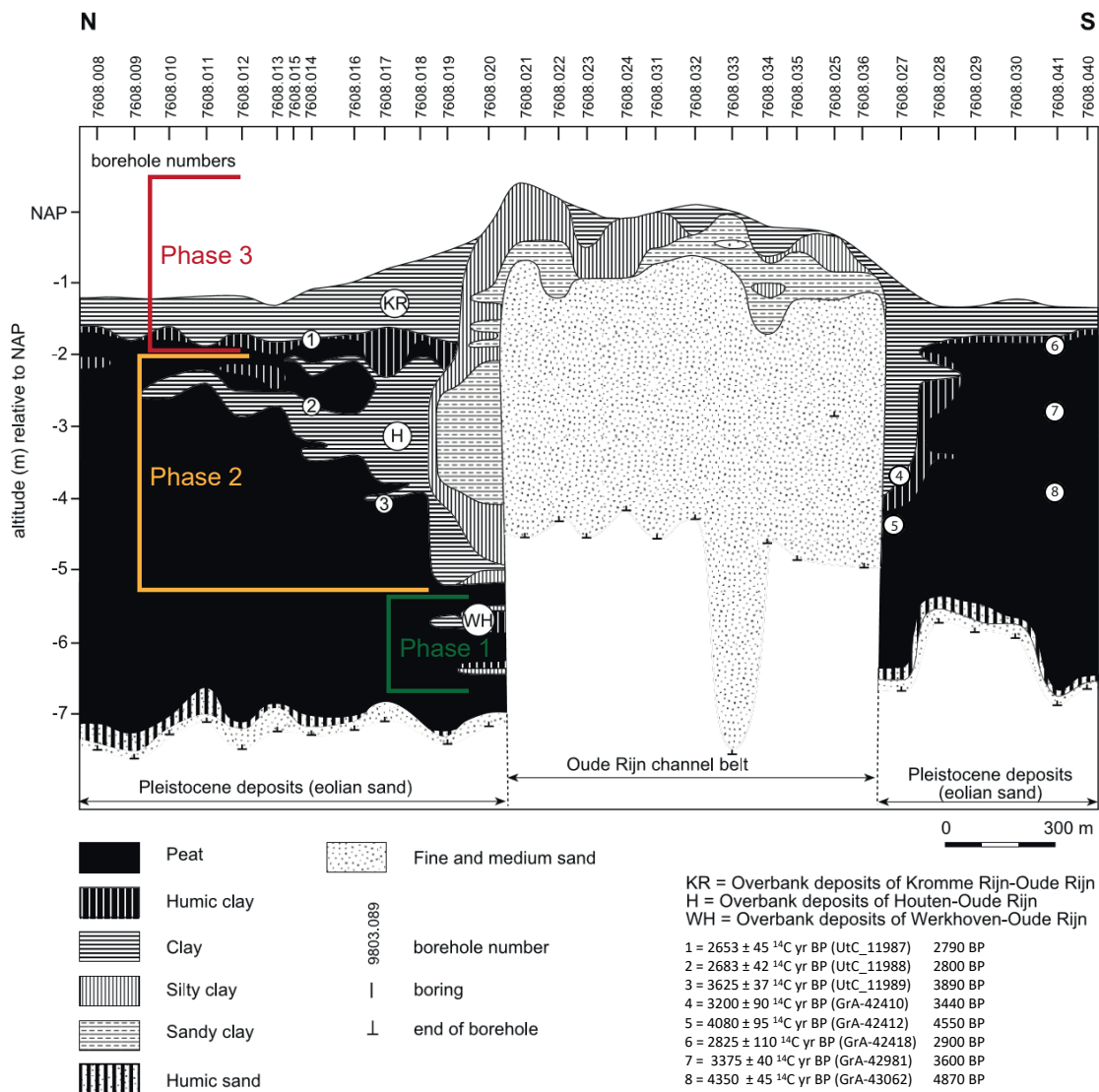


Figure 2.9: Sedimentological cross-section of Old Rhine overbank deposits at fieldwork location 1 (Figure 3.3), based on Stouthamer (2005) with added datings from Van Asselen (2010). Phases in levee deposits are renamed to phase 1, phase 2 and phase 3.

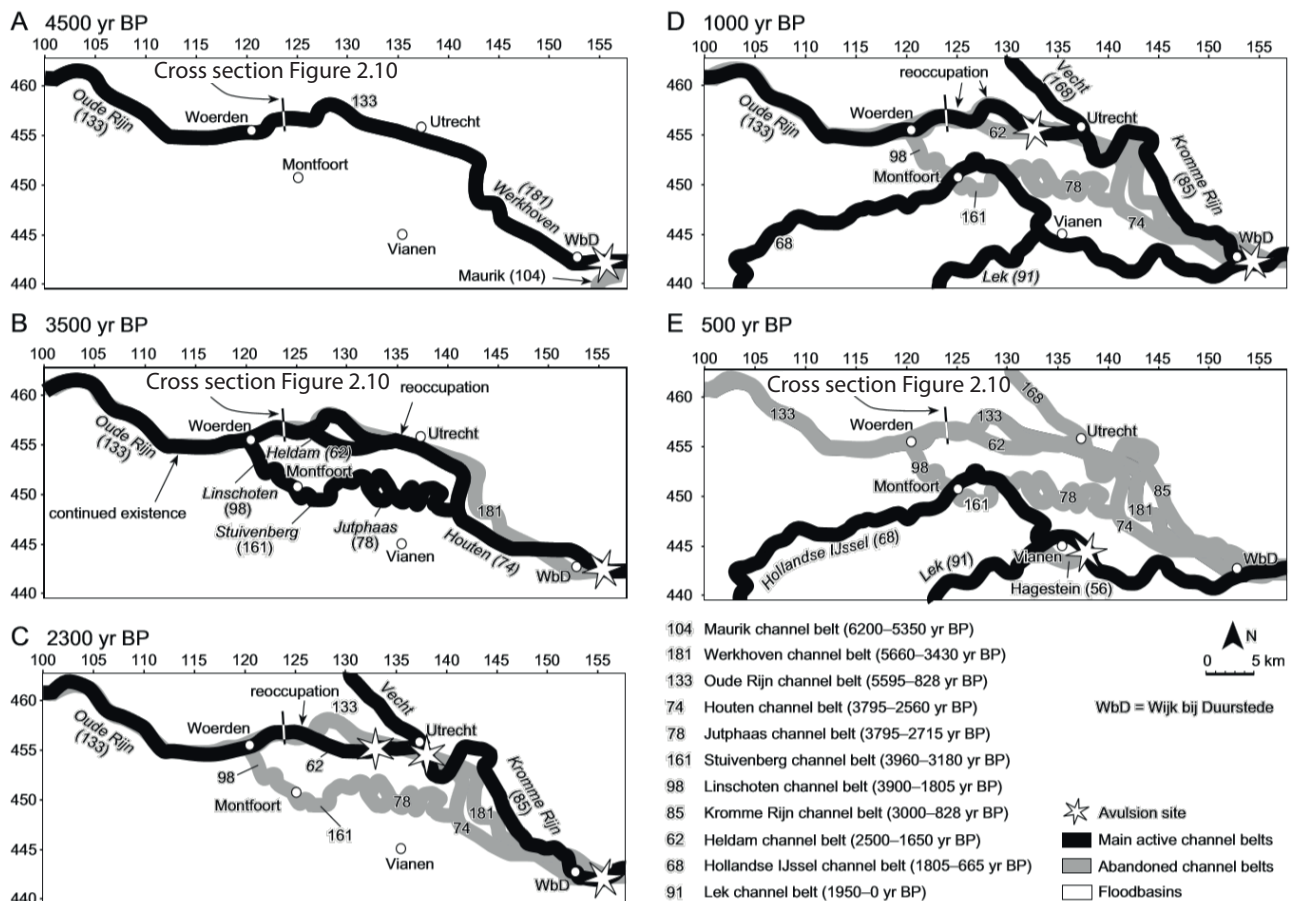


Figure 2.10: Paleogeographic evolution of the Old Rhine river system. Coordinates are Dutch map coordinates (km). Source: Stouthamer (2005).

2.6 Knowledge gaps

Despite the extensive amount of research on fluvial and estuarine morphodynamics, levee morphology and evolution has mostly been studied on a small spatial scale in fluvial environments, often only focussing on levees along a short stretch of a particular river. The only exception to this rule is the study by Pierik et al. (2017) who studied levee morphology in the fluvial part of the entire Rhine-Meuse delta over time based on field data. Previous studies have suggested levee morphology end-members (Adams et al., 2004), whereas others have shown that levee morphology can change over space and time (Pierik et al., 2017; Stouthamer, 2005). As a result, questions remain open on the effects of fluvial and tidal boundary conditions on levee morphology, the combined effects of fluvial and tidal boundary conditions, and on the internal feedbacks that drive levee formation. The two major knowledge gaps are therefore:

- The effects and combined effects of fluvial and tidal boundary conditions on levee evolution and morphology.
- The influence of internal or autogenic feedbacks on levee evolution and morphology.

2.7 Hypotheses

2.7.1 Boundary conditions

From Filgueira-Rivera et al. (2007) we know that levee height is limited by maximum water level and that levee width is mainly controlled by flood basin hydraulics and sediment transport capacity, which is endorsed by Pierik et al. (2017) and Adams et al. (2004). Temmerman et al. (2004) found that in tidal environments an equilibrium exists between levee height and basin elevation, controlled by negative feedbacks on sedimentation rates. Based on these examples the following hypotheses can be proposed:

- All boundary conditions that affect maximum water levels will affect maximum levee height. Consequently, increasing discharge magnitude, peak discharge and/or tidal amplitude will increase levee height.
- All boundary conditions that increase the amount of sediment transport out of the channel will increase levee width. Therefore, larger discharges, larger tidal amplitudes and/or larger volumes of sediment will increase levee width.
- The boundary conditions that increase the energy in the overbank environment will affect levee morphology and sedimentology. Especially tidal boundary conditions will influence the latter by decreasing levee width.

2.7.2 Hydromorphological feedback mechanisms

Adams et al. (2004) observed two end-member levee morphologies coupled to different floodplain settings; 1) wide and gently sloping levees in unconfined floodplains and 2) high and narrow levees in confined floodplains (Figure 2.4). The cross-sectional sedimentological profile in Figure 2.9 created by Stouthamer (2005) however shows that levee morphology is not static but experiences phases and evolves over time and space even if floodplain conditions remain relatively similar over time. As explanation for the presence of the different levee phases upstream avulsions are used (Stouthamer, 2005). Stouthamer (2005) argumentation however is not able to explain the differences in levee morphology of the phases. The fact that the evolution of levee morphology cannot solely be explained by shifts in boundary conditions or floodplain settings leads to the following hypotheses:

- The availability of accommodation space for levees to form will influence hydrodynamics and sediment transport, therefore influencing levee morphology. Accommodation space can be created by both high water levels and compaction of the substrate.
- When levees form and evolve they will first fill the proximal accommodation space. As this accommodation space is filled flow velocities and sediment transport over the levees will change inducing changes in levee morphology over time.
- Feedback mechanisms between accommodation space, hydrodynamics and levee morphology as described above can be as important for levee evolution as changing boundary conditions.

3 | Methods

Two distinct methods were applied for this thesis; numerical modelling and field research. Therefore, this chapter will be divided as such. Numerical modelling allows complete control over the boundary conditions of the fluvial-tidal domain, something that is impossible in nature. In this way numerical modelling allows us to study the effects of discharge magnitude, tidal amplitude and concentration of fines on the evolution, morphology and sedimentology of levees in the fluvial-tidal domain. Despite the advantages, numerical modelling has a couple of important drawbacks. Numerical models simplify natural processes and the results are sensitive to the chosen modelling parameters. To partly overcome these disadvantages, comparing the numerical results to field data is essential. To accomplish a meaningful comparison the numerical model is roughly based on the natural system that is used as a case-study; the Old Rhine. It must be noted that due to limitations in computer power the size of the model and the magnitude of the forcings are scaled down. This implies that the model domain, the river discharge and the tides are smaller than they were in the Old Rhine system. Downscaling was the only option as the cell size used in the model was already optimized between efficiency and resolution.

Next to numerical modelling, field research is needed for different reasons. First, for gaining knowledge on a wide range of boundary conditions and hydromorphological feedback mechanisms that influence levee formation, evolution and morphology. Second, to validate trends in levee evolution, morphology and stratigraphy in the models with nature. Third, to couple levee evolution to larger scale delta evolution.

Within the numerical modelling part of this chapter the hydrodynamic and morphological model will be described, the different modelling scenario's will be discussed and the methods of analysing the model results will be presented. Within the field research part of this chapter, the methods applied in the field and in the lab will be described and discussed.

3.1 Numerical modelling

3.1.1 Hydrodynamic and morphological model

The numerical modelling was conducted in Delft3D (FLOW2D3D Version 6.02.13.7658M from tag 7545) (Deltares, 2017). Delft3D is an open source software in which hydrodynamics and morphodynamics of fluvial, tidal and coastal systems can be simulated. Delft3D is widely used, tested and validated (Lesser et al., 2004). In Table 3.1 the most important morphodynamic settings applied in the model are presented. They will be discussed in further detail below. For the input files of Delft3D see Appendix B.

In Delft3D a rectangular tidal basin is created that is partly closed by two barrier islands on the seaside and is fed with river discharge on the landward side of the basin (Figure 3.1). To reduce computational time, speed up the process of channel formation and to have more control on levee formation an initial, straight, river channel is included in the initial bathymetry of the basin. The river channel trumpets out when reaching the barrier islands to simulate the natural bathymetry of

an estuary. The total dimension of the domain is 20 by 10 km, consisting of 7.5 by 10 km sea and 12.5 by 10 km of fluvial-tidal basin (Figure 3.1). Within the domain a Cartesian coordinate system is used with 200 grid cells along the length the basin (M-direction) and 200 grid cells along the width of the basin (N-direction). The individual grid cells therefore have a length of 100 meter and a width of 50 meter.

To properly model differentiation in lithology and sedimentology between depositional units, six sediment fractions were used for calculations. Four of which were sand, ranging from coarse to very fine. Two of the fractions were mud, one silt and one clay. The composition of the bed is saved and tracked over time, which allows for studying lithology, sedimentology and stratigraphy over time and space.

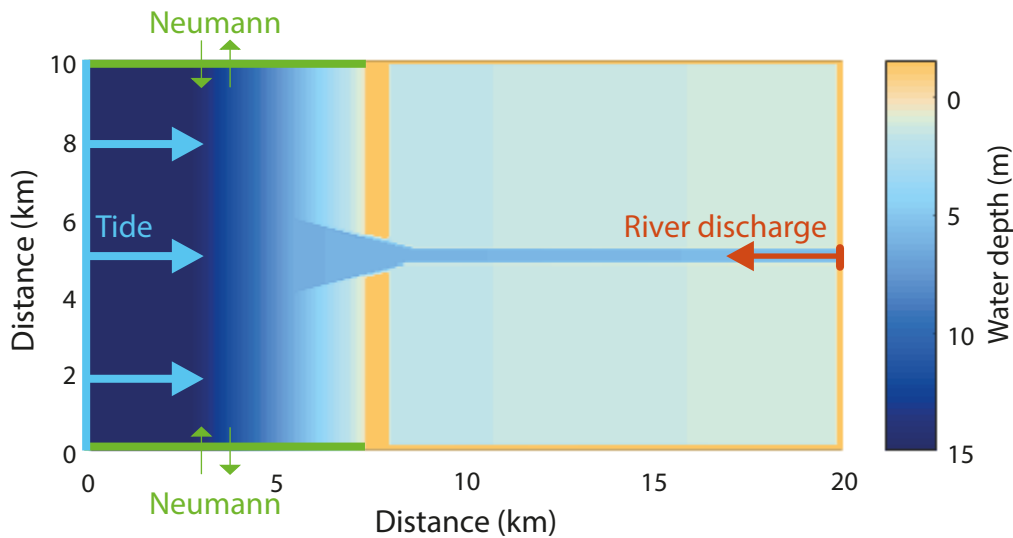


Figure 3.1: Model configuration showing initial bathymetry, boundary conditions and forcings

Boundary conditions

The modelled basin is influenced by tides coming from the seaward boundary and discharge coming from the river (Figure 3.1). Along the North and South side of the basin Neumann boundaries are applied with a gradient of zero. The tidal wave therefore does not propagate along shore but propagates directly into the basin. Neumann boundaries with a zero gradient specify that a zero concentration gradient exist at the boundary; concentration at the boundary equals the concentration just inside the model domain. As a result, very little accretion or erosion occurs near the model boundaries. The tide in the model consists of two components; the principal lunar semidiurnal (M2) and the shallow water overtides of the principal lunar (M4). The use of two tidal components creates tidal asymmetry resulting in a sediment importing system. The amplitude of the tides differs between the model runs. However, in general the M2 has an amplitude of 0.75 m and the M4 an amplitude of 0.075 m (see Table 3.1) with a phase difference of 75°. The amplitude of the M2 and M4 tidal components are coupled; the amplitude of M4 is 10% of the M2 amplitude.

As described above the discharge of the river differs per model run. However, in general the discharge equals to 700 m^2/s (see Table 3.1). The dimensions (width and depth) of the initial river channel are determined based on simple geometric relations ($Q = w * h * u$) and the aim for an initial flow velocity of 0.5 m^2/s . Due to the used geometric relations the dimensions of the initial river channel change when river discharge is altered. On the river an equilibrium sand concentration boundary is applied for 4 sand fractions with different grain sizes. On the contrary, the concentration of the two fine fractions in the incoming fluvial flow is pre-described to the model, with a general value of 0.01 kg/m^3 for the silt fraction and 0.01 kg/m^3 for clay (see Table 3.2). For more detailed information on the sediment characteristics see Table 3.2.

Table 3.1: Key morphodynamic settings

Parameter	Value	Unit	Motivation or reference
Duration run (morph. years)	100	years	-
Hydrodynamic time step	0.5	min	Based on grid cell size and flow velocity
Morphological scale factor	200	-	Relatively high to reduce computation time
Spin-up time at cold start	7.20e+02	min	Default value Delft3D
Grid size (width x length)	10 x 20	km	Enveloping fluvial and tidal part of basin
Cell size (width x length)	50 x 100	m	Trade-off between efficiency and resolution
Sediment transport equations	Van Rijn et al. (2007)	-	Van Rijn et al. (2007) & Van Rijn et al. (2004)
River discharge	700	m ³ /s	0.5 x approximate discharge Old Rhine
Tidal amplitude (M2-M4)	0.75 - 0.075	m	0.5 x tidal amplitudes along Dutch coast
Tidal periods (M2-M4)	12.42 - 6.21	hours	Natural occurring periods

Table 3.2: Sediment characteristics and parameters

Sediment property		Value	Unit
<i>Sand - 4 fractions</i>		<i>Fraction</i>	
Specific density	all	2650	kg/m ³
Dry bed density	all	1600	kg/m ³
Reference density for hindered settling	all	1600	kg/m ³
Median diameter D ₅₀	1 MS	300	μm
	2 MS	250	μm
	3 FS	125	μm
	4 VFS	75	μm
Initial sediment layer thickness at bed	1	20	m
	2	15	m
	3	10	m
	4	5	m
<i>Mud - 2 fractions</i>		<i>Fraction</i>	
Specific density	all	2650	kg/m ³
Dry bed density	all	500	kg/m ³
Reference density for hindered settling	all	1600	kg/m ³
Settling velocity	1 silt	2.5E-04	m/s
	2 clay	1.5E-04	m/s
Critical bed shear stress for sedimentation	all	1000	N/m ²
Critical bed shear stress for erosion	all	0.2	N/m ²
Erosion parameter	all	1.0E-04	kg/m ² /s

Flow

The hydrodynamics in Delft3D are solved based on the Navier-Stokes equations for incompressible fluids, under the shallow water and Boussinesq assumptions (Deltares, 2017). The most important components of the Navier-Stokes equations are the conservation of mass (equation 3.1) and conservation of momentum (equation 3.2 and equation 3.3). The conservation of mass describes that a change in water depth is caused by a gradient in discharge flux in the x and/or y direction. The conservation of momentum describes the change in velocity in the x and y direction over time due to advection, eddy diffusivity, friction, changes in water depth and stream line curvature (Lesser et al., 2004).

$$\frac{\partial h}{\partial t} + \frac{\partial hu}{\partial x} + \frac{\partial hv}{\partial y} = 0 \quad (3.1)$$

$$\frac{\partial u}{\partial t} + u \frac{\partial u}{\partial x} + v \frac{\partial u}{\partial y} + g \frac{\partial z_w}{\partial x} + \frac{gu\sqrt{u^2 + v^2}}{C^2 h} - V \left(\frac{\partial^2 u}{\partial x^2} + \frac{\partial^2 u}{\partial y^2} \right) + F_x = 0 \quad (3.2)$$

$$\frac{\partial v}{\partial t} + u \frac{\partial v}{\partial x} + v \frac{\partial v}{\partial y} + g \frac{\partial z_w}{\partial x} + \frac{gv\sqrt{u^2 + v^2}}{C^2 h} - V \left(\frac{\partial^2 v}{\partial x^2} + \frac{\partial^2 v}{\partial y^2} \right) + F_y = 0 \quad (3.3)$$

where h is water depth (m), t is time (s), u is the depth-averaged flow velocity in the x -direction (m/s), v is the depth-averaged flow velocity in the y -direction (m/s), g is the gravitational acceleration (m/s^2), C is the Chezy roughness ($m^{0.5}/s$), z_w is the free water surface level (m), V is the horizontal eddy viscosity (m^2/s) and $F_{x,y}$ is the acceleration term due to stream line curvature (m/s^2) (Schuurman et al., 2013). The advantage of the Navier-Stokes equations over for example simplified flow models described by Friedrichs and Aubrey (1988) comes from the terms containing second derivatives of depth-averaged flow velocities in the momentum equations (equations 3.2 and 3.3). These terms are important at locations where quick changes in flow velocities occur, e.g. on top of levees.

Sediment transport and bed level evolution

The calculations of sediment transport in the model are divided between bed load transport and suspended sediment transport. Both modes of transport are calculated based on formulations of Van Rijn et al. (2004). In the model bedload transport by currents is calculated as follows (instantaneous form) (Van Rijn et al., 2007):

$$q_{b,t} = 0.5\rho_s d_{50} D_*^{-0.3} \left(\frac{\tau'_{b,c,t}}{\rho_l} \right)^{0.5} \left(\frac{\max(0, \tau'_{b,c,t} - \tau_{b,cr})}{\tau_{b,cr}} \right) \quad (3.4)$$

where $q_{b,t}$ is the instantaneous sediment transport, $\tau'_{b,c,t}$ is the instantaneous grain-related bed-shear stress due to currents, $\tau_{b,cr}$ is the critical bed-shear stress according to Shields, ρ_s is the sediment density (kg/m^3), ρ_l is the fluid density (kg/m^3), d_{50} is the mean particle size (m). The bedload transport is mostly influenced by the instantaneous grain-related bed-shear stress $\tau'_{b,c,t}$ which value is dominated by the current-related friction coefficient f_c which is again dominated by the bed roughness by grains $k_{s,grain}$. For further details on the bedload transport formulation I would like to refer to Van Rijn et al. (2004) and Van Rijn et al. (2007).

The basis of suspended sediment transport in the model is formed by an advection-diffusion equation. This equation takes the suspended transport of clay, silt and sand in account (Van Rijn et al., 2007). Solving the advection-diffusion equation numerically for current related suspended transport gives, according to Van Rijn et al. (2007):

$$\begin{aligned} S_{s,c,x} &= \int_a^h \left(uc - \varepsilon_{x,x} \frac{\partial c}{\partial x} \right) dz \\ S_{s,c,y} &= \int_a^h \left(vc - \varepsilon_{x,y} \frac{\partial c}{\partial y} \right) dz \end{aligned} \quad (3.5)$$

where $S_{s,c,x/y}$ is the current related suspended transport rates in x - and y -directions, u, v are flow velocity components (m/s), c is the mass concentration of sediment (kg/m^3) and $\varepsilon_{x,x/x,y}$ are the eddy diffusivities of the sediment (m^2/s). It must be noted that equation 3.5 is the three-dimensional formulation of the suspended sediment transport, whereas in this thesis a two-dimensional depth-averaged approach is used. Therefore, the formulation of the suspended transport is averaged over depth. For determining bed level changes, transport gradients in the x - and y -direction are being used in the sediment continuity equation, also known as the Exner equation:

$$\frac{\partial z_b}{\partial t} + \frac{\partial(S_{b,x} + S_{s,x})}{\partial x} + \frac{\partial(S_{b,y} + S_{s,y})}{\partial y} = 0 \quad (3.6)$$

where $S_{b,x/y}$ is the bed-load transport in respectively the x - and y -direction and $S_{s,x/y}$ is the suspended-load transport in respectively the x - and y -direction. The Exner equation describes conservation of mass between sediment in the bed and sediment that is being transported. Bed elevation increases proportionally to the amount of sediment that falls out of transport and decreases proportionally to the amount of sediment being entrained by the flow. The formulation therefore controls the morphological change in the basin.

Bed composition

Bed composition is of great importance for this thesis as mud (silt and clay) and fine sand is the dominant sediment in natural levees and therefore must be modelled correctly. In addition, the mud content determines the cohesive behaviour of the bed and therefore erosion. Studying levee lithology and sedimentology in the model is thereby needed for comparison with natural levees from the field. For these reasons, a bed module is used, developed by Van Kessel et al. (2012), that accounts for sediment mixtures and the effect of bed composition on erosion properties. In addition, the module tracks and saves the bed composition. In the module the bed is split in 50 Eulerian bottom layers and 1 Lagrange top layer. In the Eulerian framework the position of the layers is kept constant. Aggradation/degradation is accounted for by changing the thickness of the top layer (Van Kessel et al., 2012). In the Lagrangian framework, the thickness of the layers is constant and the set of layers moves with aggradation/degradation by means of an artificial advection velocity (Van Kessel et al., 2012). The advantage of using a mixed Eulerian-Lagrangian approach is limiting the artificial diffusion due to grid movement while preventing undesired layer thickness effects resulting in a realistic mass flux and bed composition (Van Kessel et al., 2012).

3.1.2 Modelling scenarios

The model was run for different scenarios to study the effects of different boundary conditions on levee evolution and morphology. The boundary conditions focussed on were: 1) discharge magnitude, 2) tidal amplitude, 3) concentration of fine sediment and 4) discharge variability (for summary of characteristics see Table 3.3). The magnitude or set-up of these boundary conditions was varied to be able to study the individual effects of the four boundary conditions. Fluvial discharge magnitude was varied between 400 m³/s and 1500 m³/s. The tidal amplitude of the M2 component was varied between 0 and 1.25 m with steps of 0.25 m. Consequently, the M4 component was varied between 0 and 12.5 cm. The concentration of fines in the incoming river flow was varied between 0 g/m³ clay and silt, and 20 g/m³ clay and silt resulting in a total mud concentration of 40 g/m³. The influence of yearly discharge variability is tested by forcing a yearly discharge peak and varying the magnitude of this peak (see 3.2-A for graphical representation and 3.3 for peak magnitudes). To keep the different scenarios the total yearly discharge is kept constant. In addition, the influence of discharge variations on a larger temporal scale is tested with one model forced by variations in discharge with a period of 25 years (3.2-B).

It must be mentioned that the variability of the discharge presented in Table 3.3 and Figure 3.2 corresponds to the morphological time within the model and not the hydrological time. In addition, a small sensitivity analysis was executed on the effect of the '*critical shear stress for erosion*' parameter in Delft3D. See Appendix G for the results and discussion of this sensitivity analysis. A summarized overview of all the model runs used in this thesis is presented in Table 3.4.

Table 3.3: Summary of tested boundary conditions. Note that 1. Discharge magnitude, 2. Tidal amplitude (M2) and 3. Concentration fine (silt&clay) are varied based on magnitude. Whereas, 4. Discharge variability is varied based on peak discharge magnitude and peak duration.

Parameter	Unit	Absent	Low	Medium	High	Very high
1. Discharge magnitude	m ³ /s	-	400	700	1000	1500
2. Tidal amplitude M2	m	0	0.25 - 0.5	0.75	1	1.25
3. Concentration fine (silt & clay)	g/m ³	0 & 0	5 & 5	10 & 10	15 & 15	20 & 20
		Peak Q	Normal Q	Mean Q	Peak	
		(m³/s)	(m³/s)	(m³/s)	duration	
4. Discharge variability		1000	692	700	10 days	
		1250	685	700	10 days	
		1500	678	700	10 days	
		1000	400	700	25 years	

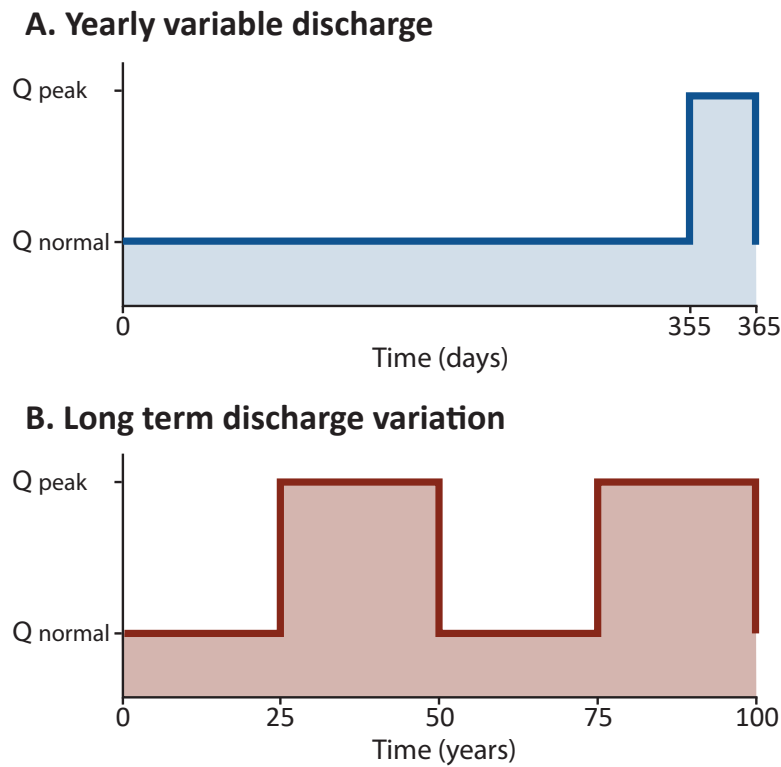


Figure 3.2: Schematization of implemented variable discharge; A. Yearly variable discharge, with one peak discharge of 10 days and B. Long term discharge variation, with periods of low and high discharge with a 25 years duration.

Table 3.4: Model runs overview. Colours represent the tested parameter groups. Green = discharge magnitude, light blue = tidal amplitude, yellow = fine concentration, dark blue = discharge variability, and pink = larger critical shear stress for erosion. Model 12 is of a different colour (grey) as it functions as the control scenario. Note that the numbering of the runs are expressions of how the models are stored for analyses.

Model nr.	Q mag. (m ³ /s)	Tidal amp. M2-M4 (m)	Conc. fine c-s (g/m ³)	Q variability	Additional
011	400	0.75-0.075	10-10	-	-
012	700	0.75-0.075	10-10	-	-
013	1000	0.75-0.075	10-10	-	-
014	1500	0.75-0.075	10-10	-	-
018	700	0-0	10-10	-	-
023	700	0.25-0.025	10-10	-	-
015	700	0.50-0.050	10-10	-	-
016	700	1.00-0.100	10-10	-	-
017	700	1.25-0.125	10-10	-	-
022	700	0.75-0.075	0-0	-	-
019	700	0.75-0.075	5-5	-	-
020	700	0.75-0.075	15-15	-	-
021	700	0.75-0.075	20-20	-	-
031	692-1000	0.75-0.075	10-10	Peak 10 days	
032	685-1250	0.75-0.075	10-10	Peak 10 days	
033	678-1500	0.75-0.075	10-10	Peak 10 days	
034	692-1000	0-0	10-10	Peak 10 days	
037	400-1000	0.75-0.075	10-10	25 yrs variation	
038	700	0-0	10-10		Larger critical shear stress for erosion
039	700	0.50-0.050	10-10		0.5 N/m ² instead of 0.2 N/m ²
040	700	0.75-0.075	10-10		
041	700	1.00-0.100	10-10		
042	692-1000	0.75-0.075	10-10	Peak 10 days	

3.1.3 Analysis of model results

Data from the models were analysed over space and time. Hence, evolution of levee morphology and stratigraphy at specific locations as well as evolution of the entire basin were followed. Both quantitative and qualitative analyses were used to study the data. The analysis can be divided into morphodynamics, sedimentation patterns and stratigraphy, and hydrodynamics.

Morphodynamics

The morphodynamic analysis can be divided into levee and crevasse related morphodynamics and basin evolution. Levee height over time and space, levee width over time and space and crevasse channel area over time were studied. In the morphodynamic analysis of levees and crevasses only the fluvial dominated part (upper 5 km) of the basin is considered. This is part of the basin in which clear levees and crevasses formed.

Levee height over time is studied by finding the maximum elevation in the levee complex for every time step. Levee height over space is studied by cross-sections over the levees at set locations. Final levee topography is studied as well, based on hypsometry plots over the levee crests. Levee width over time and space is studied based on three different characteristics that fit to the definition of a levee in Chapter 2; 1) planform lithology, 2) height above floodplain and 3) height above zero water level. For method 1) *planform lithology*, the outer boundary of the levee is determined as the transition between an average grain size that represents silt and other fractions. For method 2) *height above floodplain*, the floodplain height is determined based on the height that would be reached if all overbank deposits were spread evenly over the entire overbank area. For method 3) *height above zero water level*, levee width comprises the distance between the most proximal point to the channel above the zero water level and the most distal point on one cross-section.

Crevasse channel area over time is studied based on cross-sections over the levees. From these cross-sections the width and depth of the crevasses breaching them is determined with the *findpeaks* function in MATLAB. This function is able to find local maxima and can be optimized by specifying the minimum distance between peaks and the minimum prominence of the peak (relative importance). In the calculations a minimum peak distance of 5 cells was forced and a minimum prominence of 1. Hereafter the cross-sectional crevasse area is assumed to be *width·depth*. For basin infilling analysis the area above and below the water level is studied over time. To make this analysis representative the data is normalized with the initial depth of the basin.

For the morphological evolution of the entire basin the area located above and below the water level over time and plan view bathymetry were studied. The bathymetric results of the model were not detrended with the initial basin slope as the basin fills up rapidly and the initial slope is not clear in the later timesteps.

Sedimentation patterns and stratigraphy

Planform sedimentation patterns were qualitatively studied based on the planform distribution of D_{50} grain sizes. To study sedimentology and stratigraphy, cross-sections over the levee complexes were created showing average grain sizes and the percentages of single and combined sediment fractions.

Hydrodynamics

To further assess mechanisms in basin infilling, the location along the x-axis at which the ebb velocity is larger than the flood velocity is determined in the main river channel over time. Due to the limited storing of hydrodynamic data and the morphological scaling vector the extraction of flow velocity data is not straightforward. The procedure to extract the most downstream location of ebb dominance over time is as follows: 1) locate peaks and troughs in velocity data per location, 2) extract consecutive trough values from peak values, 3) find point in time in which signal becomes ebb dominant for every location, 4) extract location of ebb dominance over time.

3.2 Field research

A field campaign along the Old Rhine in the Western part of Netherlands was conducted in the middle of September 2018. The fieldwork area followed the course of the Old Rhine from the city of Utrecht to the city of Leiden (Figure 3.3). The fieldwork was a joined effort for this thesis and for the thesis of Moree (2019) about crevasse splays along the Old Rhine. Focus of the field campaign was obtaining detailed data on the stratigraphy, sedimentology, morphology and the age of levees and crevasses along the Old Rhine. The data will be used to reconstruct the boundary conditions under which the levees evolved as sedimentology and possibly morphology reflects these conditions. In addition, the data is also used for comparison with the model. At three locations the levees of the Old Rhine were studied. Starting upstream close to Utrecht, where fluvial boundary conditions influenced evolution, and moving downstream to Leiden where both fluvial and tidal boundary conditions influenced the evolution of the system (Figure 3.3).

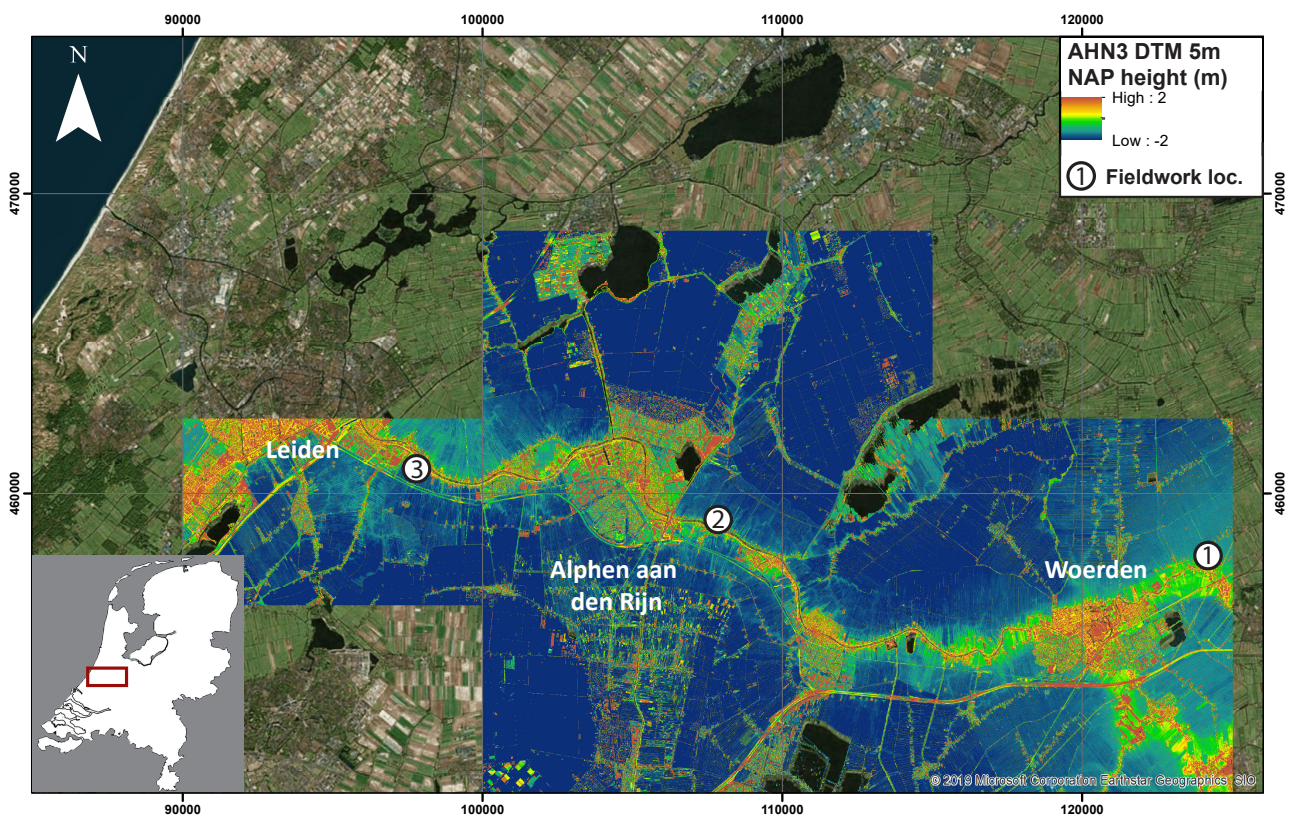


Figure 3.3: Overview of the fieldwork locations along Old Rhine system on the digital elevation model of the Netherlands (AHN). The Old Rhine alluvial ridge can be observed as an elevated (red and yellow) line meandering from the south-east of the image to the north-west.

3.2.1 Stratigraphy and lithology

At all locations stratigraphy was studied based on multiple hand-cored boreholes on a transect along the width of the levees (Figure 3.4). For every ten centimetres lithology, colour, plant remains, the redox status and the relative calcium content were determined together with other special details such as the presence of shell remains or bedded structures. Lithology in the field was described based on the Dutch classification scheme of Bakker and Schelling (1966) adjusted by Berendsen (2005) (Appendix C) and will be presented in this thesis in the USDA classification scheme. The classification scheme of Bakker and Schelling (1966) is based on fluvial and marine deposits in the Netherlands and is therefore applicable in the case of the Old Rhine.

To be able to study levee sedimentology in more detail and to be able to compare the field data with the model results, grain size samples were taken at all three locations. Samples were taken on the top, in the middle and at the bottom of the different levees at approximately the same distance from the current Old Rhine channel. This sampling strategy supports studying levee evolution over time and in a downstream direction. The ultimate goal of the sample analysis is to distinguish different influencing boundary conditions during levee evolution. The assumption is that the lithology and sedimentology of the levees will reflect the conditions they are formed under. In addition, at the most upstream and downstream locations a few sediment samples were taken in the direction of the floodplain to allow for studying levee sedimentology in this direction.

The sediment distribution of the samples was later determined in the lab based on a combination of wet sieving and pipetting. Sand was sieved and mud was pipetted. For the pipetting the mud was mixed into a glass column together with one litre of water and 2 grams of sodiumhexametaphosphate to prevent flocculation. The content of the column was thoroughly mixed after which at set time steps samples were pipetted. These were later dried and weighted to reconstruct the distribution of fines. The pipetting method is based on Stokes's law for settling velocity. Which describes that a particle with a larger radius will settle faster than one with a smaller radius. The sand was sieved with 0.5 Φ intervals (Wentworth scale), whereas the mud was pipetted with Φ intervals of 1, ranging from 5 Φ to 9 Φ . The results of the sieving and pipetting were combined and analysed based on D_{50} and average grainsize, sorting, skewness and kurtosis. All the statistics were calculated based on formulations of Folk and Ward (1997). The characteristics of the samples were used for comparing levee lithology along the channel, from upstream to downstream, and for comparing the different levee phases. As the sediments will provide insight in the hydrodynamic conditions the comparison will allow for studying the different conditions the levees were influenced by.

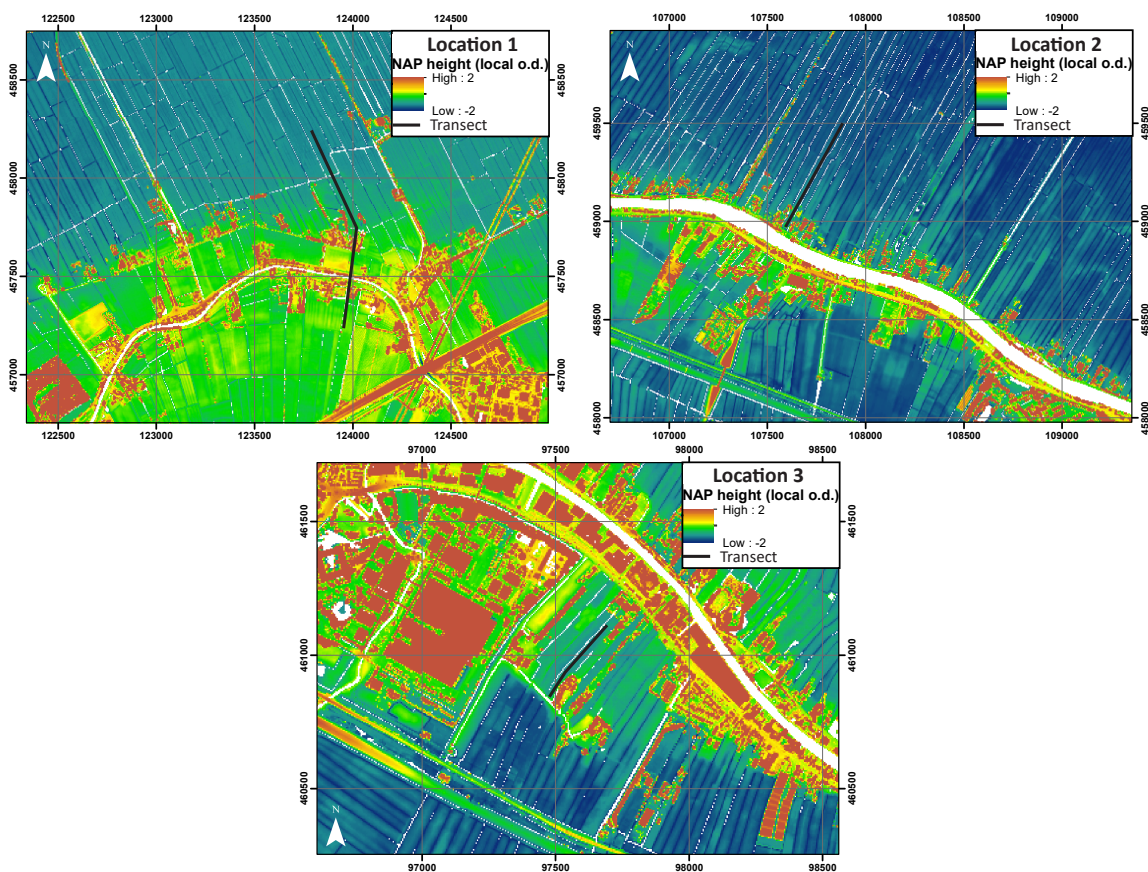


Figure 3.4: Maps of the three field locations depicting the digital terrain model AHN. Black lines indicate the transect along which coring was performed.

3.2.2 Dating the deposits

For the determination of the start and end date of the levees sediments cores were taken of peat layers below and on top of the levee or connecting floodplain deposits. To obtain accurate dates the sediment cores were further processed and analysed in the laboratory to determine the exact location of the transition from peat to clastic deposits or vice versa. This was done with lost on ignition (LOI) (see Heiri et al., 2001). From all the sediment cores sub samples (1 cm cubes) were extracted over the entire length of the core. Consecutively, the wet, dry and clastic weight of each individual sample was determined. This was done respectively by weighing the samples after extraction from the core, after a night in a stove at 100 °C and after igniting all organics for 4 hours in an oven at 550 °C. With this data, curves were created with organic content over depth. Based on these curves the exact location for the sample was determined. Ultimately, the macro-remains from these samples were dated with carbon-14 dating. Carbon-14 dating, or radiocarbon dating is a method for determining the age of a deposit based on the radioactive decay of radiocarbon. For a detailed review of the carbon-14 sampling method see Törnqvist and Dijk (1993). It must be noted that the results of the C14 dating became available after handing in this thesis.

3.3 Comparison between model and field data

For the qualitative and quantitative comparison of model and field data multiple analyses are executed. The morphology, stratigraphy, sedimentology and lithology of modelled and natural levees is quantitatively and qualitatively compared. For lithological analyses the same statistical methods were used to define D_{50} , sorting, skewness and kurtosis (Folk and Ward, 1997). The comparison between modelled and field morphology, stratigraphy, sedimentology and lithology has multiple purposes. The comparison will be used to assess how well the model can represent natural levee deposits in the fluvial-tidal domain. Comparing will thereby show if similar feedback processes influence levee stratigraphy in the field as in the model. Further, levee width and shape over space and time is qualitatively compared and coupled to different conditions along natural rivers.

4 | Results

4.1 General morphological and sedimentological development

4.1.1 Planform development

The set-up of the boundary conditions has a significant influence on the morphodynamic and sedimentological development of levee complexes. Figure 4.1 shows the bathymetries and plan view median grain size of key model set-ups after 100 years of morphological development. The key models are; 1. a model without tides with a constant discharge (nr. 018 in Table 3.4), 2. a model without tides with a variable discharge (nr. 031 in Table 3.4), 3. a model with a small tidal amplitude and constant discharge (nr. 023 in Table 3.4), 4. a model with a larger tidal amplitude and constant discharge (nr. 012 in Table 3.4) and 5. a model with a smaller concentration of fines (nr. 019 in Table 3.4). From Figure 4.1 the large-scale effects of fluvial processes, tides and concentration of fines on levee morphology can be derived.

In absence of tidal fluctuations most of the sediment brought in by the river is deposited within the basin confined by the barriers and only a small part is exported through the outlet. All significant morphological change occurs within the basin (Figure 4.1-1,2). In the presence of tidal fluctuations most of the sediment brought in by the river is still deposited within the basin. However, morphological change occurs within the basin as well on the seaward side of the barriers, where an ebb tidal delta forms (Figure 4.1-3,4,5). Based on morphology the basins in which tidal fluctuations occur can be divided in three main sections; 1. ebb-tidal delta (~4-7.5 km), 2. tidal dominated part (~7.5-15 km), 3. fluvial dominated part (~15-20 km).

When a constant discharge is forced into the basin and water level fluctuations are absent clear and smooth levees form on both sides of the channel that decrease in width downstream (Figure 4.1-1). When small water level fluctuations are introduced with a yearly frequency, by peak discharges, the levees are breached by crevasse channels after a stage of undisturbed levee development (Figure 4.1-2). The crevasse channels breach the levees in the upstream part of the basin. Due to the breaching the final levee morphology becomes more complex. At the locations of the crevasse channels the levee becomes wider due to levee formation along the crevasse channels themselves. When larger tidal water level fluctuations are introduced into the basin with a two-daily frequency, levees and crevasses form simultaneously resulting in a complex final morphology consisting of multiple different levees and crevasses interplaying and dissecting each other (Figure 4.1-3 and Figure 4.1-4). The larger the tide the larger the complexity of the final morphology. If the concentration of fines supplied to the basin is limited the levee-crevasse complex significantly decreases in width (Figure 4.1-5).

The grainsize maps in Figure 4.1 show that despite differences in boundary conditions and energy in the models, all levees and levee complexes consist mainly of silt (Φ 4-8). Under zero to low tidal influence, the levees gradually transfer into a clay ridge floodplain (Figure 4.1-1,2,3). When tidal amplitude becomes larger and tidal prism increases, the floodplain clays are either not able to deposit and are washed out of the basin (Figure 4.1-4,5).

In Figure 4.1-3 there is a clear difference in crevasse direction between the downstream and upstream

crevasses. The downstream crevasses are oriented landwards, whereas the upstream crevasses are oriented seawards. To understand the orientation of the crevasses better the maximum and mean flow velocities of the model with a small tidal amplitude (model 023, see Figure 4.1-3) were studied. They are visualised in respectively 4.2-A and 4.2-B. The maximum and mean values were based on the first 15 years of development. The direction of the maximum flow velocities along the edges of the main channel are directed landward in the downstream part of the basin (8-15 km), whereas they are directed seawards in the upstream part of the basin (15-20 km). The mean flow velocities in the basin are all directed seaward due to the presence of river flow in the basin. Mean flow velocities along and in the channel are smallest just outside of the channel in the downstream part of basin.

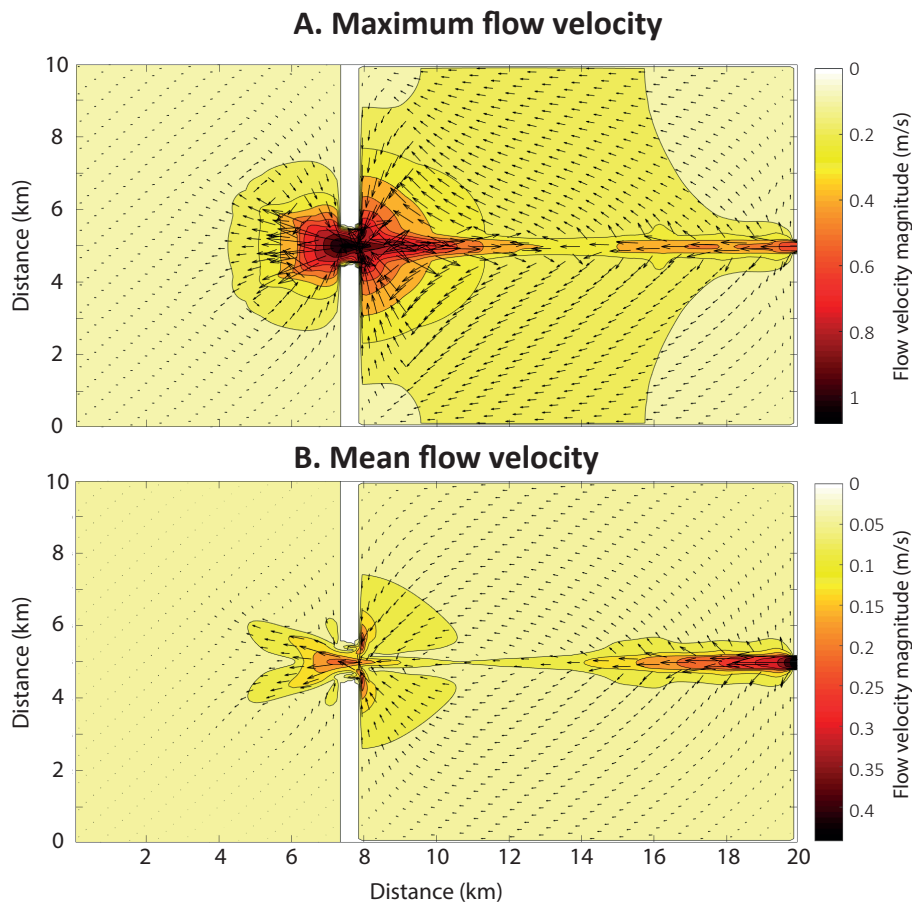


Figure 4.2: Maximum (A.) and mean (B.) flow velocity magnitudes and directions for model 023. Model 023 corresponds to the final bathymetry and sedimentology of 3. in Figure 4.1

4.1.2 Cross-sectional development

The development of levees was studied in more detail by looking at cross-sections over the levee complexes (Figure 4.3). To identify the different stages of development the combined silt and fine sand fraction are plotted in percentages for a cross-section at 18.3 km in Figure 4.3. The combined silt and fine sand content is plotted as the grain size maps in Figure 4.1 clearly show that lithology is a great indicator for the presence of levee deposits.

In general, the development of the levees can be described by three morphological phases; 1. levee heightening, 2. levee widening and 3. crevasse influence (Figure 4.3). During the first phase levees grow in height, filling the proximal accommodation space along the channel. The shape of the levee during this phase is best described as triangular. During the second phase the levees start to widen in the direction of the floodplain resulting in a more trapezoid shape. The third phase is characterised by the influence of crevasse channels breaching the levees. The crevasses build up their own levees

causing the expansion of the levee-crevasse complex width. The increase in width caused by the development of crevasse levees is large; at certain locations the pre-crevasse levee width is doubled. The timing of onset of the three phases differs between the models. Furthermore, when fluvial discharge is constant and tides are absent crevasses do not form causing the third levee phase related to crevasse formation to be absent (Figure 4.3-A).

When river discharge is constant and tides are absent, the heightening phase has a duration of ~10 years at this location (Figure 4.3-A). Hereafter, the levees start to widen up to the end of the modelled time. If river discharge is variable and tides are absent (Figure 4.3-B) levee heightening again has a duration of ~10 years. Hereafter, levees start to widen. At this specific location, after 70 years from the start of the modelled time crevasses start to influence the sedimentation patterns. The crevasse channels breach the levees and start to build up their own levees on the distal side of the levee complex.

If large water fluctuations are present on a bi-daily scale caused by tidal fluctuations, the previous described levee phases can still be recognised however they are more intertwined (Figure 4.3-C). The levee heightening phase has a duration of 3 years, after which levees start to widen. Despite the name 'widening phase' the resulting levee morphology from this phase is different than from the previous fluvial examples. During the widening phase the levee grows in height significantly and the levee crest moves away from the main channel. The third phase related to the influence of crevasse channels is more complex than in domains without tides or with smaller tides. The duration of the phase is longer, causing crevasse channels to form, silt up and form again. The extended duration of the phase results in thicker deposits (Figure 4.3-C).

As morphology results from gradients in sediment transport and sediment transport results from the hydrodynamics, the cause of distinct morphological levee phases could hypothetically be found in the hydrodynamics. To study the likely relation between the hydrodynamics and the morphological levee phases flow velocities, flow velocity gradients and sediment transport gradients over the levees (at 18.3 km) are plotted over time in Figure 4.4-A,B and Figure 4.5 respectively. Note that due to the presence of water level fluctuations in some models and the time step of data saving it was necessary to apply a moving mean to the velocity magnitude to smooth the signal for plotting. For all cases and timesteps the flow velocity magnitude on top of the levee is higher than in the floodplain for (Figure 4.4). For the model without tides and with a constant discharge (model 018) flow velocity magnitude is largest in the first 15-20 years after which it drops. For the case with a variable discharge and no tides (model 034) the same is true, except after 70 years flow velocity increases again (Figure 4.4-A). In the case with tides (model 012) flow velocity magnitude evolves in a complex path, but in general the magnitude increases over time.

Sediment deposition and erosion are the results of gradients in flow velocity, therefore the flow velocity gradient between the levee and the floodplain is plotted over time in Figure 4.4-B. Within Figure 4.4-B the timing of the morphological levee phases from Figure 4.3 is illustrated by vertical dotted lines and coloured bullets with numbers corresponding to the phases. For the models without tides, in which the morphological transition from heightening to widening is very clear (Figure 4.3), the transition from heightening to widening (around 10 years) coincides with a drop in the magnitude of the velocity gradient (see Figure 4.4-B). The timing of the transition from the widening phase to the crevasse influenced phase in the model with a variable discharge (model 034) again coincides with a change in flow velocity gradient. For the model with a large tidal amplitude (model 012) the distinction between morphological phases is less clear. The transition between phases however does coincide with peaks and troughs in the velocity gradient.

When studying the gradients in sediment transport over time (Figure 4.5) it becomes evident that for the models without tides (018 and 034) changes in transport gradients coincide with changes in levee morphology. The transition from a heightening levee to a widening levee, after ~10 years, occurs at

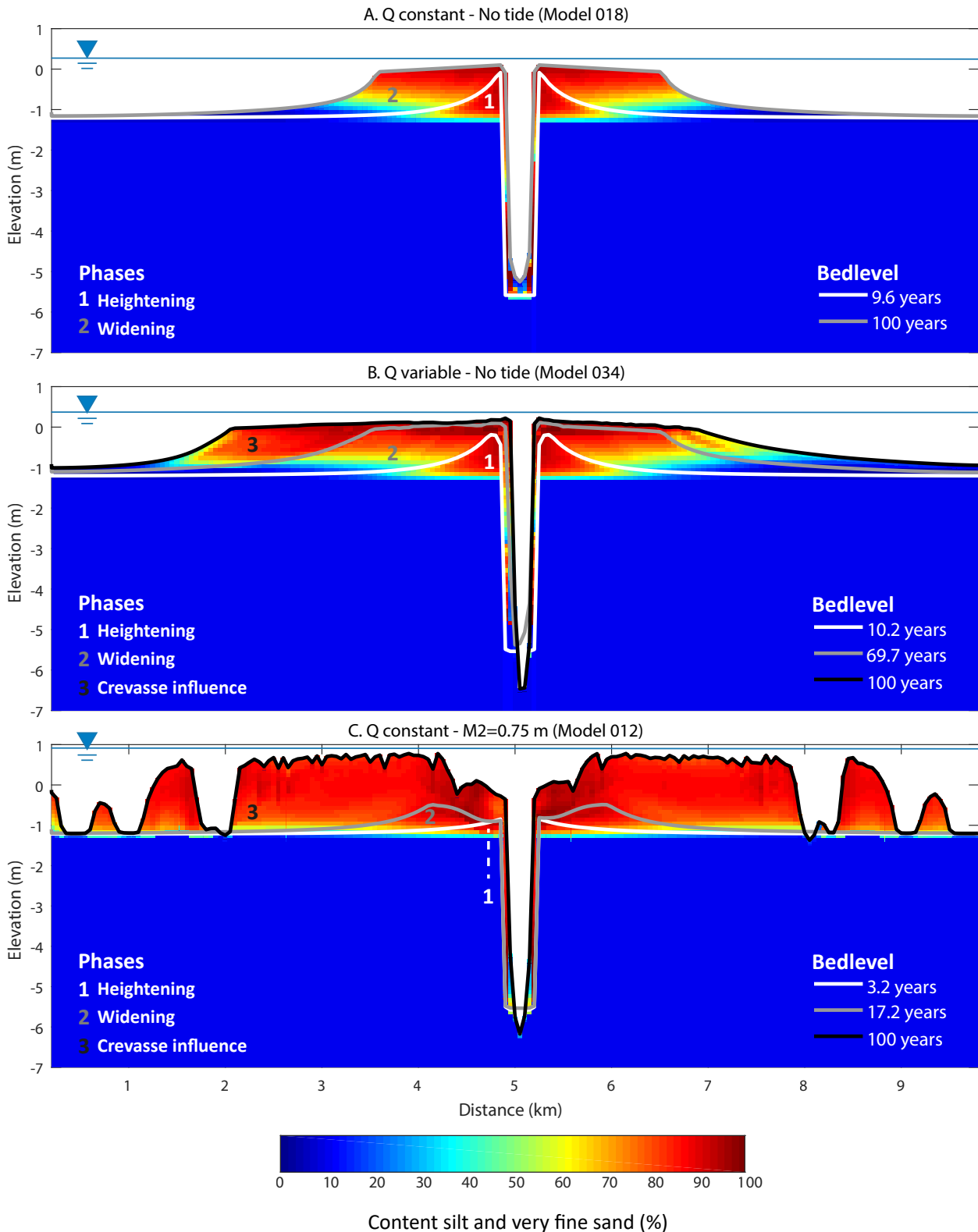


Figure 4.3: Cross-sectional levee development at 18.3 km represented by percental silt and very fine sand content and characteristic bed levels. The depicted bed levels represent the end stage of a certain development phase. Blue lines represent the maximum water level.

the time when the magnitude of the sediment transport gradient is becoming smaller. The transition from the widening levee to the levee influenced by crevasse channels in model 034 occurs at the time when the magnitude of the sediment transport gradient again starts to decrease. For the case with a significant amount of tides (model 012, $M_2=0.75$ m), the identified morphological phases of Figure 4.3 do not coincide with changes in transport gradients. Despite that, it is clear that the occurrence of morphological levee phases is correlated to shifts in sediment transport gradients. The correlation between these two phenomena and the direction of the relation will be further discussed in Chapter 5.

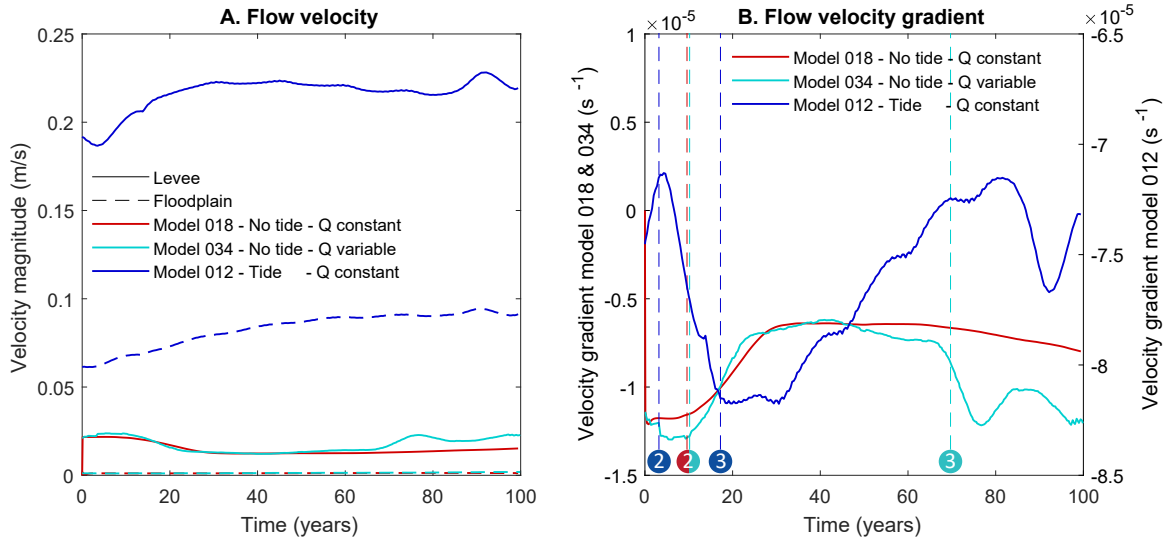


Figure 4.4: A. Flow velocity magnitude on levee crest ($y=19.7$ km) and in floodplain ($y=7.5$ km) for the three modelled cases presented in Figure 4.3. B. Flow velocity gradient from levee crest to floodplain ($y=19.7 - 7.5$ km) over time for the three modelled cases presented in Figure 4.3. Within the figures the vertical dotted lines depict the start of the phases (numbers in coloured bullets) presented in Figure 4.3. Note that y-axis differs for the models.

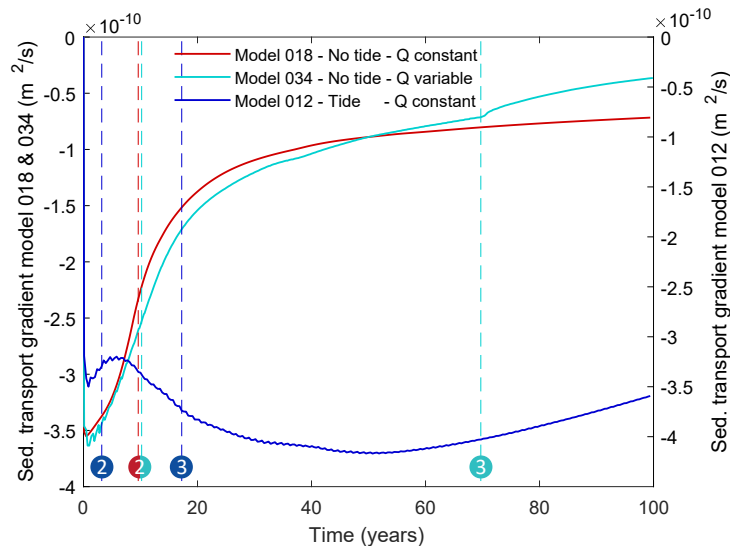


Figure 4.5: Total sediment transport gradient from levee crest to floodplain ($y=19.7-7.5$ km) over time for the three modelled cases presented in Figure 4.3. Values are negative as sediment transport on top of the levee is larger than in the floodplain. Within the figures the vertical dotted lines depict the start of the phases (numbers in coloured bullets) presented in Figure 4.3. Note that y-axis differs for models.

4.2 Levee and crevasse morphology

The effects of boundary and initial conditions on levee and crevasse morphology can be quantified by studying levee height and width over time (Figure 4.6, Figure 4.7 and Figure 4.9), by relating these measures to water levels (Figure 4.8) and by studying the cross-sectional crevasse area over time (Figure 4.12). Below levee height over time and space, maximum levee height in relation to water levels, levee width and crevasse dimensions are discussed in this order.

4.2.1 Levee height

Data on maximum levee height presented in Figure 4.6 are divided in the four tested boundary conditions; A. discharge magnitude, B. tidal amplitude, C. fine concentration, D. variable discharge. It must be noted that for the tidal amplitude the M2 amplitude is considered and that for the fine concentration the depicted concentration represents the individual concentration silt and the individual concentration clay. E.g. a concentration of 5 g/m^3 in the graphs, implies 5 g/m^3 of clay and 5 g/m^3 of silt. Which together results in 10 g/m^3 of mud. Independent of the parameter setting the development of levee height is fastest in the first 20-30 years, in which most of the growth appears. After this the growth slows down and ultimately stops. When studying the evolution of levee height over time in detail wiggles can be observed in the first ten years. These are due to the combination of the tidal cycle and the morphological acceleration factor in the model (Morffac). Below the development of maximum levee height over time is discussed separately for the four parameter groups.

The maximum levee height increases faster over time for higher constant flow discharges. In addition, the final maximum levee height is larger when the discharge magnitude is larger (Figure 4.6-A). The differences between maximum levee height are however small, within the order of centimetres. The growth of the maximum levee height in the first 20 years is faster for smaller discharges than for larger discharges. However, after 30-40 years the levees that formed under larger discharges outgrow the levees formed under smaller discharges.

Tidal amplitude has a significant effect on the final maximum levee elevation as well as the evolution of levee height over time (Figure 4.6-B). Larger tidal amplitudes result in higher levees (Figure 4.6-B). The increase in tidal amplitude seems to be directly related to the increase in final maximum levee height. E.g. levees formed in a basin with a M2 amplitude of 0.25 m are 0.25 m smaller in height than levees formed in a basin with a M2 amplitude of 0.50 m. Therefore, tides seem to be the primary driver behind maximum levee height. The development of levee height in the first couple of years is faster for larger tidal amplitudes. For the smallest tidal amplitudes, the evolution of levee height is characterised by rapid height increase in the first ~20 years, followed by height stabilisation. For larger tidal amplitudes (0.75 m - 1.25 m) the evolution of levee height is characterised by two successive height increase and stabilization phases.

Increasing or decreasing the concentrations of fines also affects the evolution of maximum levee height and the final maximum levee elevation. In general, higher concentrations of fines result in larger maximum levee height and a faster development towards this maximum height. The final maximum levee height is however not directly related to the concentrations of fines; For high concentrations ($10\text{-}20 \text{ g/m}^3$) the final maximum levee height is equal, whereas for smaller concentrations the levee height increases when concentrations increase. Nonetheless, the final maximum levee height is reached earlier for larger concentrations of fines.

When applying variable discharge in various ways the evolution of maximum levee elevation is influenced. In general, the larger the peak discharge the higher the maximum levee elevation (Figure 4.6-D). Although the difference in maximum levee height under peak discharges of 1000 and $1250 \text{ m}^3/\text{s}$ does not differ much. This can be explained by tides being the primary driver of maximum levee height. The evolution of levee height under a peak discharge of $1500 \text{ m}^3/\text{s}$ however shows that

if a certain threshold discharge is met peak discharge magnitude becomes the main factor controlling maximum levee height.

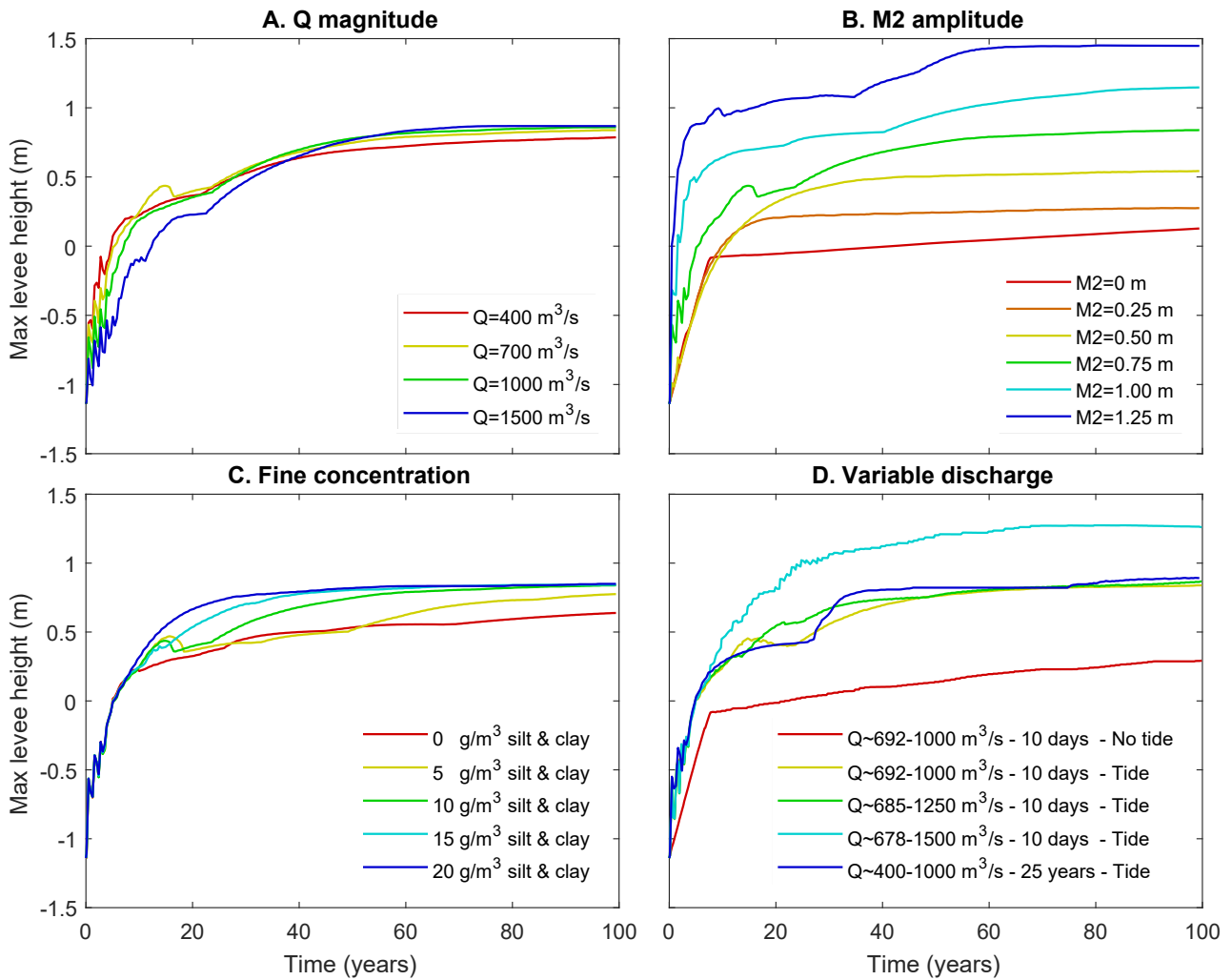


Figure 4.6: Evolution of maximum levee elevation over time for different boundary conditions: A. Discharge magnitude, B. Tidal amplitude (M2), C. Concentration of fines (silt and clay), D. Discharge variability.

To study the overall levee topography hypsometry plots are created from cross-sections over the final levees (after 100 years of morphology) along the main channel (see Figure 4.7). Again, the data are divided over the four boundary conditions; A. discharge magnitude, B. tidal amplitude, C. fine concentration, D. variable discharge. The hypsometries demonstrate that an increase in discharge magnitude (Figure 4.7-A) and an increase in tidal amplitude (Figure 4.7-B) both increase the topographical variation in the levee complex. E.g. for a small tidal amplitude of 0.5 m the hypsometric curve is almost horizontal indicating a small amount of topographical variation, whereas for a large tidal amplitude of 1.25 m the hypsometric curve is almost diagonal indicating a large amount of topographical variation. The hypsometries in Figure 4.7-C demonstrate that an increase in fine concentration increases the elevation of almost the entire levee complex. Despite the increase in elevation the lowest elevation in the levee complex remains similar for all concentrations. The hypsometric curves for different variable discharge cases (Figure 4.7-D) resemble the hypsometric curve from model 012 with a tide of 0.75 m (Figure 4.7-B green). With an exception for the hypsometric curve of the variable discharge case without tides who resembles the hypsometric curve of the small tidal amplitude case (Figure 4.7-B orange). All hypsometric curves from the variable discharge cases indicate only a small amount of topographical variation in levee topography, with a large amount of the levee complex (>70%) being above a certain height.

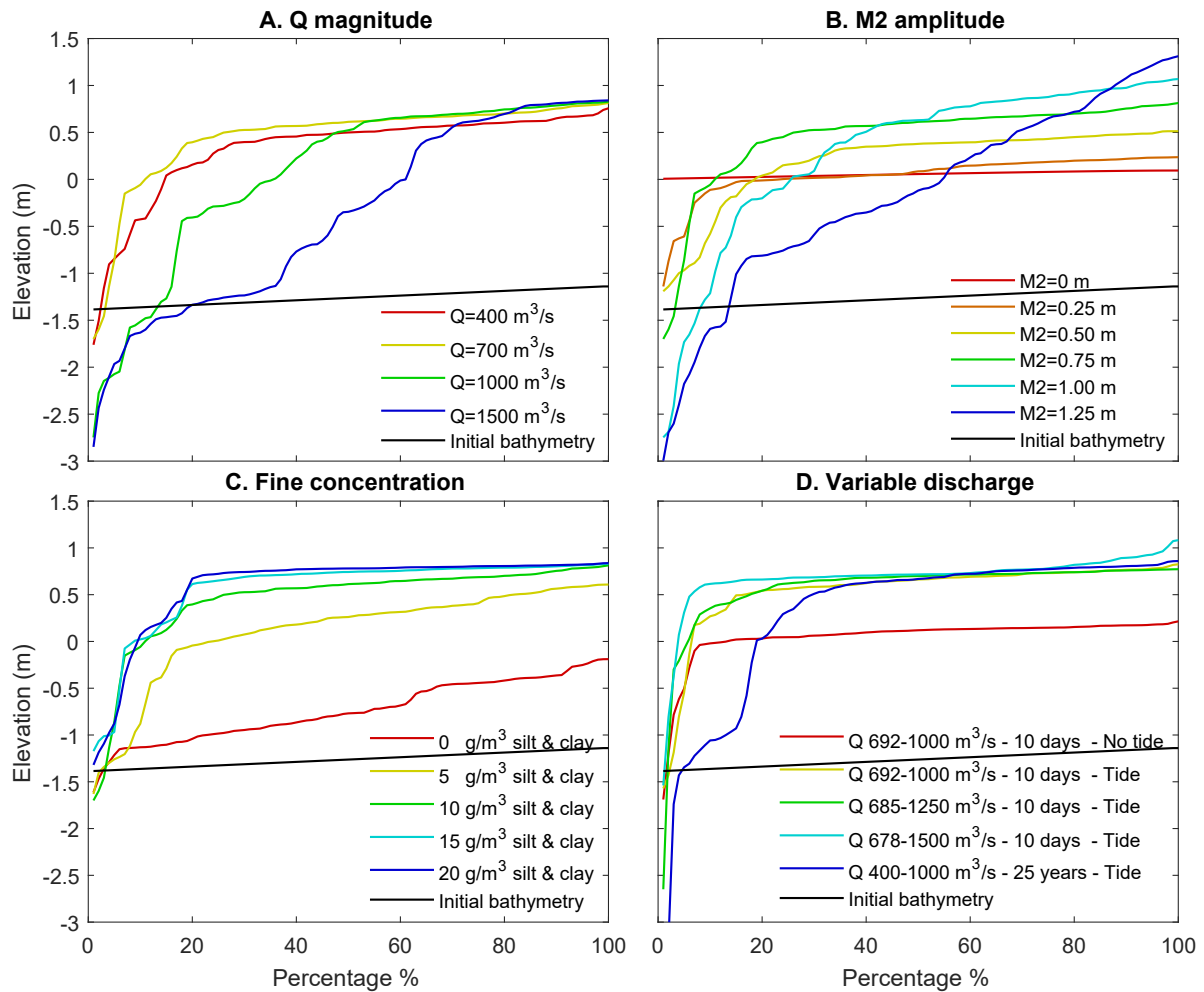


Figure 4.7: Hypsometry of final cross-sectional levee height for different boundary conditions: A. Discharge magnitude, B. Tidal amplitude (M2), C. Concentration of fines (silt and clay), D. Discharge variability.

4.2.2 Maximum water level and maximum levee height

In section 4.2.1 it is suggested that there is a relation between maximum levee height and discharge magnitude, tidal amplitude and concentration of fines. Discharge magnitude and tidal amplitude affect water levels, and according to Filgueira-Rivera et al. (2007) maximum levee height is determined by water levels. To study the nature of the relation between the different fluvial and tidal conditions and levee height in more detail the maximum water levels and final maximum levee height for the different boundary conditions are plotted in Figure 4.8.

For all discharge magnitudes and tidal amplitudes the maximum levee height follows the maximum water level; the maximum levee height is approximately 10-14 cm lower than the maximum water level in the basin resulting in linear correlation coefficients of 0.99 and 1.00 respectively. The approximate difference of 10-14 cm between maximum levee height and maximum water level is a modelling artefact related to the minimum water depth (10 cm) for sediment transport calculations. For the different concentrations of fines the direct linear relation between maximum water level and maximum levee height is absent. For high concentrations of fines (10-20 g/m³ silt and 10-20 g/m³ clay) the difference between maximum water level and maximum levee height is approximately 12 cm. However, for smaller concentrations (0-5 g/m³ silt and 0-5 g/m³ clay) the difference between maximum water level and maximum levee height becomes larger than 12 cm. This results in a lower linear correlation coefficient than in the previous cases. Implying, that if the concentration of fines is lower than a certain threshold the maximum levee height is not necessarily linked to the maximum water level.

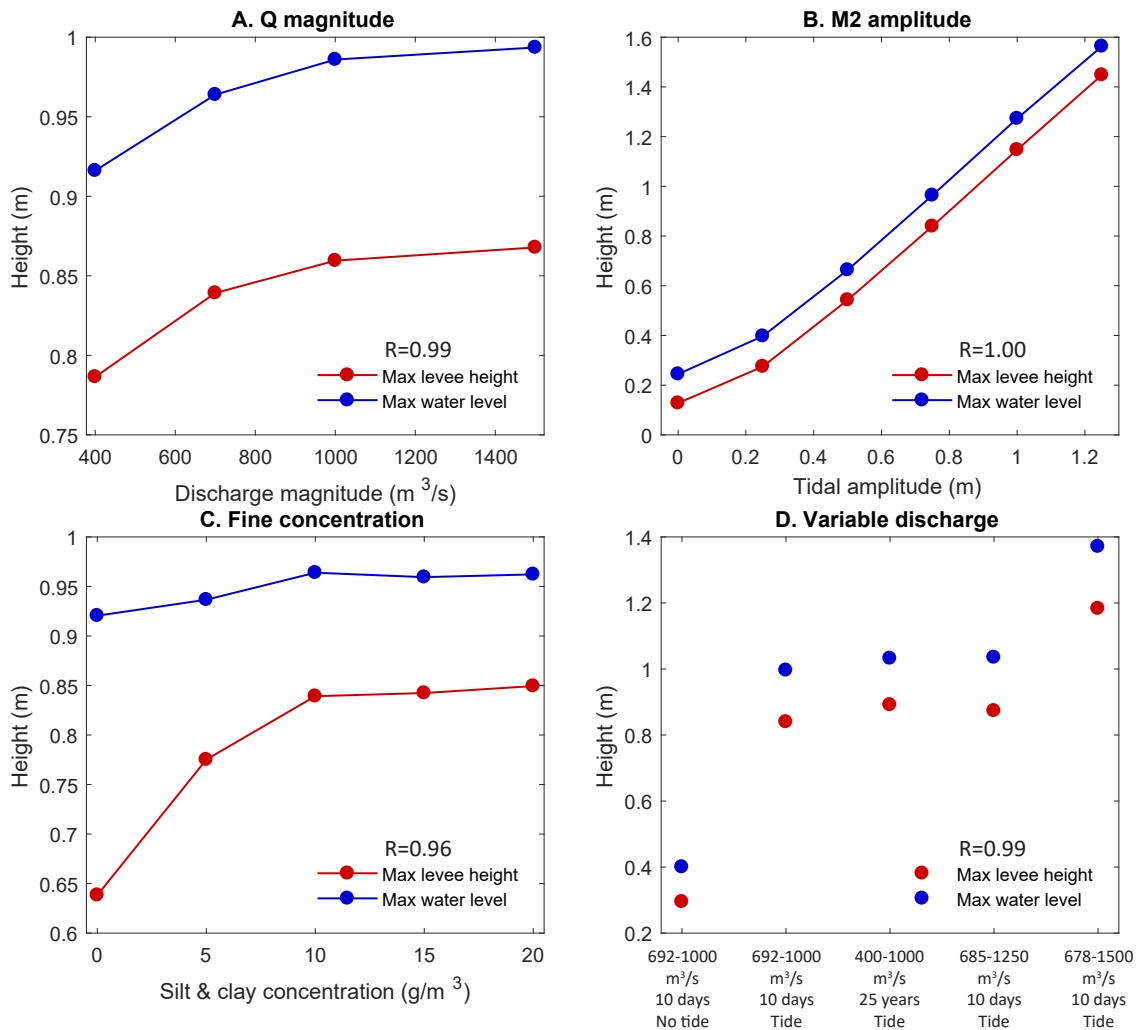


Figure 4.8: Maximum water level and maximum levee height for different parameter groups: A. Discharge magnitude, B. Tidal amplitude (M2), C. Concentration of fines (silt and clay), D. Discharge variability, with the linear relation coefficient for every parameter group. Note: for the discharge variability, the different scenarios are ordered based on the maximum water level. The different variable discharge scenarios are not directly linked, a connecting line between the dots is therefore absent.

When the discharge is variable the maximum levee height approximately follows the maximum water level (see Figure 4.8-D). However, the differences between maximum water level and maximum levee height differs more, between 10 and 19 cm. With larger differences for higher peak discharges. Although the scenarios do not relate to each other the linear correlation coefficient between the maximum water levels and the maximum levee height is 0.99.

4.2.3 Levee width

The definition of a levee in Chapter 2 states that levee deposits are characterised by their lithology and by their elevated position relative to the floodplain. For determining levee width in the model both the lithological and morphological characteristic can be used separately. Below levee width determined by relative height above the floodplain will be used to discuss the influence of different boundary conditions on levee width (4.9). Hereafter, the effect of three different methods on determining levee width will be discussed.

Levee width under different boundary conditions based on elevation above floodplain

The average levee width based on elevation above the floodplain is studied over time (Figure 4.9). The results are again divided along the four boundary conditions; A. discharge magnitude, B. tidal amplitude, C. concentration of fines and D. discharge variability. Before starting with discussing the

results per parameter group one observation can be made for all the boundary conditions; average levee width at timestep one is not zero. From timestep zero to timestep one sediment deposition already occurred in the basin, causing small levees to form. As the average sediment deposition in the basin at the first timestep is also small the resulting levee width is already significant.

Higher fluvial discharges result in wider levees (4.9-A). With a final average width difference of 700 metres between levees formed under the largest and the smallest discharge magnitude. The rate at which the levees widen over time is similar for all four tested discharge magnitudes. Similar statements hold for increasing tidal amplitudes (Figure 4.9-B). Increasing tidal amplitude results in wider levees. Except for the case with a tidal amplitude of 0.75 m, which has less wide levees than the case with a tidal amplitude of 0.5 m. Further, the rates at which width increases are similar. The only exception to this statement is the case without tides, where the growth rate is smaller.

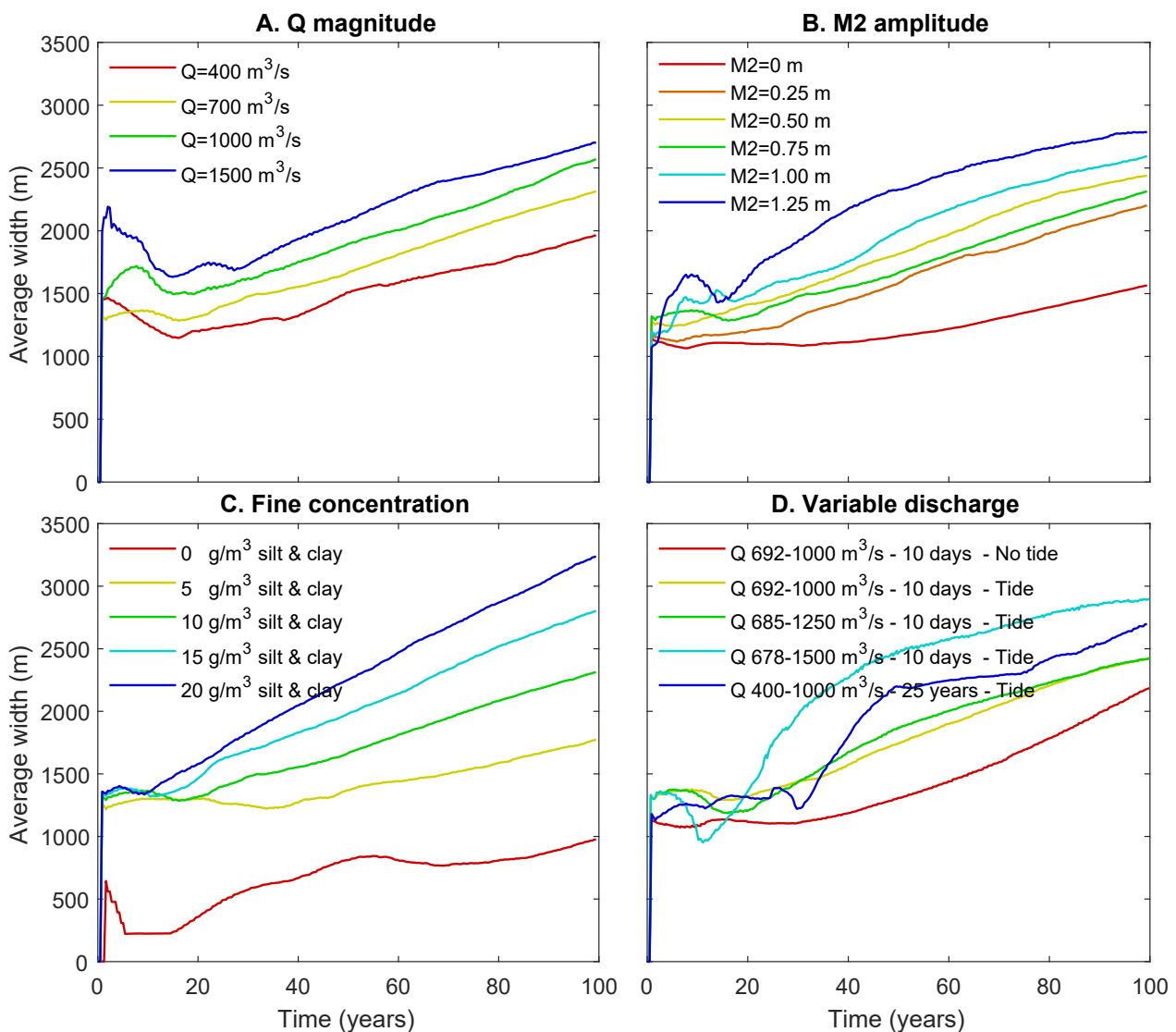


Figure 4.9: Levee width based on baseline for four boundary conditions: A. Discharge magnitude, B. Tidal amplitude (M2), C. Concentration of fines (silt and clay), D. Discharge variability.

When the concentration of fines is increased levee width increases (Figure 4.9-C). The rate at which the width increases becomes larger when the concentration of fines is enlarged. When fines are absent levee width is limited in comparison with the other model set-ups. Even at the first timestep the width is significantly smaller. Showing that levee development is inherently coupled to the presence of finer fractions.

Introducing a variable discharge to the systems results in deviating development of levee width over time (Figure 4.9-D). For cases in which yearly variable discharges were introduced the width development roughly follows the same trend as it does under constant discharges. However, it must be noted that for the largest peak discharge ($1500 \text{ m}^3/\text{s}$) the development of levee width resembles more the development of levee width under a tidal amplitude of 1.25 m. When variability is introduced on a 25 years' time scale, levee width experiences period of increased growth when discharge is enlarged (after 25 and 75 years).

Comparison of three different methods for levee width determination

The discussion on levee definition in Chapter 2 showed that levee width can be determined based on sedimentological and morphological properties. To study the effects of different levee definitions on levee width three methods were used to determine average levee width; 1. height above the floodplain, 2. top view grain size, 3. height above zero water level (see Chapter 3 for description of the methodology). In Figure 4.10 the results of these three different methods are presented for different tidal boundary conditions. It has been chosen to compare the methods based on different tidal boundary conditions as they depicted the differences most pronounced. For the influence of the three methods on levee width under different fluvial discharge magnitudes see Appendix E.

In general the three different methods all show that increasing tidal amplitude results in wider levees (Figure 4.10). However, major differences between the methods can be observed in the evolution of levee width over time, the magnitude of final average levee width and in the evolution of levee width for different tidal boundary conditions relative to each other. To start with the former, the evolution of levee width over time calculated based on the floodplain height shows relatively linear trends (Figure 4.10-A). The evolution of levee width based on top view grain sizes is characterised by a period of rapid increase, a period of rapid decrease and a period of gradual increase for cases with relatively small tidal amplitudes (Figure 4.10-B). This pattern can be explained based on the top view grain size itself (see Figure 4.11). After approximately 18 years (depending on the model setting), clay is deposited on top of former silty levee deposits, resulting in a less wide levee classification. Levee width over time based on height above the zero water level depicts non-linear trends with an increasing slope for smaller tidal amplitudes ($M2=0-0.5 \text{ m}$) and a decreasing slope for larger tidal amplitudes ($M2=0.75-1.25 \text{ m}$) (Figure 4.10-C).

The range in final average levee width is similar when the *floodplain height* and *top view grain size* method are used. Final average width for these methods ranges between 1500 and 3000 metres. Final average levee width calculated based on the *zero water level* ranges between 600 and 2500 metres. The width based on this method is relatively smaller as it only accounts for the terrestrial part of the levee, whereas the other methods also account for the submerged part of the levee.

Despite the similar range of final average levee width of the *floodplain height* and *top view grain size* method, levee width is different when the individual model runs are studied. Levee width, based on floodplain height, increases when tidal amplitude increases except for one run. On the other hand, levee width based on top view grain size becomes larger when tidal amplitude ($M2$) is increased from 0 m to 0.5 m and smaller when tidal amplitude is further increased from 0.75 m to 1.25 m. This is probably due to the hindering of deposition of fine material by strong tidal flows.

Note that when the three methods are compared based on fluvial boundary conditions the differences become smaller (see Appendix E). Indicating that the method chosen to determine levee width is especially important in cases where tidal boundary conditions changed. Further, it is interesting that in the levee width evolution based on top view grain size, wiggles can be observed. These wiggles are again caused by the combination of the tidal signal and morphological acceleration factor of the model. They are only visible for the method based on top view grain size as strong tidal flows greatly influence the deposition of fines.

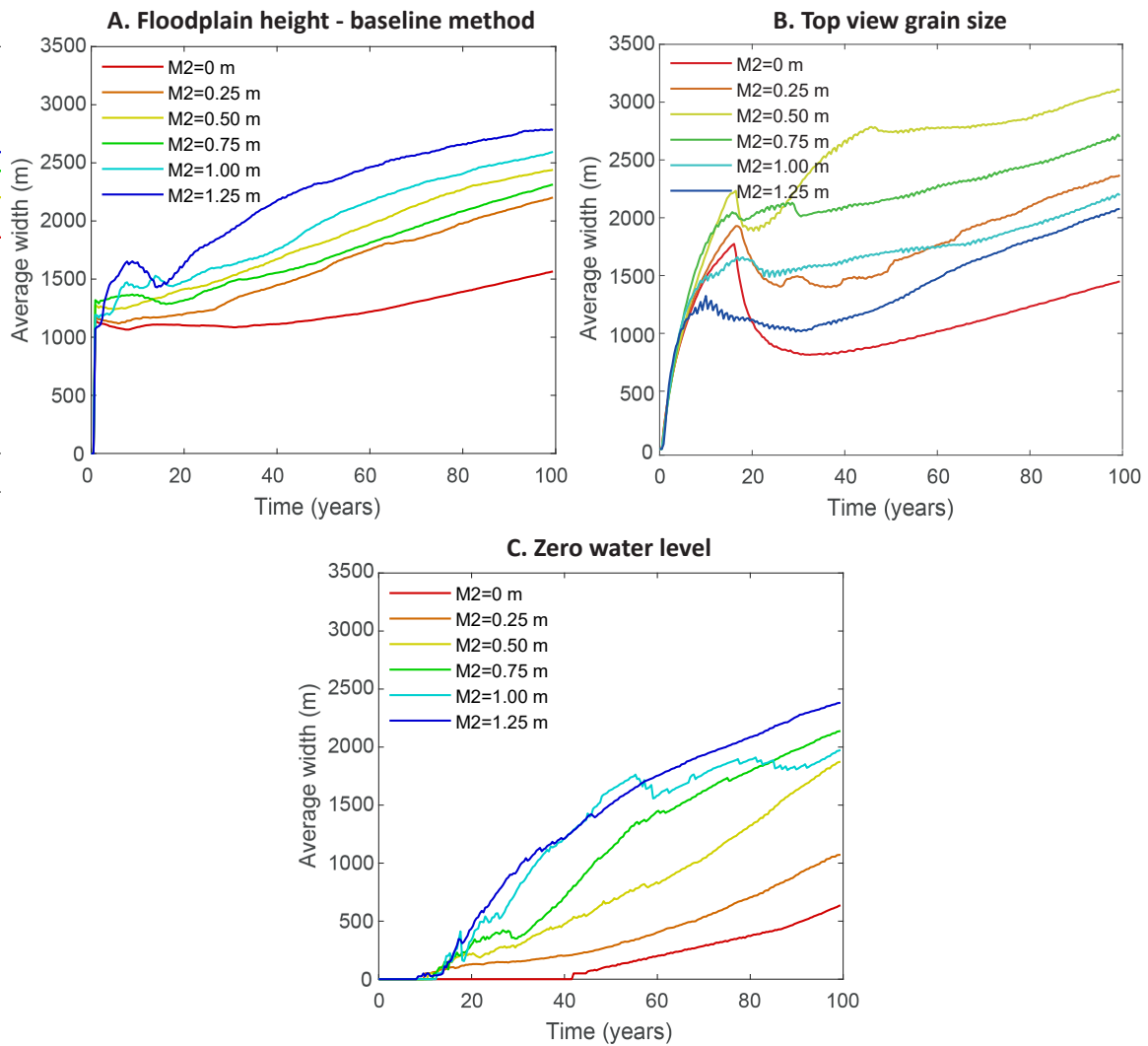


Figure 4.10: Average levee width for different tidal amplitudes over time calculated based on three different methods; A. floodplain height, B. top view grain size, C. zero water level.

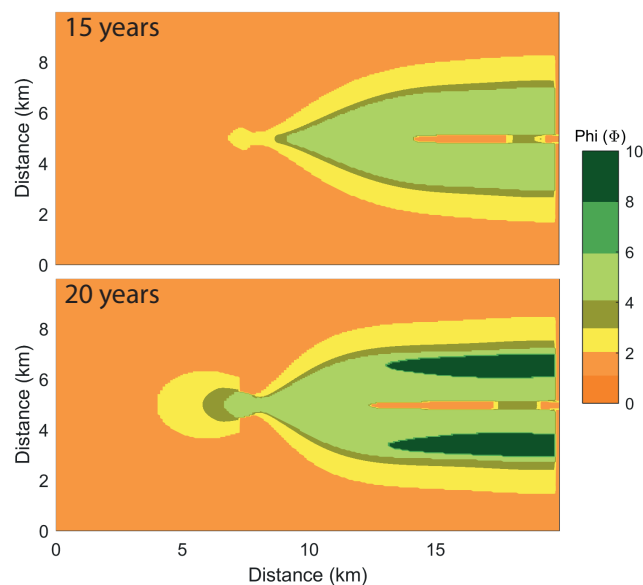


Figure 4.11: Top view average grainsize for model 018 with a constant discharge ($700 \text{ m}^3/\text{s}$) and no tides, for two timesteps (15 and 25 years).

4.2.4 Crevasse dimensions

Crevasse channels dissecting the levees can be characterized by their cross-sectional area. For the different boundary conditions the total cross-sectional crevasse area is plotted (Figure 4.12). The total cross-sectional crevasse area is based on all the crevasses dissecting the levee in the fluvial dominated part of the basin (upper 5 km). Below the evolution of the cross-sectional crevasse areas per boundary condition are discussed.

In general the maximum and final cross-sectional crevasse area is larger for larger discharge magnitudes (Figure 4.12-A). The only exception is the extreme discharge magnitude case ($1500 \text{ m}^3/\text{s}$). The reason for a lower cross-sectional crevasse area in the case of an extreme discharge can be found in the bathymetric results of this model run (see Appendix D - Q magnitude, model 014). The bathymetry in the middle of the basin deviates from the rest of the runs; it resembles one very wide and shallow crevasse channel. This channel is not recognised as a crevasse channel, causing the total crevasse cross-sectional area to decrease for this run. Furthermore, for all discharge magnitudes the total cross-sectional crevasse area first increases where after it starts to decrease, suggesting infilling of the channels (Figure 4.12-A). Ultimately, the cross-sectional area starts to stabilize, which is clear for the cases with discharge magnitudes of 400 and $700 \text{ m}^3/\text{s}$ but less for the models with larger discharges.

A larger tidal amplitude also results in a larger final cross-sectional crevasse area (Figure 4.12-B). The evolution of the cross-sectional crevasse area under different tidal amplitudes can be split into two groups; 1. tidal amplitudes that first allow the crevasse area to grow where after it decreases and the crevasses silt up (Figure 4.12-B, $M2=0-0.75 \text{ m}$), and 2. tidal amplitudes that allow the crevasse area to grow and continue to grow (Figure 4.12-B, $M2=1.00-1.25 \text{ m}$). Apparently, when tides are large enough the tidal flows are able to keep the crevasses open and even to let them grow.

Larger concentrations of fines cause the maximum cross-sectional crevasse area to increase (Figure 4.12-C). On the other hand, the final cross-sectional area does not seem to be dependent on the concentration of fines as the final area is very similar for different concentrations. Only the absence of fines results in a $\sim 80\%$ reduce of the final cross-sectional crevasse area. The growth of the cross-sectional crevasse area is fastest for the highest concentrations. However, the crevasses formed under higher concentrations of fines also start to silt-up earlier. It could be hypothesised that the larger initial cross-sectional area under larger concentrations of fines is caused by a more effective focussing of the flow, due to a decrease in bank erodibility, and therefore deepening of the crevasse channels.

Yearly variability in discharge also influences the cross-sectional crevasse area. Studying the trends for yearly variations, a peak discharge of $1000 \text{ m}^3/\text{s}$ in combination with the absence of tides results in the largest maximum cross-sectional crevasse area. For this case the cross-sectional crevasse area grows rapidly after which it starts to decrease and stabilises. When tides are introduced the maximum and final cross-sectional crevasse area decrease. When peak discharges are higher the final cross-sectional crevasse area becomes smaller. When variations in discharge occur on a scale of 25 years the cross-sectional crevasse area evolves different. With periods of rapid change during periods of higher discharge.

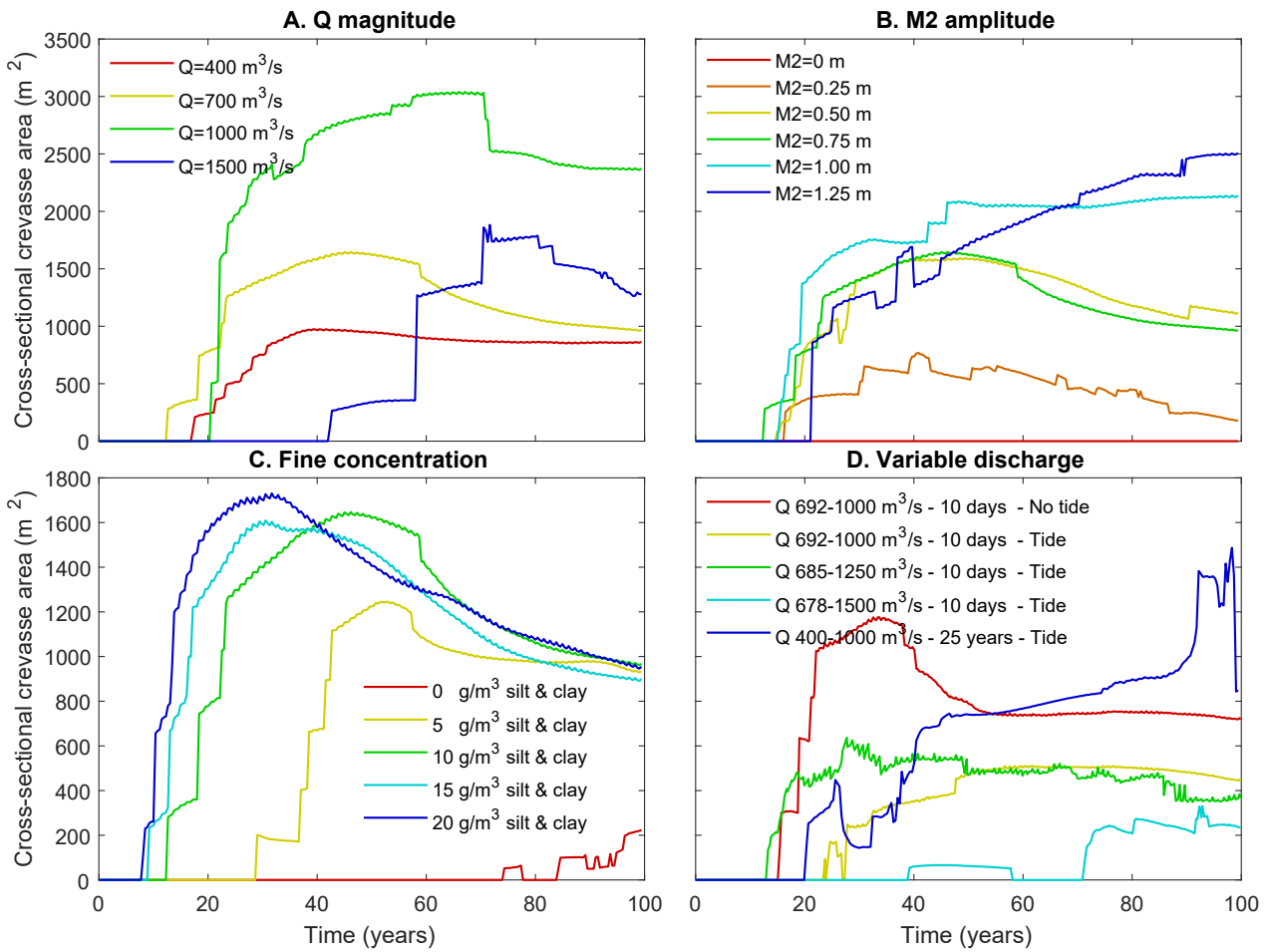


Figure 4.12: Cross-sectional crevasse area over time for different parameter groups: A. Discharge magnitude, B. Tidal amplitude (M2), C. Concentration of fines (silt and clay), D. Discharge variability.

4.3 Role of levee evolution on hydrodynamics & basin infilling

To understand the role of levee formation in the development of tidal basins, the infilling of these basins must be studied over time under different boundary conditions. In this chapter this is done in two ways. By studying the location along the main channel where ebb velocity is larger than flood velocity over time (Figure 4.13), and by studying the infilling of the basin through the area above and below mean water level over time (Figure 4.14).

At the first time step the location where ebb flow velocity is larger than flood flow velocity (from now on *the point of ebb dominance*) is located further downstream for model set-ups which are relatively more fluvial dominant. Thus, larger discharges shift the point of ebb dominance further downstream as well as smaller tidal amplitudes (Figure 4.13-A,B). Relatively smaller fluvial discharges and larger tidal amplitudes have the reverse effect. They result in an upstream shift of the point of ebb dominance. Higher concentrations of fines cause a downstream shift of the point of ebb dominance (Figure 4.13-C). Also, the rate at which the point of ebb dominance shifts seawards is higher for larger concentrations. Indicating that fluvial flow is better focussed. The effect of variable discharges on the location of the point of ebb dominance remains unclear due to noise in the data created by the variable discharge (Figure 4.13-D). Note that the steps in the graphs are a result of the combination between the timestep of data saving, the morphological acceleration factor (MorFFac) and the tidal cycle.

To quantify the infilling of the basin over time for the different boundary conditions the area above and below zero are studied. This area is normalised by dividing it by the initial maximum basin volume determined by the maximum water level and the initial bathymetry of the basin, including the initial river channel. Normalisation had to be applied as different maximum water levels and different channel dimensions result in different accommodation space volumes and therefore a different pace of infilling. As a result, the normalised area below zero in Figure 4.14 (left column) at $T=0$ years is not equal for the different discharge magnitude runs (Figure 4.14-A) and for different tidal amplitudes (Figure 4.14-B). For all model set-ups the change in the tidal part of the basin is minimal. Largest changes in this zone occur when tidal amplitude is increased (Figure 4.14-B). An increase in tidal amplitude causes an increase in area above zero in the tidal part of the basin for all time steps. An increase in fluvial discharge, which is linked to decreasing the tidal dominance in the basin, has the opposite effect. Increasing the discharge results in a decrease in area above zero in the tidal part of the basin.

In the fluvial part of the basin changes are more significant, with larger increases in area above zero over time. An increase in fluvial discharge increases the normalized area above zero for all time steps. The increase in area is however not linearly related to the discharge magnitude (Figure 4.14-A), as an increase from $400 \text{ m}^3/\text{s}$ to $700 \text{ m}^3/\text{s}$ is more effective than an increase from $1000 \text{ m}^3/\text{s}$ to $1500 \text{ m}^3/\text{s}$. The same counts for an increase in the concentration of fines (Figure 4.14-C). Increasing the tidal amplitude has a more complex influence on the normalized area above zero in the fluvial part of the basin over time (Figure 4.14-B). When increasing the tidal amplitude (M_2) from 0 m to 0.5 m the normalized area above zero increases as well for all time steps. Increasing the tidal amplitude further to 0.75 and 1 m, results in a decrease in the final area above zero. Even further increasing the tidal amplitude, this time up to 1.25 m, has an increase in final area above zero as result in respect to the 1.0 m tidal amplitude case. This trend could indicate that there is an equilibrium area above zero in the fluvial domain around which the results slightly vary. The model set-ups with variable discharges (Figure 4.14-D) show the following results: Larger peak discharges result in an increase in the normalized area above zero and the absence of tides results in a highly significant decrease in the normalized area above zero in the fluvial part of the basin. Summarizing, tides highly influence the distribution of sediment in the basin and larger fluvial discharges provide extra sediment into the basin.

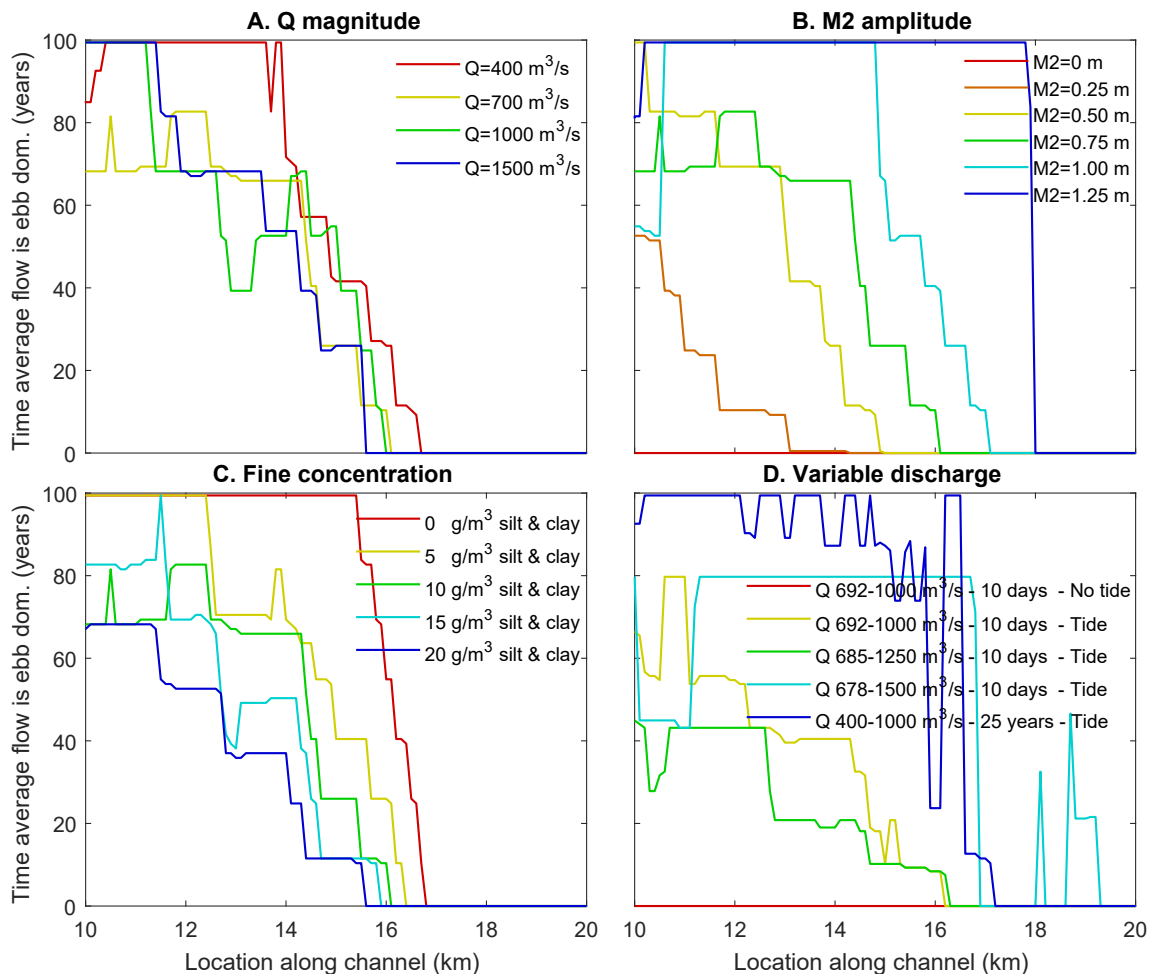


Figure 4.13: Time it takes for the peak ebb flow velocity to become larger than flood flow velocity for every location in the main channel for different parameter groups: A. Discharge magnitude, B. Tidal amplitude (M2), C. Concentration of fines (silt and clay), D. Discharge variability

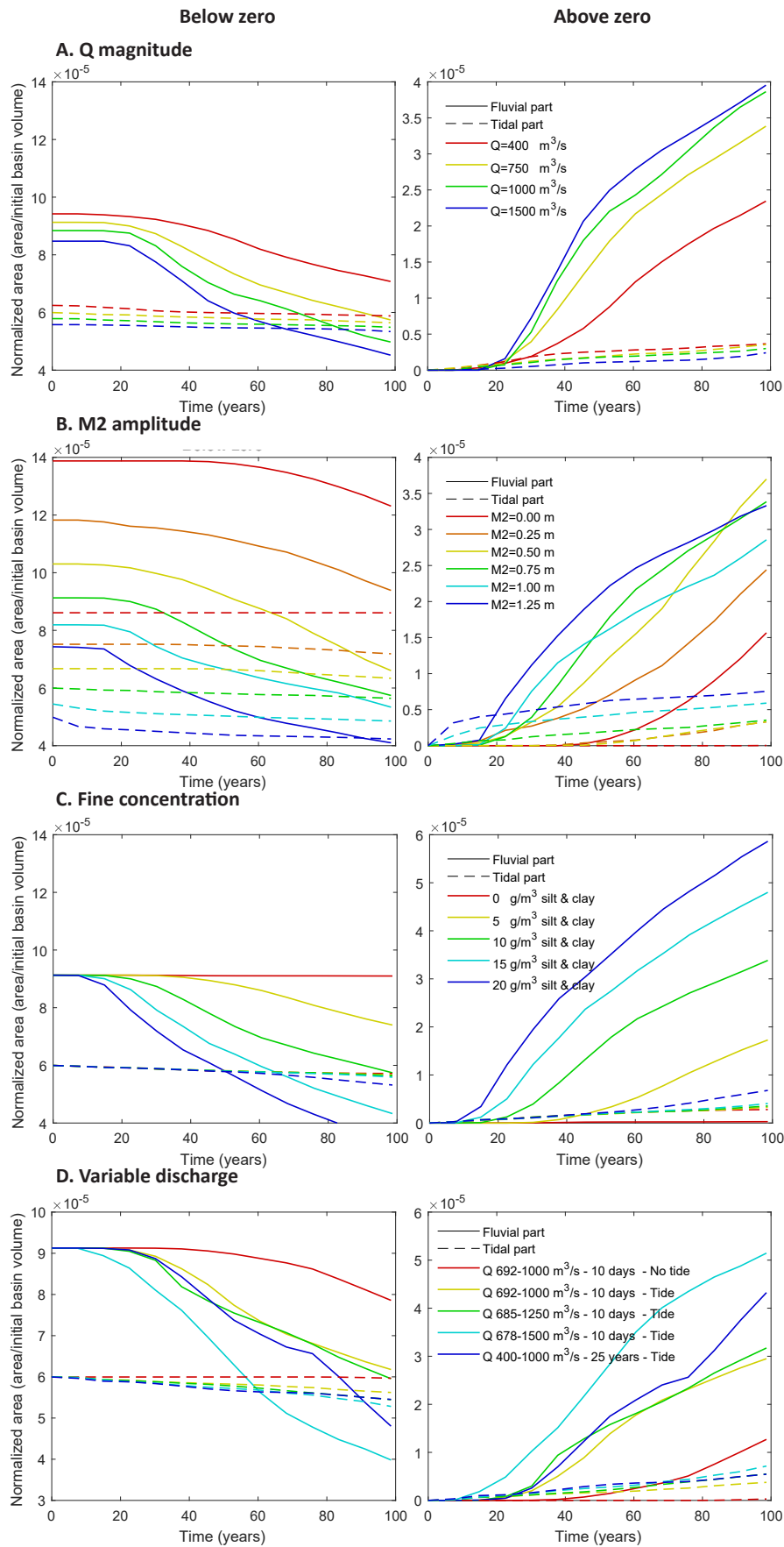


Figure 4.14: Normalised area above and below mean water level (0 m) over time for different parameter groups: A. Discharge magnitude, B. Tidal amplitude (M2), C. Concentration of fines (silt and clay), D. Discharge variability. Area is normalized with the initial basin volume below mean water level (0 m).

4.4 Levee stratigraphy and sedimentology

The set-up of the boundary conditions has a significant influence on the sedimentological and morphological development of levees resulting in varying stratigraphies. To determine the main trends and characteristics in stratigraphical development of levees under different boundary conditions lithological cross-sections are created for the key models depicted in Figure 4.1 at 18 km. For every key run a figure is created showing the D_{50} grain size, percentage silt and very fine sand, and percentage clay. An overview of the main conditions and figure numbers is given in Table 4.1. Below the main trends and characteristics in levee stratigraphy will be discussed.

Table 4.1: Overview of key models with their key conditions and corresponding stratigraphy figures.

Model nr.	Q mag. (m ³ /s)	Tidal amp. M2-M4 (m)	Conc. fine c-s (g/m ³)	Q variability	Figure nr.
018	700	0-0	10-10	-	4.15
034	692-1000	0-0	10-10	Peak 10 days	4.16
023	700	0.25-0.025	10-10	-	4.17
012	700	0.75-0.075	10-10	-	4.18
019	700	0.75-0.075	5-5	-	4.19

The main trends and varying characteristics in levee and basin stratigraphy resulting from different model set-ups can best be described in two themes; 1. levee composition and build up, 2. floodplain stratigraphy. Starting with 1. *levee composition and build up*; In general, all levees are built up from silt and very fine sand ($\Phi=3-8$). In model set-ups without tides or with a small tidal amplitude a layer of clay ($\Phi=8-10$) can be recognised within the silty levee deposits (Figures 4.15, 4.16, 4.17). This layer is clearly visible in the cross-section visualizing percentage of clay. In the models without tides or with a small tidal amplitude, clay can also be found towards the edges of the domain forming a layer of floodplain deposits up to 40 cm in thickness.

Cross-sections of models with a larger tidal amplitude do not portray the clay layer described above (Figures 4.18, 4.19). Despite the lack of representation of clay in the D_{50} analysis, clay is not absent in the stratigraphy of these models. When studying the percentage of clay in further detail, one can recognise layers that consist of 30% to 40% clay. In Figure 4.18 a thick layer of relatively high clay content can be found on top of the initial basin floor at 2-4 and 6-8 km. A relatively smaller sloping clay rich layer can be recognised in the same profile a bit closer to the main channel. In the model with a smaller clay and silt concentration (Figure 4.19) this sloping clay rich layer is absent. For both cases with larger tidal amplitudes (Figures 4.18, 4.19) floodplain deposits are absent.

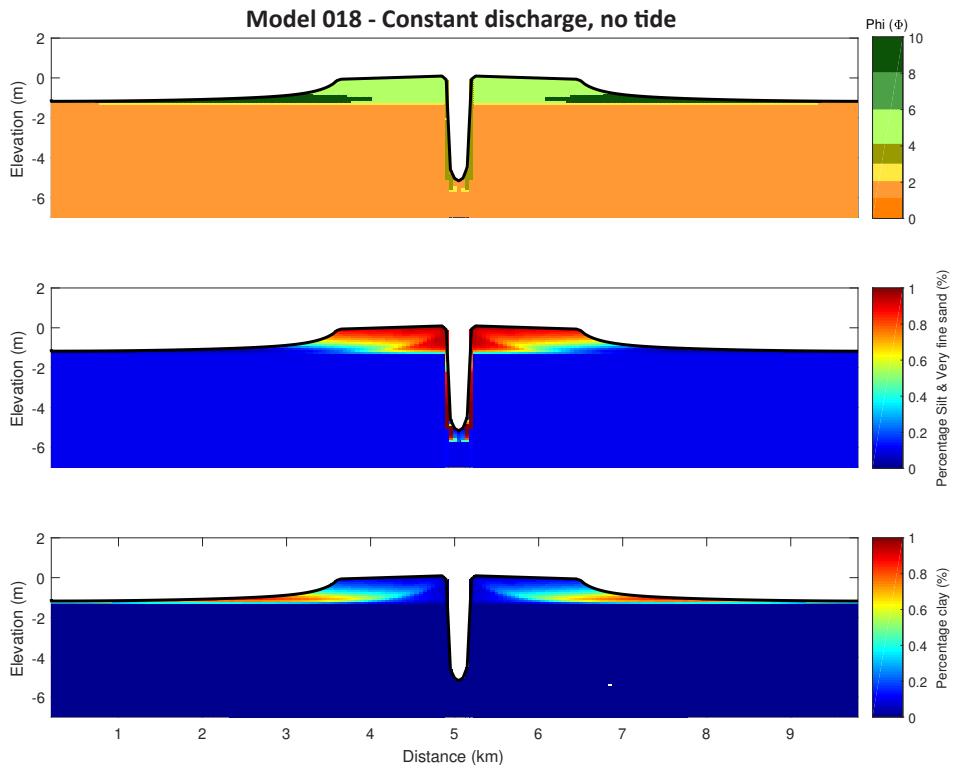


Figure 4.15: Final cross-section of a model with constant discharge without tides (model 018) at 18.3 km showing D50 grainsize (top), percentage silt and very fine sand (middle) and percentage clay (bottom)

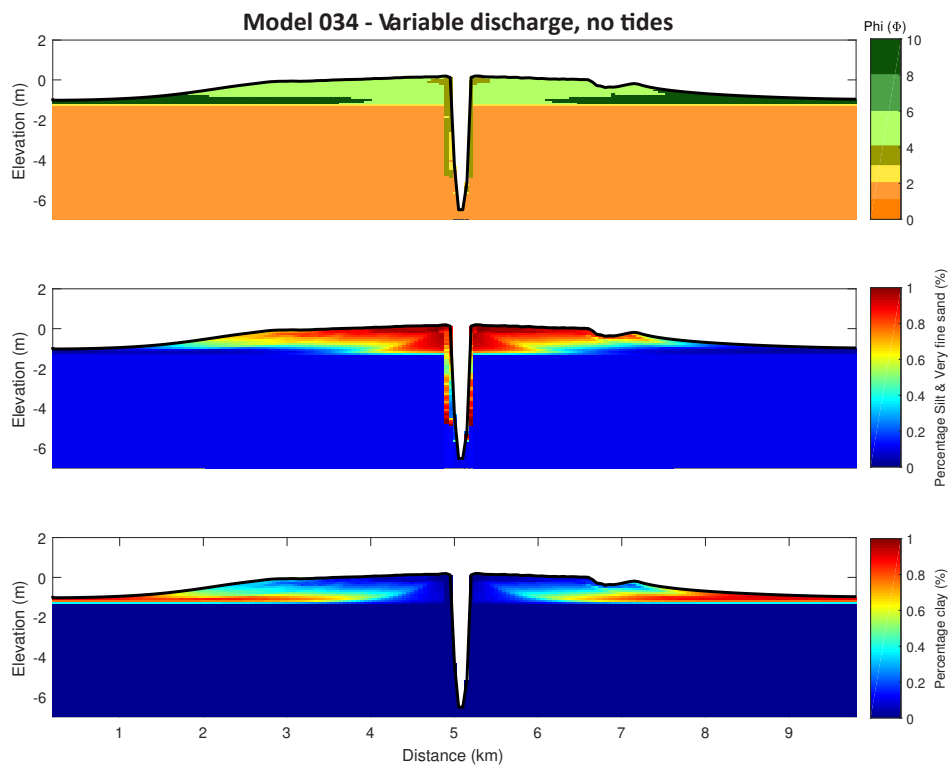


Figure 4.16: Final cross-section of a model with variable discharge without tides (model 034) at 18.3 km showing D50 grainsize (top), percentage silt and very fine sand (middle) and percentage clay (bottom)

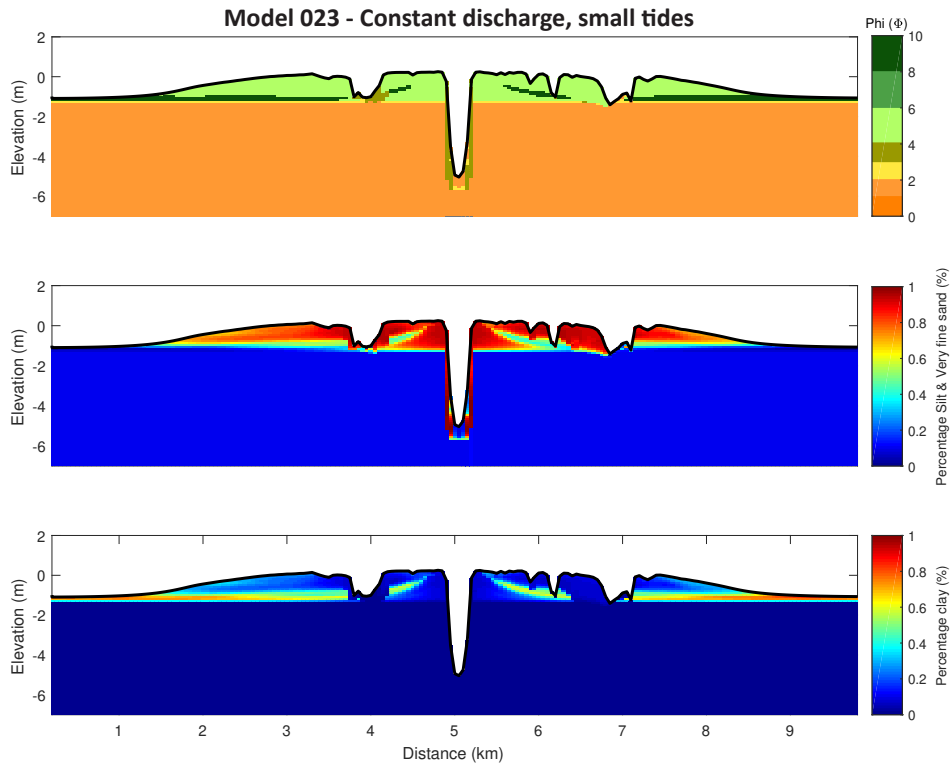


Figure 4.17: Final cross-section of a model with a constant discharge and small tides (model 023) at 18.3 km showing D50 grainsize (top), percentage silt and very fine sand (middle) and percentage clay (bottom)

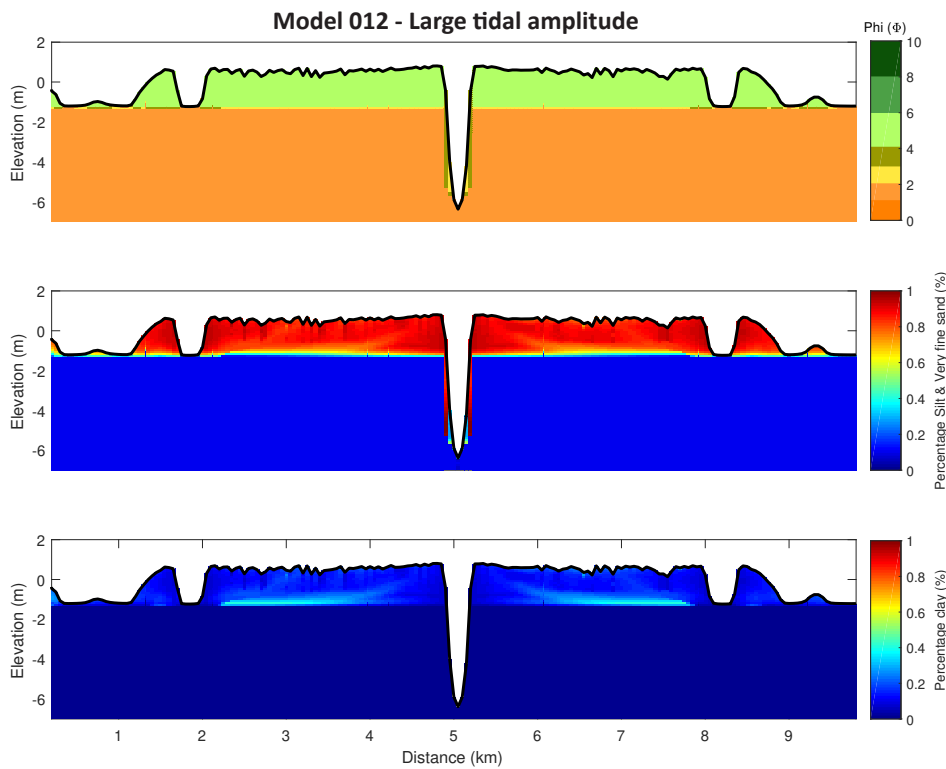


Figure 4.18: Final cross-section of a model with a constant discharge and large tidal amplitude (model 012) at 18.3 km showing D50 grainsize (top), percentage silt and very fine sand (middle) and percentage clay (bottom)

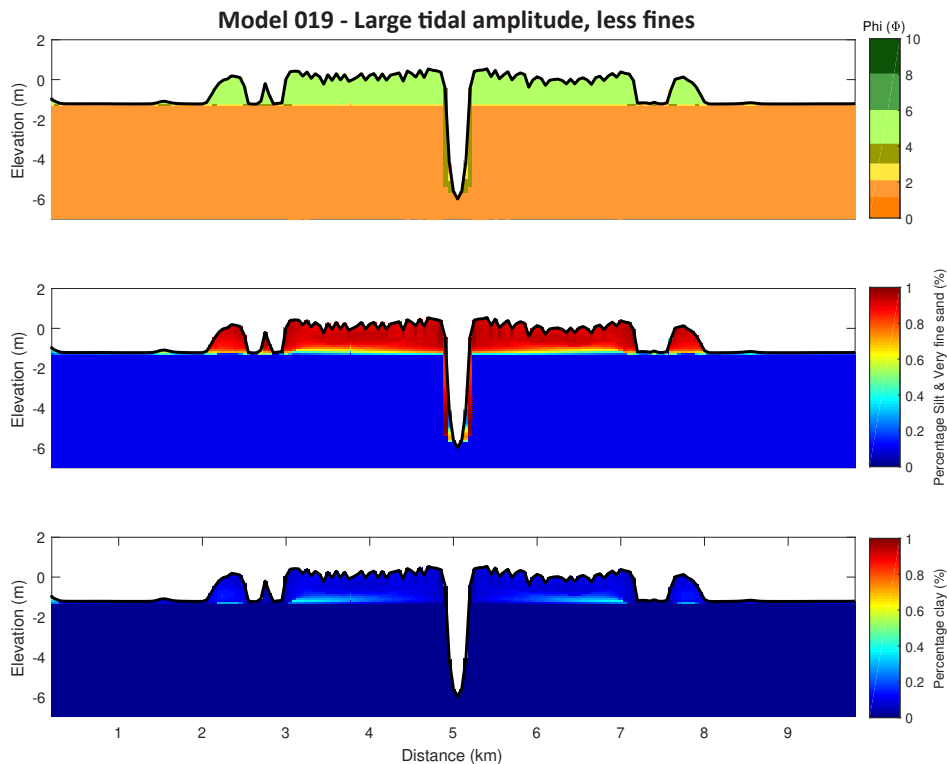


Figure 4.19: Final cross-section of a model with constant discharge large tidal amplitude and with less fines (model 019) at 18.3 km showing D50 grainsize (top), percentage silt and very fine sand (middle) and percentage clay (bottom)

To further quantify the sedimentary composition of the different levees the final lithology of every cell in the levees of model 018, model 034, model 023 and model 012 is plotted in lithological triangles (see Figure 4.20). These four models represent four distinct boundary condition set-ups and therefore give insight in the effects of these different conditions on levee lithology. Figure 4.20 shows that the levee lithology of model 018, model 034 and model 023 are rather similar and that the lithology of model 012, with a large tidal amplitude ($M_2=0.75$ m), deviates. In the models where levee evolution is dominated by fluvial flow (Figure 4.20-A,B,C), the levee lithology in general has a wide distribution ranging from sandy silt to almost pure clay. When tides dominate levee evolution (Figure 4.20), levee lithology has a narrow distribution dominated by silt. It is interesting to note that the presence or absence of fluvial discharge fluctuations does not seem to influence levee lithology much (Figure 4.20-A,B). The one notable difference is that in the levees formed under fluctuating discharges a bit more sandy material is present than in levees formed under a constant fluvial discharge. The introduction of a small amount of tidal energy into the basin results in a small shift in lithology (Figure 4.20-C), with less clayey material in the levees than in the levees that are purely influenced by fluvial processes.

The effects of tidal amplitude on levee lithology are further analysed in Appendix F. The lithological triangles in this appendix show that when tidal amplitude of the M_2 constituent is increased from 0 m to 0.75 m the distribution in lithologies becomes smaller and more clayey material is lost. When tidal amplitude is increased further up to 1.0 m and 1.25 m the distribution in lithology becomes wider again as more sandy material is trapped in the levee-crevasse complex.

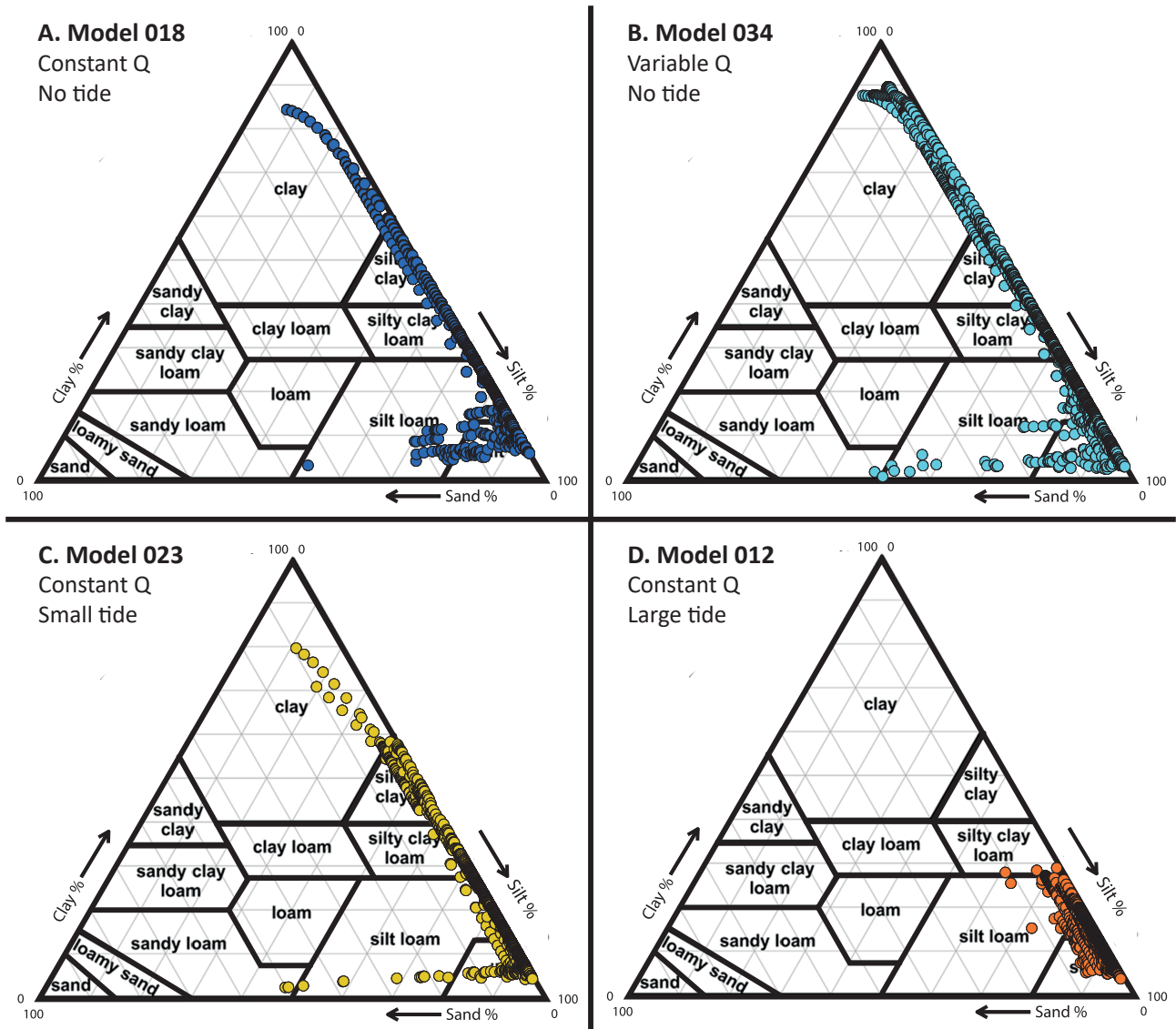


Figure 4.20: Lithology of levees at 18 km for four distinct set-ups depicted in the lithological triangle of Bakker and Schelling (1966) adjusted by Berendsen (2005). A. Model 018, constant fluvial discharge without tides; B. Model 034, variable fluvial discharge without tides; C. Model 023, constant fluvial discharge with small tides ($M_2=0.25$ m); D. Model 012, constant fluvial discharge with large tides ($M_2=0.75$ m).

4.5 Field results - Cross-sections and grain size analysis

The levees along the Old Rhine river system were studied at three locations, from more upstream to downstream, as described in Chapter 3. They were studied based on lithological and sedimentological observations in the field and in more detail by grain size analysis in the lab. First, the results of the sedimentological and lithological observations will be discussed based on cross-sections from up- to downstream (see Appendix H for the borelogs). Hereafter, the longitudinal connectivity between these profiles will be elaborated on. At last, the results of the detailed grain size analysis will be presented.

4.5.1 Old Rhine levee cross-sections

Location 1: Upstream

As previous studies by Stouthamer (2005) and Van Asselen (2010) created detailed sedimentological cross-sections at the upstream location of our fieldwork we are partly using their results (see Figure 2.9 and Figure 4.21 for adjusted version). The deposits presented in Figure 4.21 can be divided into a large body of channel belt deposit on the southern side, overbank deposits consisting of levee and floodplain deposits located next to the channel, and peat deposits distal of the channel belt. The overbank deposits are separated by peat layers, indicating multiple phases of overbank deposition. Stouthamer (2005) couples these phases to upstream channel belts, as described in section 2.5. To temporarily remove the morphogenetic interpretation by Stouthamer (2005), the phases are renamed in section 2.5 based on their relative position. Below the phases in overbank deposits in the cross-section of Figure 4.21 will be described.

At the lowest stratigraphical location (-7 to -5.5 m below NAP), two small layers of overbank deposits can be recognised north of the channel body, separated by a layer of peat (see 4.21, phase 1). These small overbank deposits are seen as the starting of the Old Rhine river system and are therefore estimated to be formed approximately 6000 yr. BP. The layers are 20 and 30 cm in thickness, consist of clay loam, humic clay and clay, and have an extent of 150-200 meters seen from the channel body to the peat deposits. Higher up in the stratigraphical record (-5.2 below NAP) the beginning of a period of larger scale overbank deposition can be recognised (see 4.21, phase 2). Based on datings of Stouthamer (2005) and Van Asselen (2010) these sediments were deposited between approximately 4000 and 2800 yr. BP. The coarser material (loam and clay loam) of this phase is being interpreted as proximal levee deposits and the finer material (clay) being interpreted as distal levee and floodplain deposits. The body of overbank deposits from this phase is approximately 3 meters thick and reaches into the peat for 200 m to 1000 m counted from the channel body. The overbank deposits of this phase start out with a limited reach into the peat of 200 m, where after the deposits start to have a larger reach into the peat, up to 1 km. The distal floodplain deposits of this phase are covered with peat, whereas the more proximal levee deposit seem to continue to higher stratigraphical levels next to the channel body. Succeeding, is the last phase of large-scale overbank deposition (see 4.21, phase 3), with an approximate age between 2700 and 2900 years Stouthamer (2005); Van Asselen (2010). Again, consisting of coarser proximal levee deposits and distal levee and floodplain deposits. The body of overbank deposits of this phase has a thickness varying between 2 meters proximal to the channel and 0.5 meters distal to the channel. Lithology is characterised by loam, clay loam and clay. The deposits reach out far into the floodplain, beyond the drawing (>1200 m).

Location 2: Middle

At location 2 (for location see Figure 3.3), a cross-section is constructed based on three borings on a southwest-northeast transect (Figure 3.4). On the southwestern side of the transect the current channel of the Old Rhine is located. In the sedimentological cross-section three phases of overbank deposits can be recognised (Figure 4.22).

At a depth of 6.5 m below NAP, at boring 20180109 a 30 cm thick layer or lens of more clastic deposits

is present in between humic clays that overlay older tidal deposits (Figure 4.22-A). These clastic deposits are interpreted as overbank deposits related to the starting phase of the Old Rhine and are therefore approximately 6000 years old (Figure 4.22-B). The elevation of these deposits, as well as its stratigraphical position are similar to the thin overbank deposits that are correlated to the starting of the Old Rhine at the most upstream location. Both are located around 6.5 meters below NAP and succeed a peat layer covering older deposits. Thereby, the lithology of the layer at this location is similar to the lithology of the layer at the most upstream location. Based on these arguments the thin layer of overbank deposits on this location is named phase 1 (Figure 4.22-B). The inherited tidal deposits from the mid Holocene in this cross-section show a topographic low at the location of boring 20180109, which is interpreted as a former tidal channel.

Higher up in the stratigraphy at boring 20180109, above a layer of compacted peat (-5.8 m NAP), 3.3 m thick clastic deposits are present (Figure 4.22-A). Based on the lithological composition, extent and location of the deposits it is interpreted as a crevasse channel succeeded by a levee (Figure 4.22-B). From -5.8 m NAP till -4.2 m NAP the deposits consist mainly of layered loam and sandy loam with a large amount of plant remains. The width of this body is very limited, as it is only found in one boring, within the topographical low of the former tidal surface (Figure 4.22-A). Moving upwards in the cross-section (from -4.2 to -2.5 m NAP), the location of the coarse deposits shifts to the southwest, in the direction of the main channel, whereas at a similar depth above the former crevasse channel clay deposits are found. The coarser deposits at a depth ranging from -4.2 to -2.5 m NAP, in boring 20180110, consist again of layered loam and sandy loam (Figure 4.22-A). However, the amount of plant remains decreased drastically in comparison with the crevasse deposits at deeper depths. The total extent of these overbank deposits is larger than the lower loamy deposits. Including clay, the overbank deposits reach 300 m into the floodplain seen from the residual channel. The lithological composition, extent and the location next to the residual channel of this body of sediment is results in this body being classified as a levee. Based on the co-evolution of levees and crevasses in the numerical modelling part of this thesis (chapter 4.1, it can be assumed that the crevasse (5.8-4.2 m -NAP) and levee deposit (4.2-2.3 m -NAP) are of approximately the same age. The crevasse deposits are slightly older but were succeeded quickly by the levee deposits, as can be concluded from the absence of peat and/or organic clay layers.

The elevation of the crevasse-levee deposit relative to NAP (5.8-2.5 m below NAP) corresponds to the second overbank phase at the most upstream location (5.2-2.0 m below NAP). The stratigraphical position is similar as well; above a layer of peat that succeeds the first clastic deposits of the Old Rhine and below a layer of peat underneath the last phase of clastic deposits. Additionally, the lithology of the sediments is similar as well. Both sedimentary bodies consist of loamy texture classes. Based on these arguments it can be assumed that the crevasse-levee deposits belong to phase 2 (Figure 4.22-B) and were deposited between approximately 4000 and 2800 yr. BP.

Above the relatively coarse clastic deposits of phase 2, a layer of peat is located that thins towards the main channel. Succeeding the peat is another phase of overbank deposits that is interpreted as distal levee deposits transitioning into floodplain deposits (Figure 4.22-B). The overbank deposits from this phase consist of silty clay and clay and have a reach that extends beyond the profile (>400 m) (Figure 4.22-A). The elevation of these deposits as well as the stratigraphical position corresponds to the third overbank phase at the most upstream location. Both phases start at an elevation of 2 metres below NAP and are the last clastic deposits along the Old Rhine, succeeding a thin layer of peat. It can therefore be assumed that the clastic deposits, between -2 and -1 m NAP in this cross-section belong to phase 3 (Figure 4.22-B). Therefore, they have an estimated age between 2700 and 2900 years.

Location 3: Downstream

At location 3 a cross-section is constructed based on five borings on a southwest-northeast transect (Figure 3.3 and Figure 3.4). On the northeast side of the transect the current channel of the Old Rhine is located (Figure 3.4). In the cross-section only one phase of overbank deposits can be recognised together with a large channel body below the levee (Figure 4.23). Below the cross-sectional sedimentology and stratigraphy will be described.

On the northeastern side of the transect at a depth of -6 up to -3.5 m NAP a body channel belt deposits are present consisting of coarse sand (Figure 4.23). On the southwestern side of this channel body, at the same depth, older tidal deposits are located. Pointbar sediments were deposited on top of the channel body, consisting of layered sandy loam and sandy clay loam. Succeeding the pointbar deposits are levee deposits consisting of loamy material proximal to the channel and consisting of clay loam at the more distal locations. Note that pointbar deposits gradually grade into levee deposits which makes it hard to distinguish them. On the southwest in the cross-section the levee deposits lay on top of a meter-thick peat layer. Overall the overbank deposits in this cross-section have a thickness varying between 2.5 and 1 m. It must be noted that at the location of profile a 30 cm thick clay layer was excavated in the early and mid-20th century for the benefit of a tile factory.

The elevation and stratigraphical position of the thick levee deposits do not directly coincide with the overbank phases at the most upstream and middle fieldwork locations (Figure 2.9, 4.22). The lithological composition and thickness of the deposit however corresponds to the second overbank phase at the upstream and middle fieldwork locations. The sediments of this body also consist of loamy textures and are approximately two meter in thickness. Thereby, it is suggested by De Haas et al. (2018a) that at the downstream reach of the Old Rhine, peat growth could only occur once the first large levees along the Old Rhine were established. Possibly explaining the lack of (preservation) of the first clastic overbank deposits from the Old Rhine (phase 1). The notion that 30 cm of clay was excavated for the benefit of a tile factory can explain the absence of the last, relatively fine overbank phase seen in the more upstream cross-sections. Based on similarities in lithology and thickness and the deviating evolution of peat and levees along the downstream reach it can be suggested that the thick levee deposits in this cross-section belong to phase 2 4.23-B) and are therefore deposited between approximately 4000 and 2800 yr. BP.

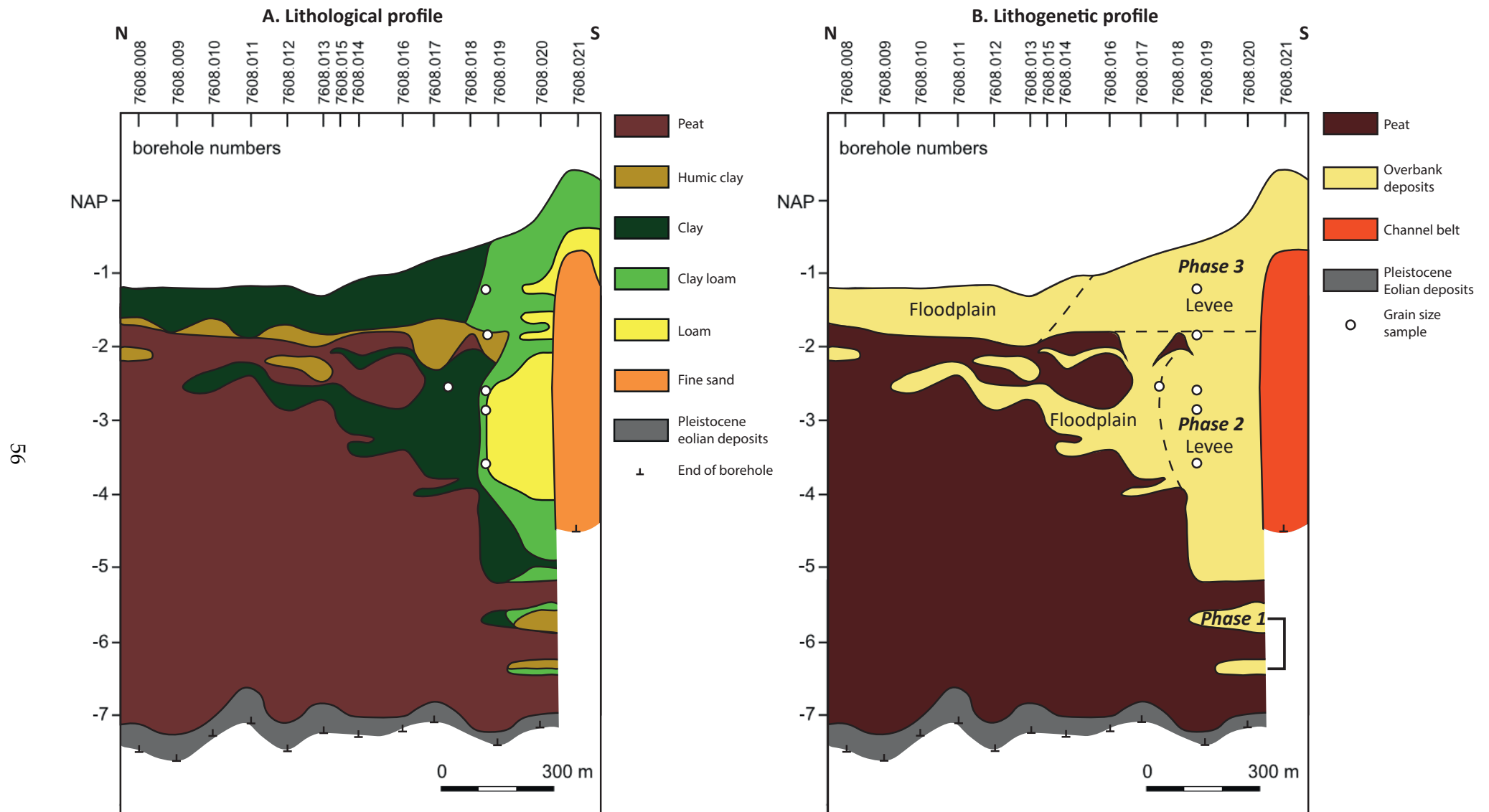


Figure 4.21: Lithological cross-section (A.) and Lithogenetic cross-section (B.) of Old Rhine overbank deposits at fieldwork location 12, upstream (Figure 3.3). Cross-section is constructed based on Stouthamer (2005) (see Figure 2.9) and two borings for the verification and fine-tuning of the lithology to the USDA scheme. Note that because of the latter the lithology in this cross-section differs from the lithology in Figure 3.3.

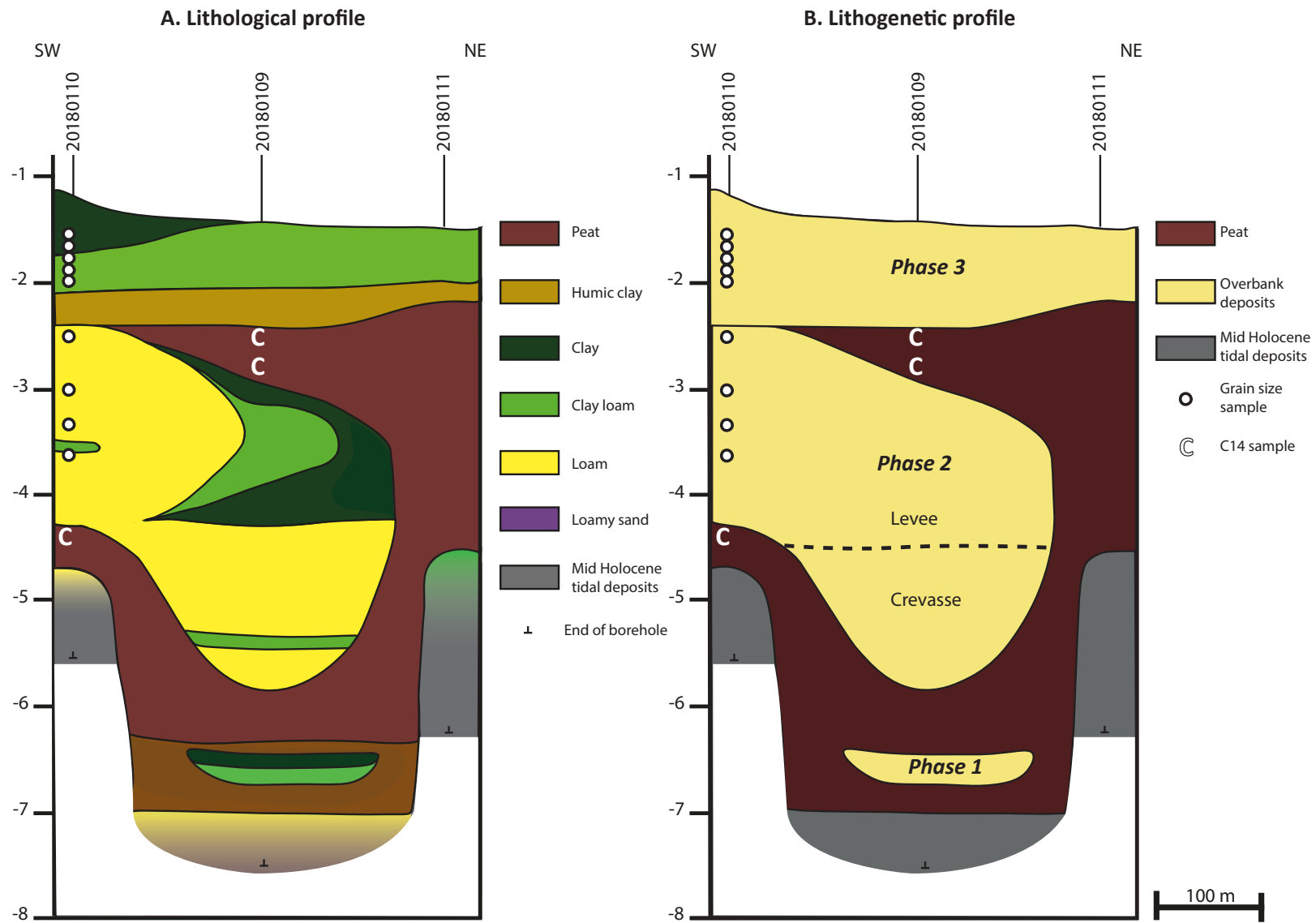


Figure 4.22: Lithological cross-section (A.) and Lithogenetic cross-section (B.) of Old Rhine overbank deposits at fieldwork location 2, middle (Figure 3.3).

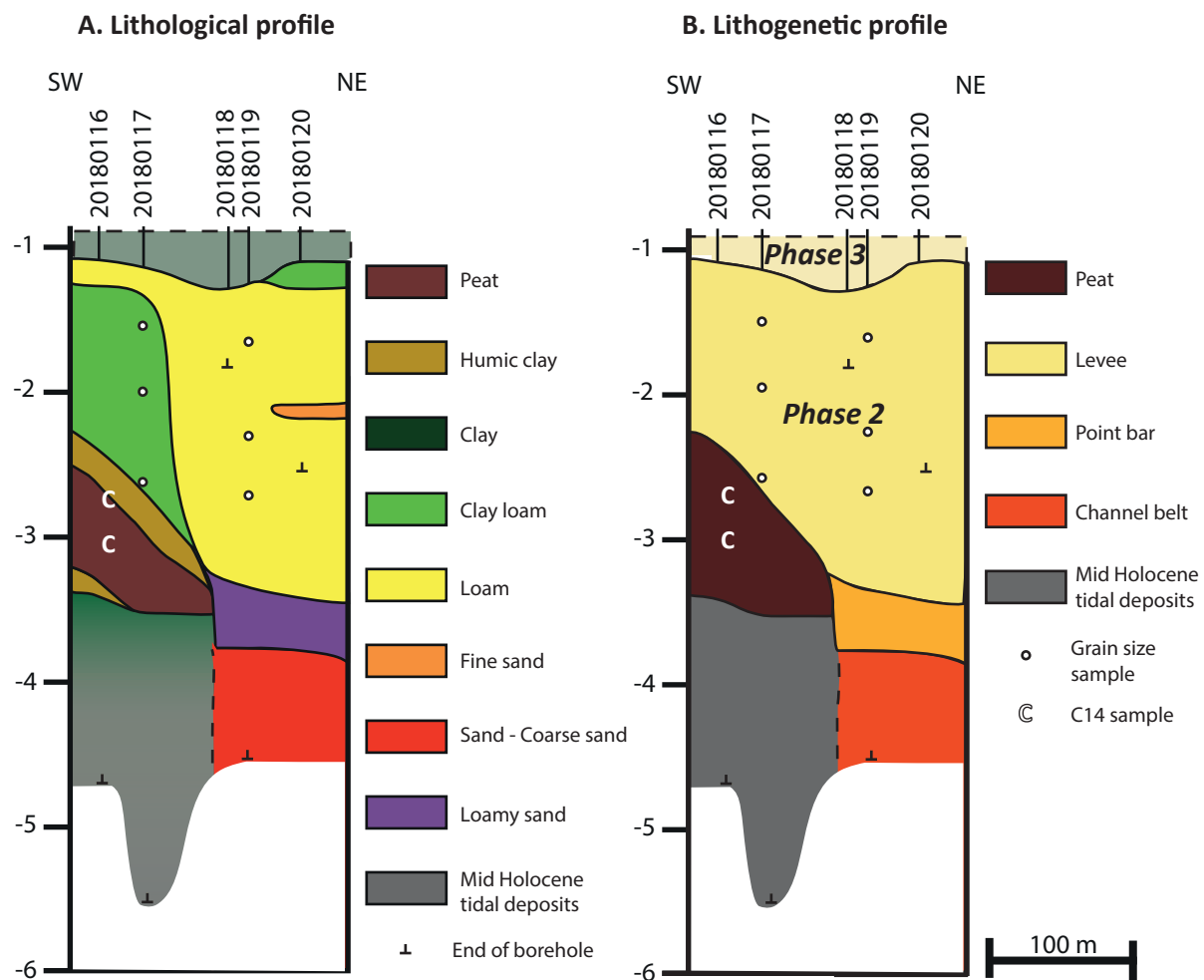


Figure 4.23: Lithological cross-section (A.) and Lithogenetic cross-section (B.) of Old Rhine overbank deposits at fieldwork location 3, downstream (Figure 3.3).

4.5.2 Comparison of the three levee phases along the Old Rhine

From the results of section 4.5.1 we know that there are multiple phases of overbank deposits along the entire Old Rhine and that the phases at different locations can be connected to each other. The evolution of these phases through time for the different locations is summarized in Figure 4.24. Showing that the first levee phase is only preserved upstream (location 1 and 2). At the most downstream location, location 3, the peat layer succeeding the second levee phase and the third levee phase were absent (Figure 4.22). However, it is known that clay was dug away at this location, which could potentially have been the sediments from phase 3. Furthermore, it is unknown if further into the floodplain the peat layer that separates the phases is present.

Within the summary the general characteristics of the phases are also depicted. This allows for a comparison between the phases (Figure 4.24). Comparison of the characteristics can provide insight in the boundary conditions under which the phases formed. The overbank phase related to the starting phase of the Old Rhine, phase 1, consists mainly of clayey material at all locations along the river. The second overbank phase consists of coarser material along the entire river. During the third phase finer material was again deposited along the entire river, containing higher percentages of clay. Hence, the phases differ in composition but the along channel location does not seem to influence large scale lithology and sedimentology (Figure 4.24) (more on this in Section 4.5.3).

The thickness of the different overbank phases also differs significantly (Figure 4.24). The first phase is only 20-30 cm in thickness at both locations where this phase is observed. The second phase has a maximum thickness ranging from 2.5 to 3 m, with a small thinning downstream trend. The third

phase has a maximum thickness of 2 m. A clear trend along the river could not be determined due to the absence of this phase at the most downstream location.

The first overbank phase has the smallest extent, with at maximum 200 m of width at both the upstream and middle fieldwork locations (Figure 4.24). The second overbank phase has a larger extent, with a width of 200-1000 m counted from the channel belt. The width of this phase seems to decrease in downstream direction. It is thereby interesting to note that at the most upstream location (location 1) the extent of this phase increased over time. Starting out with a limited width and extending into the floodplain later in time. The third overbank phase has the largest extent, with widths larger than 1000 m at both the upstream and middle fieldwork locations.

The significant differences between the three levee phases and the trends along the river channel could hypothetically be linked to changes in boundary conditions and possibly internal feedbacks. For an in-depth discussion in which levee characteristics, from the field and the model are linked to boundary conditions and internal feedbacks see Chapter 5.

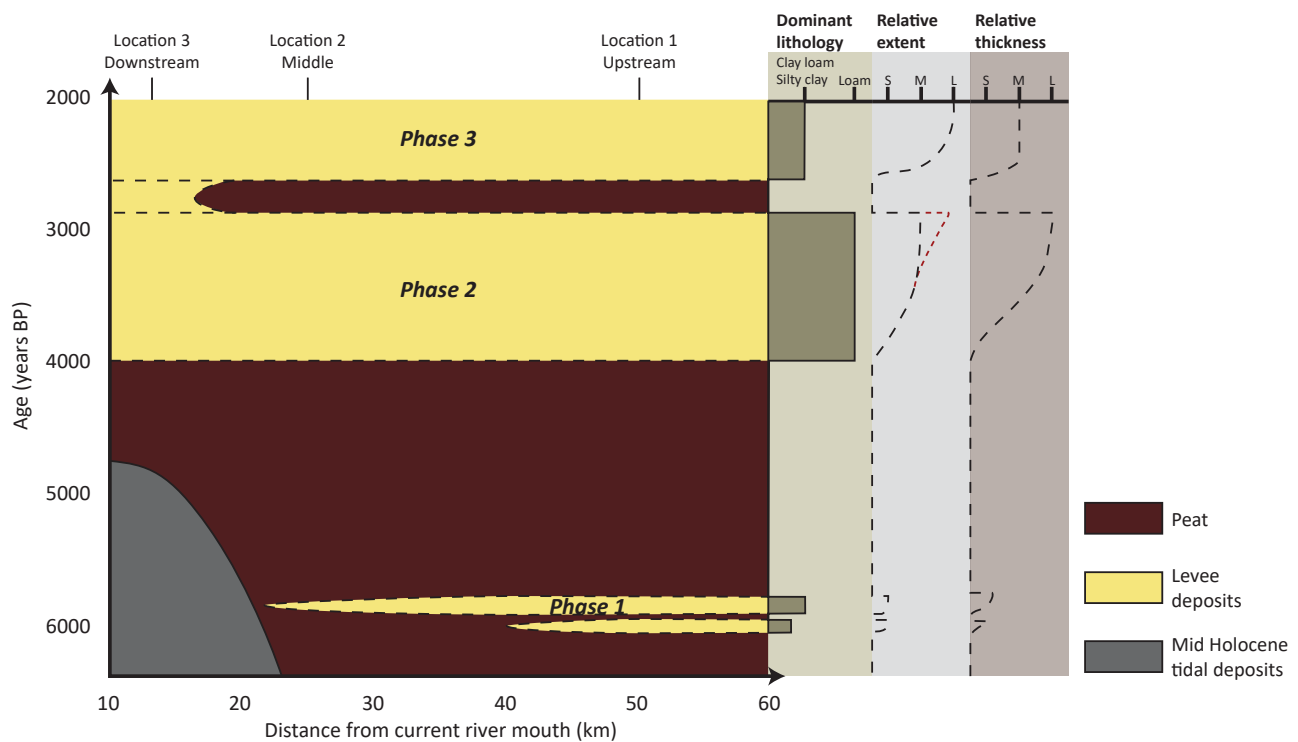


Figure 4.24: Graphical summary of levee evolution along the Old rhine through time and along the channel. The summary depicts the timing of the different levee phases and peat deposits in the along channel direction. Furthermore, the lithology, thickness and extent that dominates the phases is visualised. Note that the trends in of these variables over time are solely hypothetical.

4.5.3 Detailed grain size analysis

The statistical results of the detailed grain size analysis are visualized in Figure 4.25 and summarized in Appendix I. Figure 4.25 provides detailed insight in the lithological composition and variation of levee deposits in relation to location and phase. Locations are indicated by colours, phases by symbols and relative distance from river by symbol size.

The first observation that can be made is that within *phase 2* the lithology of the samples differs per location. The distribution of the samples of *phase 2* at location 1 (upstream) has a larger variability than the distribution of the samples of *phase 2* at location 2 and 3 (Figure 4.25). At location 1 the levee lithology varies from loamy sand to silty clay. Whereas, at location 2 and 3 the lithology of the levee

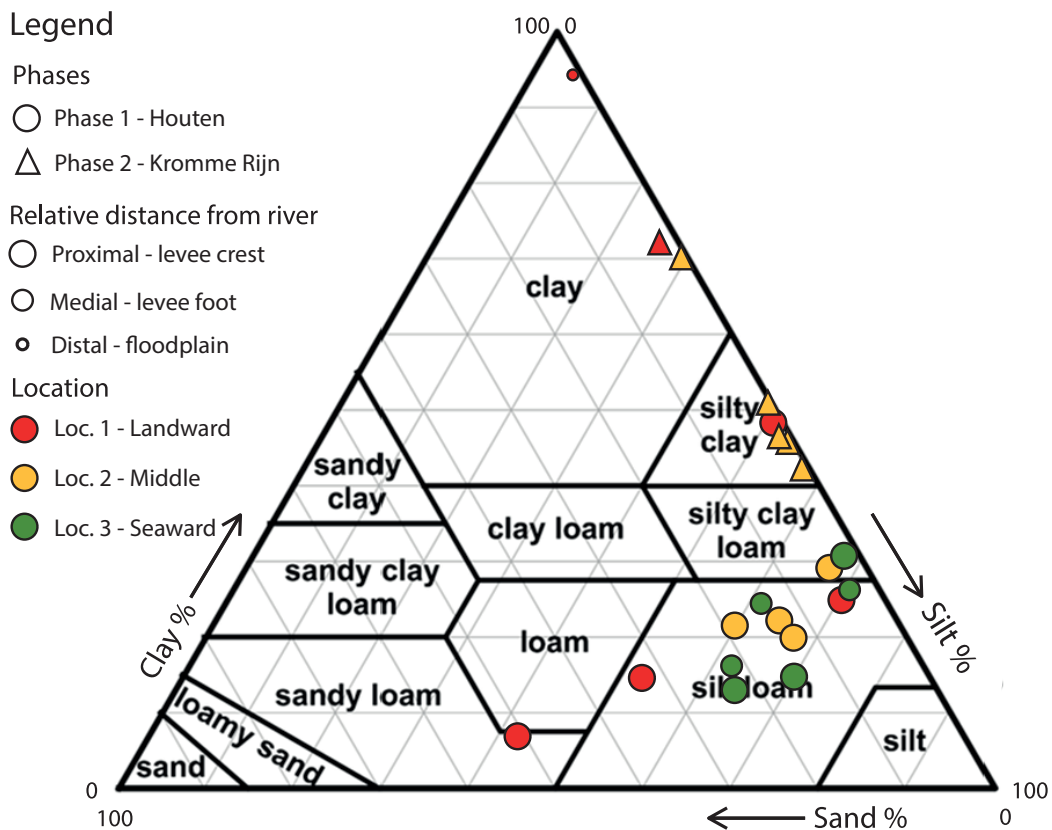


Figure 4.25: Results of detailed grain size analysis on levee deposits presented USDA grain size triangle. Distinction in hypothesised phases, relative distance from main river channel and location is visualized via symbology.

is mainly characterised in the region of silt loam and silty clay loam. The difference in lithological distribution between the upstream location (location 1) and the more downstream locations (location 2 and 3) suggest different conditions along the river under which the levees of this phase have been formed.

Furthermore, as the profiles and the phase comparison already showed the phases are characterised by different lithologies. In which *phase 3* is finer grained than *phase 2* (Figure 4.25). For both the upstream and middle location (location 1 and 2) the samples of *phase 3* are finer than of *phase 2*. The difference in composition between the phases suggest the evolution of these phases under different boundary conditions.

The last thing that can be noted is that next to the differences in median grain size between the phases the lithological distribution of the individual samples within the phases differs too. In phase 2 the distributions of all the individual samples are (very) positively skewed or symmetrical, except for sample HW A-III (Appendix I). On the contrary, the distributions of the individual samples of phase 3 are all very negatively skewed (Appendix I). Implying that phase 2 has a higher abundance of coarse grains, even in the samples with a smaller D_{50} , and that fine grains are abundant in phase 3.

5 | Discussion

In this chapter the results of the study will be discussed. As the objectives of this thesis are divided in assessing the influence of boundary conditions and hydromorphological feedbacks on the evolution, morphology and sedimentology of levees in the fluvial-tidal realm, the discussion of the results will be divided as such. Consequently, the results from the model and from the field will be combined. Furthermore, the results of the sensitivity analysis will be discussed as well as the possible effects of model simplifications.

5.1 The effects of fluvial and tidal boundary conditions on levee evolution and properties

5.1.1 General morphological development

The general morphological development of the levee complex is mainly influenced by the presence of fluctuating water levels. If water level fluctuations are absent smooth unbreached levee complexes form on both sides of the river (Figure 4.1-1). When water level fluctuations are introduced, either by fluvial discharge variability or tides, crevasses form (Figure 4.1-2 till 5). The increase of fluvial discharge during floods and the introduction of tides in the basin, cause differentiation of flow velocities and sediment transport along the levee crests which triggers the formation of crevasse channels.

Despite the triggering of crevasse formation by both fluvial discharge variability and tides the evolution of crevasses formed under these conditions differ. Under purely fluvial conditions a relatively small levee is formed before crevasses start to breach the levee complex whereas under tidally influenced conditions, crevasses and levees develop simultaneously. The difference can be explained by the magnitude of water level fluctuations and the flow velocities related to these fluctuations in the model. Forcing a peak discharge into the basin where no tides are present, causes water level fluctuations in the order of millimetres. On the other hand, when tides are introduced in the model water level fluctuations are in the order of centimetres to metres. These larger water level fluctuations cause stronger differential flows over the levees, which explains the early formation of crevasse channels. In purely fluvial conditions the first crevasses are formed at the upstream part of the basin, as the water level changes are largest upstream. Over time as levees grow the formation of crevasses slowly progrades downstream (Figure 4.1-2). Due to levee growth the river flow is better focussed which causes enhancement of water level fluctuations downstream. During the downstream progradation of crevasse initiation new crevasses are still formed upstream later on in the modelled time. As time continues in purely fluvial set-ups crevasse channels also start to silt-up.

Under tidal influence, the first crevasse develops just upstream of the centre of the basin after which more crevasses form down- and upstream. In the centre of the basin the fluvial and tidal flows meet which causes the water level fluctuations and flow velocity directed out of the channel to be largest here. The location of the first crevasse is just upstream (1 km) of the location where at time step one the ebb-flow velocity is larger than flood flow velocity (Figure 4.1-3 till 5 at and Figure 4.13-B). Furthermore, crevasses remain open over the modelled time when influenced by a significant amount of tidal flow. With the used model set-up this is the case for model runs with tidal amplitudes (M2) of

1-1.25 m (Figure 4.12-B) (model 016 and model 017).

When tides are relatively small, $M2 \leq 0.25$ m, the crevasses in the model that form upstream are directed seawards, whereas the downstream crevasses are directed landwards. De Haas et al. (2018a) mention that the perimarine crevasse systems along the Old Rhine, so the once influenced by tides, are mainly directed landwards, whereas more diverse directions can be observed further upstream. Based on the data from Figure 4.2 it can be stated that the directions of the crevasses in the model are linked to the dominant water flow direction during their formation. The directional trends in maximum flow velocity in the model coupled with the resulting crevasse directions endorse the hypothesis that the direction of crevasses is depended on hydrodynamic gradients influenced by tides and river discharge proposed by De Haas et al. (2018a).

The importance of tides on levee-crevasse morphology and formation is further endorsed by literature discussed in Chapter 2. Van Dinter (2013) and De Haas et al. (2018a) showed that an increased number of long and complex crevasse systems were present in the downstream reach of the Old Rhine. The landward extent of the increased number of crevasses corresponds to characteristic back-water length along which tides have influence on the hydrodynamics (De Haas et al., 2018a). De Haas et al. (2018a) explains the increased number of crevasses in the tidal reach of the river as follows; perimarine crevasse systems are formed when water level rise in the lower reach of the river blocks fluvial discharge which enhances the formation of crevasses. Purely based on the model results it cannot be concluded that the number of crevasses is larger when tides are present. Possibly because of the limited extent of the basin. However, the total cross-sectional crevasse area does increase when tidal amplitude is enlarged or when fluvial discharge magnitude is increased (Figure 4.12). Following a similar trend as the one proposed by Michelazzo et al. (2018), who showed that the width of the crevasse breach scales with the discharge in the main channel. To be able to quantitatively compare the relation constructed by Michelazzo et al. (2018) with the model results further analysis is needed.

5.1.2 Levee dimensions

The dimensions of the levees in the model fall within the dimensions observed in the field. Maximum levee height reaches values close to 1.5 m and final levee width ranges from 1 to 3 km. The model levees therefore have a width that is comparable to the levees along the Columbia river (Adams et al., 2004; Filgueira-Rivera et al., 2007), the Mississippi river (Saucier, 1969) and the Amazon river (Latrubesse and Franzinelli, 2002). As already stated in literature (Filgueira-Rivera et al., 2007), it is found that maximum water levels control maximum levee height, due to negative feedbacks between flow velocity and sediment deposition (Temmerman et al., 2004). The data in Figure 4.8-A,B,D reveals that all boundary conditions that increase or decrease maximum water level affect maximum water level likewise. The data in 4.8-C exposes that not only water levels influence levee height. A decrease in fine concentration below a certain threshold will lead to limited levee height growth. Therefore, based on the data in Figure 4.8-C it is possible to expand the statement by Filgueira-Rivera et al. (2007) to; maximum levee height is controlled by maximum water level *if* the concentration of fine sediments is large enough. In the used model set-up levee height is limited under concentrations smaller than 10 g/m^3 clay and 10 g/m^3 silt (equals 20 g/m^3 of mud). One can argue that as most of the levee is build up by silt, clay concentrations could be smaller than 10 g/m^3 without limiting levee height if at least the concentration of silt reaches values higher than 10 g/m^3 .

The data presented in Figure 4.9 and discussed in Chapter 4 provide insights in the factors and processes that control levee width. Increasing the discharge in the basin, by increasing fluvial discharge magnitude or increasing tidal amplitude, will cause an increase in levee width. The increase in width can be explained by more effective distribution of sediments towards the flood basin as discharge, flow velocities and sediment transport over the levees increase (Figure 4.4 and Figure 4.5). However, only when the tidal amplitude increase is translated to an increase in discharge a fair comparison can be made between the effects of discharge magnitude and tidal amplitude. The tidal amplitude is translated to a discharge by multiplying basin area by tidal amplitude and dividing the results by

the duration of the tidal cycle. The results of these calculations are presented in Table 5.1. Using the average tidal discharge for comparing the effects of discharge magnitude and tidal amplitude on levee width one important observation has to be discussed; a relatively small increase in discharge magnitude (e.g. from 700 to 1000 m³/s) has a larger widening effect than a relatively large increase in tidal discharge (e.g. increasing tidal amplitude from 0.75 m to 1 m, thus increasing tidal discharge by ~1400 m³/s), see Figure 4.9 and data from Table 5.1. The different effects of a discharge increase by fluvial sources or by tides can be explained based on floodplain hydraulics. As discussed by Adams et al. (2004); Filgueira-Rivera et al. (2007); Pierik et al. (2017), floodplain hydraulics influence levee width by enabling or preventing sediments from settling or eroding. In the cases where tides are strong and floodplains are bounded by valley edges or other channel belts, flow velocities in the flood basin are large (see Figure 4.4-A, model 012) which will prevent sediments from settling and will enable the flow to erode earlier deposit sediments.

Table 5.1: Tidal amplitude converted to average discharge by tides for six model runs

Model nr.	Tidal amp. (m)	Tidal prism (m³)	Average discharge by tides (m³/s)
018	0	0	0
023	0.25	6.00 · 10 ⁸	1389
015	0.50	1.20 · 10 ⁸	2778
012	0.75	1.80 · 10 ⁸	4167
016	1.00	2.40 · 10 ⁸	5556
017	1.25	3.00 · 10 ⁸	6944

In addition to the effective distribution of sediments and floodplain hydraulics, the concentration of fines has a significant effect on the evolution of levee width (e.g. Figure 4.9-C). Larger concentrations of mud will increase levee width and will increase the velocity at which levee width grows. Showing that mud is of vital importance to the morphodynamics of levees in fluvial and fluvial-tidal environments, an observation also made for the general morphodynamic development of fluvial and fluvial-tidal systems (e.g. Kleinhans, 2010; Braat et al., 2017; Kleinhans et al., 2018). The influence of changing mud concentrations is also reflected in the data from the Old Rhine. In the lithological cross-sections of location 1 (Figure 2.9) and location 2 (Figure 4.22) the upper overbank sedimentation phase (phase 3) corresponds to a period in which fluvial discharge in the Old Rhine started to decrease (Stouthamer, 2005; De Haas et al., 2018a) while the concentration of mud in the entire Rhine system increased as a result of deforestation in the hinterland (Erkens, 2009). The increase in mud concentration in a silting up Old Rhine possibly triggered the formation of a last, relatively thin and wide, overbank sedimentation phase. The development of levees in the model under large mud concentrations supports this hypothesis. According to De Haas et al. (2018a) the last large-scale overbank deposits in the downstream reach of the Old Rhine are caused by enhanced estuarine overbank clay deposition as a result of decreasing fluvial flow. Based on the model results it could also be hypothesised that the enhanced estuarine overbank clay deposition observed in the downstream reach of the Old Rhine could be triggered due to a decrease in tidal flow, as the river mouth started to close, and/or as a result of the increase in mud supply from the hinterland.

In addition it must be discussed that the method used for the determination of levee width can have a large effect on the results, especially when tidal boundary conditions vary in time and/or space (Figure 4.10). This hypothesis was already partly discussed in Chapter 2. Herein, it was stated that the shape-based definition of geomorphologist makes it harder for geologist to recognize levees in the geological record. This could cause an underestimation of the preservation potential of levees in the geological record and could cause misinterpretations of past river styles, landscape configurations and source/sink conditions. To quantify the effects of the different methods for levee width determination the results of the methods can be compared, as was done in Section 4.2.3. The results

clearly show that width determination based on lithology can cause underdetermination of levee width when tidal flows are small or absent. Under these conditions small amounts of clay are being deposited on top of silt on the distal parts of the levees. As geologists often define levees as the body of sediment between channel and floodplain sediments this could possibly explain the small volume of levees being identified in the rock record. When levees are being defined based on average water level levee width becomes significantly smaller as the submerged part of the levees are not taken into account. In the model, levee width determination based on floodplain height gives the most consistent results over time and for different boundary conditions. The method indirectly accounts for differential settling of fines via morphology and directly for overall basin aggradation. Nonetheless, this method cannot directly be applied in all geological studies. Most of the levees in sedimentary and rock records have been deformed due to synsedimentary or postsedimentary compaction, making reconstructing of former surface profiles difficult. To overcome this problem further research is needed to understand how levee morphology and sedimentology evolve under processes working on longer time scales, e.g. peat compaction underneath levees.

5.1.3 Levee sedimentology

Modelled levees dominated by tidal flows ($M2 > 0.5$ m) are dominated by silty sediments, in which small amounts of clay are mixed in (Figure 4.18, Figure 4.19, Figure 4.20 and Appendix F). The small amount of clay causes the levees to be more poorly sorted. Levees dominated by fluvial flows have more distinct layers of clay and silt and the layers themselves are better sorted (Figures 4.15, Figure 4.16 and Figure 4.17). Thus, levees formed under tidal conditions contain relatively smaller amounts of clay than levees formed under more fluvial conditions. In addition, the clay in tidal levees is mixed with the silt whereas in fluvial levees clear clay layers can be distinguished. The explanation for both observations can be found in flow velocities and sediment transport. Under significant tidal influence, flow velocities in the basin are large and constantly change direction. Resulting in less differential settling of silt and clay in the direction of the floodplain and a lower preservation of clay layers in the stratigraphy. When tidal influence is limited, flow velocities in the basin are smaller and unidirectional, allowing for differential settling of silt and clay and the preservation of clay in the stratigraphical record.

The results from the detailed grain size analyses on the second phase of levee deposits of the Old Rhine (Figure 4.25) show similar patterns as described above based on the model results. The most upstream location (Location 1), which is only under the influence of fluvial boundary conditions (Stouthamer, 2005), contains a wide variety of sediments. From loamy sand ('*zeer sterk lemig zand*') to clay ('*matig zware klei*'). According to De Haas et al. (2018a) and Van Dinter (2013) the two more downstream locations are influenced by fluvial as well as tidal boundary conditions. This is based on backwater calculations and indirectly by the location of the increased number of crevasses. The variety in sediments between the samples at these two locations is smaller. All the pipetted samples can be classified as silt loam or silty clay loam. Thus, the levees that were formed under the influence of tides are more mixed and fall in a small range of lithoclasses. Whereas, the levee formed under purely fluvial conditions shows clearer signals of different lithoclasses. The sorting of the individual samples is similar for the upstream and downstream locations.

To compare levee lithology under different boundary conditions in the model with the field, both results are combined in Figure 5.1. A distinction has been made between *modelled levees* and *field levees* formed under *fluvial* and *tidal* dominated conditions. The boundary of fluvial-tidal domination in the field has been defined based on backwater calculations (De Haas et al., 2018a) and crevasse presence (Van Dinter, 2013). In the model it is assumed that the levees are tidally dominated when the $M2$ tides is equal or larger than 0.75 m, which corresponds to a shift in morphology and lithology. As described earlier, fluvial dominated levees show a wider range in lithoclasses ranging from sandy silt to almost pure clay, as also observed by e.g. Saucier (1969); Farrell (1987); Nicholas and Walling (1997); Cazanacli and Smith (1998); Adams et al. (2004); Filgueira-Rivera et al. (2007); Smith

and Pérez-Arlucea (2008). Whereas, tidal dominated levees contain a smaller range in lithoclasses and are mostly silt dominated. In general, the modelled trends in lithology highly resemble the trends in lithology observed in the field. Despite the large similarities, the grain size samples from the field contain a bit less silt and a bit more clay than the lithology "samples" from the model. The most plausible explanation for this discrepancy can be found in the model parameters, in this case the CSSE (critical shear stress for erosion). The models were run with a relatively low CSSE causing clay to be under-represented in the sedimentology. Despite the small discrepancy it can be stated that the modelled levee lithology corresponds well to levee lithology along the Old Rhine.

The notion that the tidally influenced levees in the model and in the field are more silt dominated in lithology and show a smaller variety in lithoclasses seem to contradict general theory on sedimentology in tidal environments (e.g. Nichols, 2009; Martinius and Van den Berg, 2011). Often in tidal environments, in particular in channels and on shoals, alternations between coarser and finer materials can be found that are related to periods of larger flow velocities and slack water periods. Tidal levees have however hardly been described. Thereby, the environment in the model as well as along the Old Rhine is not purely tidal. Fluvial discharge is always there, which possibly diminishes the effects of slack water periods. This hypothesis is support by field research from Leonardi et al. (2015). Furthermore, it must be mentioned that in the model the stratigraphical resolution is 10 cm and in the field samples were taken of a few cubic centimetres in volume. Both 'sampling techniques' result in the loss of *mm* to *cm* scaled layering.

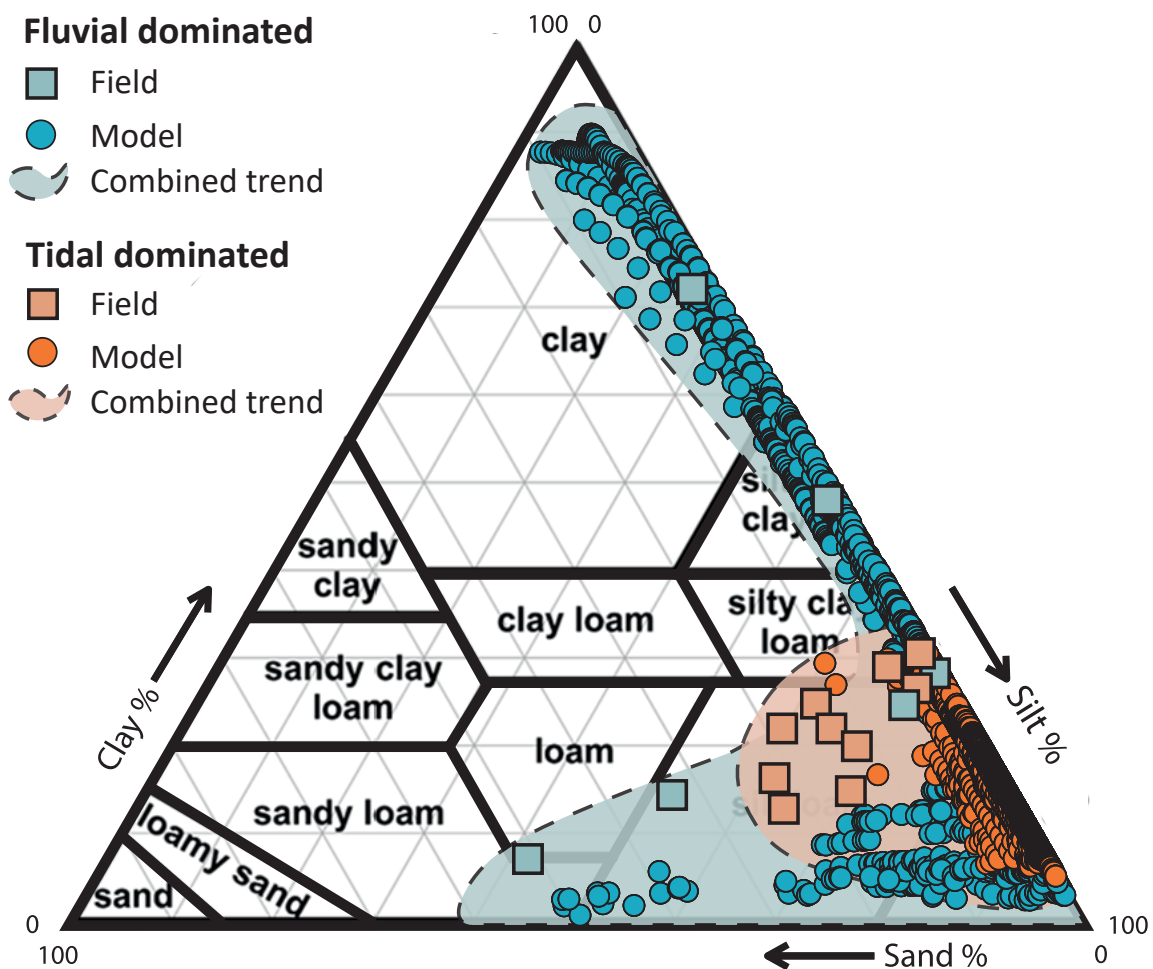


Figure 5.1: Lithological comparison between levee lithology in the field (Figure 4.25) and from the model (Figure 4.20). Distinction has been made between fluvial dominated and tidal dominated levees, and field and model levees.

5.2 The effects of hydromorphological feedbacks on levee evolution and properties

Under small to absent tidal influence (M_2 amplitude ≤ 0.5 m) the evolution of levee morphology happens in phases (Figure 4.3). The first phase is characterised by levee heightening in which the levee grows quickly in height but remains relatively narrow in width. The second phase is characterised by levee widening in which the levee grows towards the flood basin without growing in height. The third phase only occurs when water level fluctuations are present, this phase is characterised by the formation and evolution of crevasse channels. During this phase levees are breached at certain locations and sediments are brought further into the floodplain. When tides are the driver of water level fluctuations in the basin, the third levee phase related to crevasse formation occurs simultaneously with levee heightening and widening. If water level fluctuations are caused by variabilities in discharge crevasse development starts after levees have reached a threshold height. The occurrence of levee phases is linked to changes in accommodation space and transport gradients due to changes in flow velocity gradients over time (see Figure 4.4 and Figure 4.5). During the first phase, characterised by levee heightening, proximal accommodation space is large due to the low floodplain level in the model. Due to low initial floodplain level, flow velocity drops quickly when moving from the channel towards the flood basin (Figure 4.4). Resulting in large transport gradients (Figure 4.5) and therefore a large amount of sediment deposition close to the channel. Over time, the proximal accommodation space fills as the levee heightens decreasing the connectivity of the channel to the floodbasin. As a result, flow velocities on the levee decrease as well as transport gradients from the levee into the floodplain (see Figure 4.4 and Figure 4.5). This stops the process of levee heightening and triggers the onset of levee widening. Due to the low floodplain level in the model it takes time to fill up the available space in the process of levee widening. Therefore, the process of levee widening happens at a relatively slow pace.

Levee morphology during the heightening and widening phases resembles the end member morphologies proposed by Adams et al. (2004) presented in Figure 2.4. Levee morphology during the heightening phase in the model is relatively high and narrow, which was observed by Adams et al. (2004) in confined floodplain settings. Adams et al. (2004) explained the high and narrow levee morphology by the process of turbulent diffusion. An essential part in the hypothesised processes of turbulent diffusion is the creation of eddies on the free shear boundary between swiftly moving water of the main channel and relatively stagnant water of the floodplain. As the flow in the model is averaged over depth and the size of the grid cells are 100x50 m the shear eddies described by Adams et al. (2004) are not modelled in the current set-up. However, as the high and narrow levees do form in the model under a setting similar to that of a confined floodplain, an alternative explanation can be described. Like in the model, water levels in confined floodplains are high during floods as water cannot escape the valley. Hereby, a significant amount of proximal accommodation space is created with possibly steep sediment transport gradients from channel to floodplain. These steep transport gradients will be further enhanced when vegetation grows in the floodplains. As in the model the proximal accommodation space and steep transport gradients will result in high and narrow levees in confined floodplain settings. Over time it would be possible to develop wide levees in confined floodplain settings as well, as proximal accommodation space fills. The fact that (Adams et al., 2004) did not observe wide levees in confined floodplain settings can be explained by a three hypotheses; 1) the evolution of the levees in the systems he studied was limited by time, 2) the evolution of the levees was limited by the amount of sediments, 3) the evolution of levee width was hindered by strong fluvial flows in the floodplain. The latter hypothesis conforms to the observed effects of strong tidal flow in the model.

Levee morphology during the widening phase in the model is similar to the levee morphology observed in unconfined floodplain settings; wide and gently sloping (Adams et al., 2004). In unconfined floodplains water levels in proximity to the channel are not as high as in confined settings. Resulting in a smaller proximal accommodation space and larger sediment transport gradients from channel

to floodplain. This enables the formation of wide and gently sloping levees.

Similar as in the model, levee morphology in the field evolves over time. Along the Old Rhine different levee morphologies developed over time as shown and described in Figure 2.9 & Chapter 2.5.4, Figure 4.22 & Chapter 4.6.1. As described in Chapter 2.5.4, Stouthamer (2005) explains the initiation of these phases by upstream avulsions. However, the upstream avulsions do not explain the shift in levee morphology within phases and between phases. In the cross-section of Figure 2.9 the second phase of overbank deposition starts with a relatively small extent into the floodplain. Hereafter, it starts to widen. The third phase of overbank sedimentation has an even larger extent into the flood basin. More downstream at location 2 (see Figure 3.3 for location), the second phase of levee formation also has a relatively limited extent and again the third phase of overbank deposition has a larger extent into the flood basin. Apparently, levee evolution along the Old Rhine also experienced a heightening phase, characterised by relatively high and narrow levees, followed by a widening phase, characterised by overbank deposits further into the flood basin. Levee heightening, or thickening, could occur due to high transport gradients created by the vegetation in the peatlands surrounding the Old Rhine and the large amount of accommodation space that was again created by the peatlands proximal to the channel. The peat layers allowed the levee deposits to sink to lower elevations creating room for new narrow levee deposits to form on top of the old. As time continued the compaction of peat underneath the overbank deposits slowed down which limited the proximal accommodation space in which levees could heighten. This resulted in the start of a levee widening phase. It is likely that this widening started at different times along the reach of the Old Rhine. Since levee extent started to increase upstream already during the second levee phase (just before ~2900 years BP) and only during the third levee phase at the downstream locations (after ~2700 years BP). The difference in timing of the transition from levee heightening to widening along the Old Rhine could have been caused by differences in peat layer thickness and water level height. Which created differences in proximal accommodation space and transport gradients along the reach of the river. Based on the dating of levee phases by Stouthamer (2005) and the connection of the phases based on lithology in Chapter 4.6.2 it could be hypothesised that in general the start of the widening phase (~2700 years BP), triggered by internal feedbacks, co-occurred with a decreasing Old Rhine discharge and increasing fine sediment load (for timing see Figure 2.7 and Erkens, 2009; Stouthamer, 2005). On the other hand, it could be hypothesised that the levees that are prominently present in the peat are all formed during multiple widening phases and that at times were no levees are prominent levee heightening occurred. This hypothesis is however less likely as the presence of multiple widening phases also requires accelerated creation of accommodation space to allow for levees to heighten again. As no evidence has been found for the latter this hypothesis can be omitted.

The general hypothesis that high and narrow levees could develop along the Old Rhine due to peat compaction and large sediment transport gradients due to vegetation is underlined by and adds to the findings of De Haas et al. (2018a) and Van Asselen (2011). Van Asselen (2011) states that the formation of natural levees on top of peat layers causes locally high peat compaction rates, creating accommodation space which enhances the formation of thick natural levees. Which is essentially a positive feedback loop between peat compaction and levee deposition. The thick peat layers also hampered lateral meander migration (De Haas et al., 2018a) which enabled the levees to keep their position. Which on itself facilitated the evolution of the levees to experience two distinct phases; 1) levee heightening and 2) levee widening.

To summarize, both modelled levees and the levees along the Old Rhine experienced phases, likely to be caused by feedbacks between accommodation space, morphology and hydrodynamics. First, levees grew in height as proximal accommodation space was large due to high water levels in the model and thick peat deposits in the field (see Figure 5.2, upper panel). In the model compaction was not accounted for so accommodation space was created by lower initial bed levels. As the basin filled in over time in the model and peat compacted under the levees in the field, the accommodation space and transport gradients decreased over time (see Figure 5.2, middle panel). This triggered a

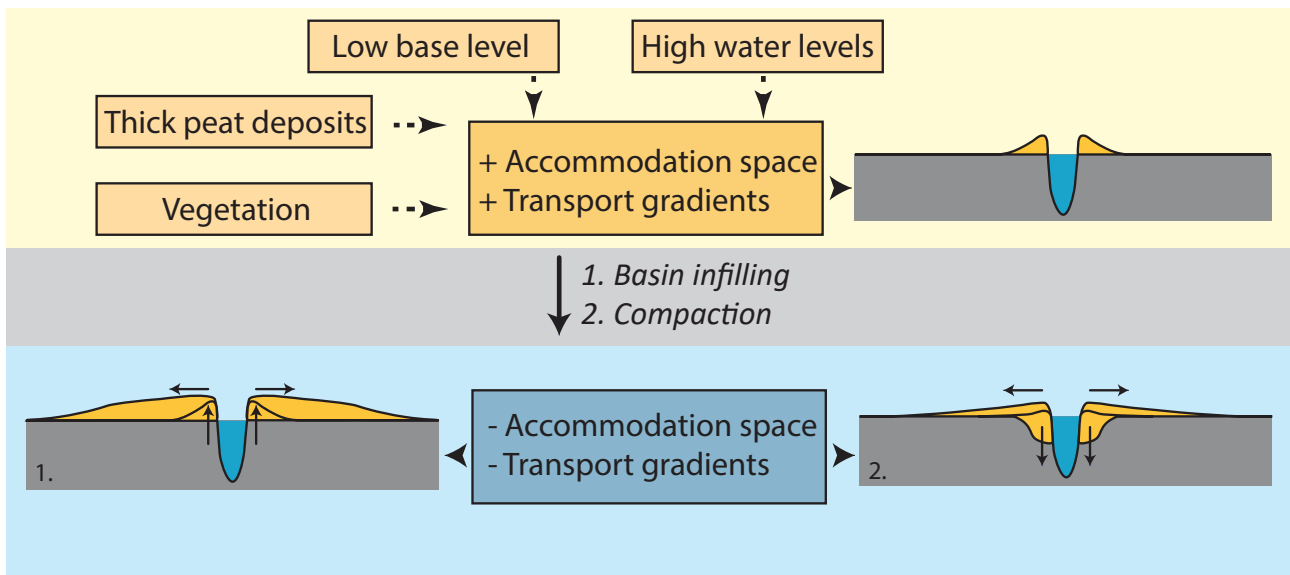


Figure 5.2: Conceptual diagram visualizing the internal processes behind levee phases in the model (1.) and in the field (2.); from high and narrow levees to wide levees.

phase of levee widening into the flood basin (see Figure 5.2, lower panel), enhanced by increased sediment supply during this period Erkens (2009).

5.3 Effects of model simplifications

Lack of vegetation, peat and subsidence

An important limitation to the model is the lack of vegetation, peat and subsidence. Vegetation has proven to be of great importance for bank stability and channel patterns in rivers (e.g. Kleinhans, 2010) as well as for the morphodynamics in estuarine environments (Lokhorst et al., 2018). Furthermore, vegetation has been proven to influence levee morphology in models and in the field, by changing sediment transport gradients (respectively Kleinhans et al., 2018; Van Asselen, 2011). Introduction of the effects of vegetation into the model will therefore likely influence morphodynamic evolution of the levee-crevasse system. It will enhance the process of levee heightening, by creating steeper transport gradients. Thereby, vegetation will influence floodplain hydraulics by hampering flow velocities by which it will enhance sedimentation and decrease erosion. Hence, influencing the development of levee width. Levee widening itself could also change the type of vegetation as the environmental conditions change.

The effects of differential subsidence or peat compaction have demonstrated to be important to levee and crevasse development (this study as well as in Van Asselen, 2011). The incorporation of peat and peat compaction in the model would allow for studying the effects of differential compaction on crevasse initiation and levee phasing in more detail. Furthermore, it would create opportunities for studying the feasibility and practicality of creating new land in sinking deltaic areas.

Meandering

In the used model set-up the river did not have a meandering pattern. The channel stayed straight for the entire modelled time. Hudson and Heitmuller (2003) and Pierik et al. (2017) demonstrated that the position of levees along the river is important for their morphology. With levees on the inner bends of meanders being relatively high in comparison to levees along the outer bends. The straight channel pattern in the model therefore hinders the quantitative understanding of the influence of meandering on levee morphology. The two factors that contributed to the lack of meandering in the model are; 1) the used sediment transport formulation, the formulation by Van Rijn et al. (2004), does not easily allow for the development of meander bends, 2) the stable position of the upstream inflow

point. Amongst others, Van Dijk et al. (2012) showed that the lack of an upstream inflow perturbation prevents the sustained formation of meander bends and that a dynamic inflow perturbation is important to enhance meander development over time. Despite the drawbacks of the absence of meandering in the model, the absence of meandering helped in distinguishing the difference between fluvial and tidal situations better. As the levees were not disturbed by the presence of obscuring meandering effects.

Mud and mud-sand mixtures

The previous section discussed the importance of mud and the influence of parametrisation of mud characteristics on the morphodynamic evolution of the levee-crevasse complex. In the model two mud fractions were implemented; silt and clay. For each of these fractions the characteristics were parametrised individually in terms of their densities, settling velocities, critical shear stress for sedimentation and critical shear stress for erosion. Despite realistic sedimentation patterns and stratigraphy, it could be argued that mud did not deposit at locations in the model where it would have in the real world due to the boundary effects along the edges of the floodplain. In addition, the difference between the settling velocity of clay and silt in the model has caused a rapid transition from levee to floodplain sediments. Whereas, along real river systems the transition from levee to floodplain is more gradual due to differential settling of widely variable sediments (Adams et al., 2004; Cazanacchi and Smith, 1998; Smith and Pérez-Arlucea, 2008; Filgueira-Rivera et al., 2007). Furthermore, the effects of salt or brackish water on the process of settling was not accounted for.

Not only realistic representation of sediment deposition in models is important also correct parametrisation of sediment erosion is essential as the previous chapter indicated. Especially the influence of sediment mixtures (mud and sand) can be of great importance for erosion patterns (Mitchener and Torfs, 1996). In the model used in this thesis the influence of sediment mixtures on erosional processes could be of influence when tides have a large influence on the hydraulics and sedimentary processes in the flood basin.

Boundary effects and domain size

Despite the realistic morphodynamic evolution of the bathymetry in the model, choices related to boundary specifications and domain size influence the results. The relatively narrow size of the tidal basin together with its closed boundaries caused unwanted morphological effects on the edges of the basin due to strong tidal flows flushing through the basin. Clays are not deposited and washed out of the system under strong tidal flows, resulting in narrow levees. The relatively small domain size also created the need for downscaling of tidal and fluvial forcings in comparison to forcings on the Old Rhine system. This mainly caused problems when flow velocities and shear stresses were large under the influence of large tidal amplitudes (> 0.75 m) or large discharge magnitudes (> 1500 m³/s). Notwithstanding the application of this model for the determination of the relative influence of tidal and fluvial boundary conditions on levee evolution.

5.4 Recommendations and future research

The model used in this thesis can be seen as the first step towards a generic and quantitative understanding of levee-crevasse morphology and evolution under fluvial and tidal boundary conditions. Combining the model results with field data has proven the morphological and sedimentological trends in the model. Furthermore, the combination of model and field data created a framework for the evolution of levees over time under the influence of internal processes. Not to mention, the use of two complementary methods also provides inspiration for further research.

The implementation of vegetation, peat and subsidence in the model set-up will help in creating more accurate predictions of morphodynamic evolution. Accurate predictions of morphodynamic responses are crucial when these morphodynamic models are used for future river and delta management. Vegetation modules to extend Delft3D exist and are well tested (e.g. Kleinhans et al., 2018;

Lokhorst et al., 2018), implementation is therefore straightforward. Modules for the implementation of peat and differential compaction do not yet exist for Delft3D. However, the expansion of knowledge on topics as subsidence over the past years provides a solid ground for the development and implementation of such modules.

Furthermore, it is of importance to further study the influence of model parameters that influence the sedimentation and erosion characteristics of sediments and sediment mixtures. The main goal should be to make depositional and erosional patterns on levees and in floodplains as representative for natural situations as possible. Comparison with field data and/or experiments should here for be evident.

At last, it would be recommended to study levee and crevasse deposits along river and estuarine systems at different places around the world. With more extensive field studies the influence of internal processes on levee evolution and morphology would become more evident. It would prove that levee evolution commonly happens in phases or that the levees along the Old Rhine form an exception. Furthermore, it could help in proving or rejecting the hypothesis that tidally influenced levees are more poorly sorted and mixed in lithology than their fluvial counterparts. Lastly, more diverse field data, including datings, would help in understanding the relative and combined influence of changing boundary conditions and internal processes.

5.5 Contribution to society

As stated in Chapter 1 natural levees influence the evolution of deltas and estuaries and their presence is linked to human occupation due their elevated morphology. Furthermore, it is stated that a deeper knowledge on levee morphology and evolution could help in sustainable delta and estuarine management in the future. The latter is of vital importance for delta communities that will face the effects of climate change, sea level rise and anthropogenic subsidence in the coming decades.

The findings presented in this thesis add to our understanding of the evolution of river, delta and tidal systems under changing boundary conditions and hydromorphological feedback mechanisms. Moreover, they provide a first step towards the development of sustainable management strategies for building new land in sinking deltas. Man-made sediment diversions are an ambitious and novel concept that is being discussed at different locations around the world. In the Mississippi delta, sediment diversions are being planned (Nichols, 2009; Allison and Meselhe, 2010) and in the Ganges-Brahmaputra-Meghna delta in Bangladesh low-lying polder dikes are partly being removed to reintroduce sediments in the hinterland (Islam and Middelkoop, 2019 in Stouthamer et al., 2019). The success of these kind of projects depends on our understanding of sediment transport and morphodynamic development of levees, crevasses and floodplains. The results of this thesis have shown that levee-crevasse complexes become larger if more sediment is transported out of the main channel, that their width is negatively affected by large flow velocities in the floodplain and that especially a low concentration of fine sediment can limit their growth. These conclusions have implications for implementation of natural land-building projects in delta areas. In fluvial-sediment starved deltas as the Rhine-Meuse delta in The Netherlands, the fine sediments will have to come from a marine source (tidal import), which implies allowing the sea to influence the land; a sensitive topic in the country that battled against the water for centuries. Furthermore, the large influence of tides on levee and crevasse dimensions provides opportunities for the development of 'natural' land building projects in tide dominated deltas around the world (Figure 1.1).

6 | Conclusions

The aim of this thesis was to create a generic and quantitative understanding of the drivers of levee evolution and morphology in different environments. This is achieved by assessing the influence of *boundary conditions* and *hydromorphological feedbacks* on levee evolution, morphology and sedimentology in the fluvial-tidal realm. Below, conclusions on the effects of boundary conditions and internal processes will be discussed.

6.1 The effects of boundary conditions

Maximum levee height is controlled by the water level and is limited temporarily if the concentration of fines drops below a certain value. Therefore, all boundary conditions that influence the water level will influence maximum levee height analogously. Levee width is controlled by the amount of sediment transport out of the channel and floodplain hydraulics. Sediment transport out of the channel is enlarged by an increase in fluvial discharge and an increase of tidal discharge (thus increasing tidal amplitude) or by increasing the concentration of fines. However, an increase in tidal amplitude also enlarges flow velocities in the flood basin which hinders settling of sediments and enhances erosion. Limiting the growth of levee width. An increase in fluvial discharge or the concentration of fines is therefore more efficient in widening levees.

The findings further indicate that levee morphology is more complex when water level fluctuations are introduced due to the formation of crevasses. Either variability in fluvial discharge or tides can cause these fluctuations. Fluctuations caused by tides are often large and occur daily causing crevasses to develop simultaneously with levees. Crevasses triggered by fluvial discharge variability only form after the levees have established a threshold height. Furthermore, it is found that large tides and strong tidal flows are essential for keeping crevasse channels open for a prolonged time.

In addition, the study has shown that levee stratigraphy and sedimentology is strongly controlled by the relative dominance of tides over fluvial discharge. When tides are dominant, levees contain less clay and their lithology is more mixed. On the other hand, if fluvial discharge is dominant, levees contain clear signals of clay layers and the individual layers are well sorted. The difference is explained by the larger and bi-directional flow velocities that tides cause. Together this hinders settling of fines and causes differential settling of silt and clay from channel to floodplain to be disturbed.

6.2 The effects of hydromorphological feedbacks

The combination of model and field results have indicated that levee evolution can be divided into two distinct morphological phases as a result of feedbacks between morphology and flow. The two phases are characterised by 1) levee heightening, in which the levees grow in height while their width stays rather limited, and 2) levee widening, in which the levees grow in width while their height remains similar.

Levee heightening occurs when proximal accommodation space is large and transport gradients from channel to floodplain are high. As proximal accommodation space fills over time and transport gra-

dients from levee to floodplain decrease, levees will start to widen. Proximal accommodation space can both be created by high water levels and thick peat layers in which the levee deposits can sink. Large transport gradients, thus levee heightening, is enhanced by the presence of vegetation in the flood basin.

The rate at which levee heightening and widening takes place is largely dependent on the concentration of fines. Higher concentrations of fines increase the rate at which levees grow, both in height and in width. Consequently, levees formed in systems or during periods of high fine concentration are generally wider in planform.

The combination of model and field data has shown that levee characteristics represent the boundary conditions and hydromorphological feedback mechanisms under which they formed. Therefore, levee characteristics can be used to reconstruct boundary conditions over space and time. In addition, the knowledge gained on the development of levees under certain boundary conditions will help to predict the morphological development of present-day levees and crevasses.

Bibliography

- Adams, P. N., Slingerland, R. L., and Smith, N. D. (2004). Variations in natural levee morphology in anastomosed channel flood plain complexes. *Geomorphology*, 61(1-2):127–142.
- Allen, J. (1964). Studies in fluvial sedimentation: six cyclothems from the Lower Old Red Sandstone, Anglowelsh Basin. *Sedimentology*, 3(3):163–198.
- Allen, J. R. (1965). A review of the origin and characteristics of recent alluvial sediments. *Sedimentology*, 5(2):89–191.
- Allison, M. A. and Meselhe, E. A. (2010). The use of large water and sediment diversions in the lower mississippi river (louisiana) for coastal restoration. *Journal of Hydrology*, 387(3-4):346–360.
- Bakker, H. d. and Schelling, J. (1966). A system of soil classification for the Nehterlands (The higher levels).
- Beets, D., Van der Valk, L., and Stive, M. (1992). Holocene evolution of the coast of Holland. *Marine geology*, 103(1-3):423–443.
- Belliard, J.-P., Di Marco, N., Carniello, L., and Toffolon, M. (2016). Sediment and vegetation spatial dynamics facing sea-level rise in microtidal salt marshes: Insights from an ecogeomorphic model. *Advances in water resources*, 93:249–264.
- Berendsen, H., Hoek, W., and Schorn, E. (1995). Late Weichselian and Holocene river channel changes of the rivers Rhine and Meuse in The Netherlands (Land van Maas en Waal). *Paläoklimaforschung/Palaeoclimate Research*, 14:151–171.
- Berendsen, H. J. and Stouthamer, E. (2000). Late Weichselian and Holocene palaeogeography of the Rhine–Meuse delta, The Netherlands. *Palaeogeography, Palaeoclimatology, Palaeoecology*, 161(3-4):311–335.
- Berendsen, H. J. A. (2005). *Fysisch-geografisch onderzoek*. Uitgeverij Van Gorcum.
- Braat, L., Kessel, T. v., Leuven, J. R., and Kleinhans, M. G. (2017). Effects of mud supply on large-scale estuary morphology and development over centuries to millenia. *Earth Surface Dynamics*, 5(4):617–652.
- Brierley, G. J., Ferguson, R. J., and Woolfe, K. J. (1997). What is a fluvial levee? *Sedimentary Geology*, 114(1-4):1–9.
- Cazanacli, D. and Smith, N. D. (1998). A study of morphology and texture of natural levees—Cumberland Marshes, Saskatchewan, Canada. *Geomorphology*, 25(1-2):43–55.
- Cloyd, K. C., Demicco, R. V., and Spencer, R. J. (1990). Tidal channel, levee, and crevasse-splay deposits from a cambrian tidal channel system; a new mechanism to produce shallowing-upward sequences. *Journal of Sedimentary Research*, 60(1):73–83.
- Cohen, K., Stouthamer, E., Pierik, H., and Geurts, A. (2012). Digitaal basisbestand Paleogeografie van de Rijn-Maas Delta. *Dept. Fysische Geografie. Universiteit Utrecht. Digitale Dataset*.

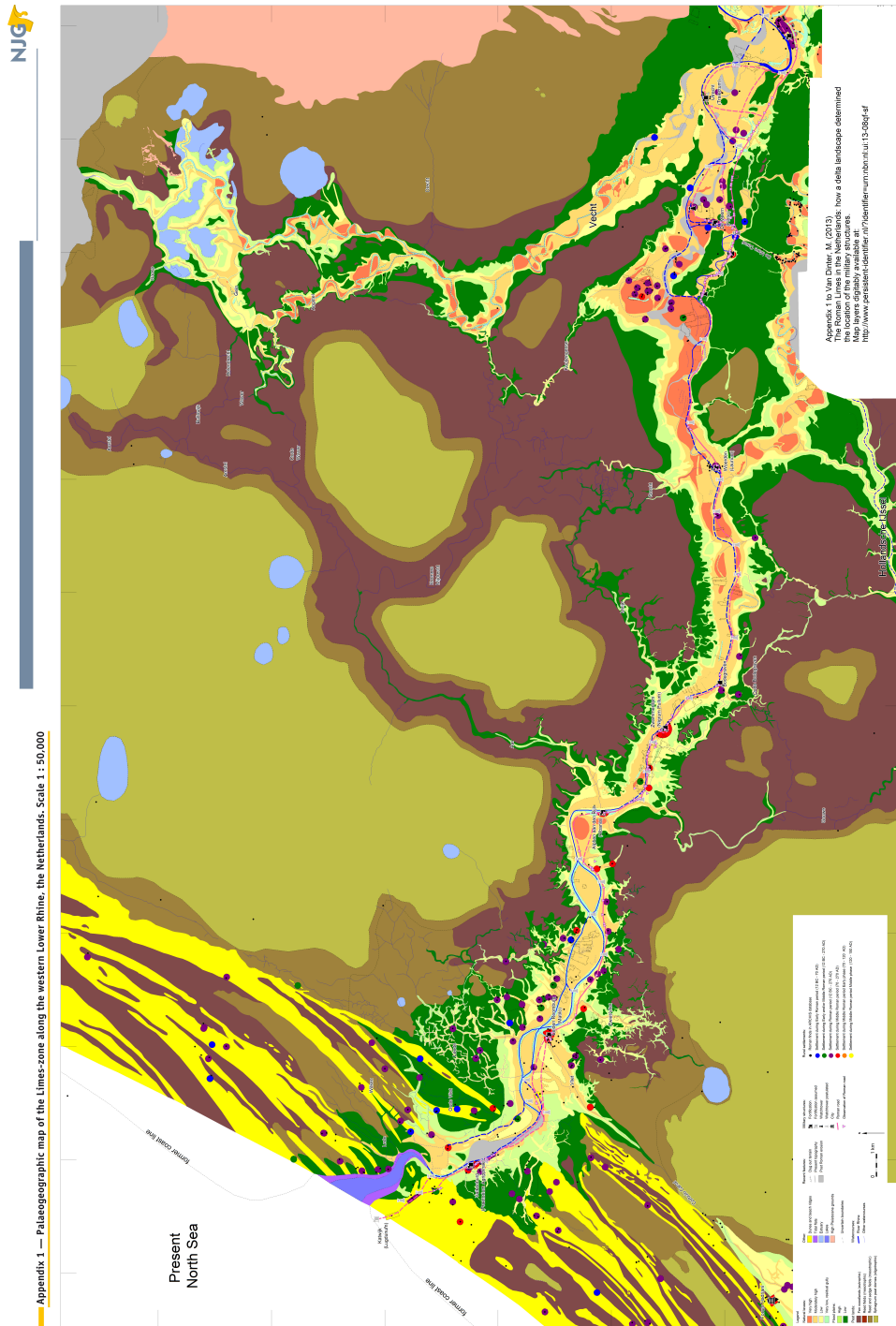
- Dalrymple, R. W., Zaitlin, B. A., and Boyd, R. (1992). Estuarine facies models; conceptual basis and stratigraphic implications. *Journal of Sedimentary Research*, 62(6):1130–1146.
- Davis, R. and Dalrymple, R. (2010). *Principles of Tidal Sedimentology*.
- De Haas, T., Van der Valk, L., Cohen, K., Pierik, H., Weisscher, S., Hijma, M., Van der Spek, A., and Kleinhans, M. (2018a). Long-term evolution of the Old Rhine estuary: unraveling effects of changing boundary conditions and inherited landscape. *The Depositional Record*, pages 1–25.
- De Haas, T., Pierik, H., Van der Spek, A., Cohen, K., Van Maanen, B., and Kleinhans, M. (2018b). Holocene evolution of tidal systems in The Netherlands: Effects of rivers, coastal boundary conditions, eco-engineering species, inherited relief and human interference. *Earth-Science Reviews*, 177:139–163.
- De Swart, H. and Zimmerman, J. (2009). Morphodynamics of tidal inlet systems. *Annual review of fluid mechanics*, 41:203–229.
- Deltares (2017). *Delft3d-FLOW, Simulation of multi-dimensional hydrodynamic flows and transport phenomena, including sediments, User Manual, Hydro-Morphodynamics*. Delft, The Netherlands.
- Edmonds, D., Caldwell, R., Baumgardner, S., Paola, C., Roy, S., Nelson, A., and Nienhuis, J. (2017). A global analysis of human habitation on river deltas. In *EGU General Assembly Conference Abstracts*, volume 19, page 10832.
- Erkens, G. (2009). *Sediment dynamics in the Rhine catchment: quantification of fluvial response to climate change and human impact*. PhD thesis, Utrecht University.
- Farrell, K. M. (1987). Sedimentology and facies architecture of overbank deposits of the mississippi river, false river region, louisiana.
- Ferguson, R. I. (1987). Hydraulic and sedimentary controls of channel pattern. *River channels: environment and process*, pages 129–158.
- Fielding, C. R., Falkner, A. J., and Scott, S. G. (1993). Fluvial response to foreland basin overfilling; the Late Permian Rangal coal measures in the Bowen Basin, Queensland, Australia. *Sedimentary Geology*, 85:475–497.
- Filgueira-Rivera, M., Smith, N. D., and Slingerland, R. L. (2007). Controls on natural levee development in the Columbia River, British Columbia, Canada. *Sedimentology*, 54(4):905–919.
- Fisk, H. N., McFarlan Jr, E., Kolb, C., and Wilbert Jr, L. (1953). Sedimentary framework of the modern mississippi delta. *Journal of Sedimentary Research*, 23(2).
- Folk, R. L. and Ward, W. C. (1997). Brazos River bar [Texas]; a study in the significance of grain size parameters. *Journal of Sedimentary Research*, 27(1):3–26.
- Friedrichs, C. T. (2010). Barotropic tides in channelized estuaries. *Contemporary issues in estuarine physics*, pages 27–61.
- Friedrichs, C. T. and Aubrey, D. G. (1988). Non-linear tidal distortion in shallow well-mixed estuaries; a synthesis. *Estuarine, Coastal and Shelf Science*, 27(5):521–545.
- Heiri, O., Lotter, A. F., and Lemcke, G. (2001). Loss on ignition as a method for estimating organic and carbonate content in sediments; reproducibility and comparability of results. *Journal of paleolimnology*, 25(1):101–110.
- Hijma, M., Van der Spek, A., and Van Heteren, S. (2010). Development of a mid-Holocene estuarine basin, Rhine–Meuse mouth area, offshore The Netherlands. *Marine geology*, 271(3-4):198–211.

- Hijma, M. P. and Cohen, K. M. (2010). Timing and magnitude of the sea-level jump precluding the 8200 yr event. *Geology*, 38(3):275–278.
- Hijma, M. P. and Cohen, K. M. (2011). Holocene transgression of the Rhine river mouth area, The Netherlands/Southern North Sea: palaeogeography and sequence stratigraphy. *Sedimentology*, 58(6):1453–1485.
- Horne, J. C. (1979). Carboniferous depositional environments in the Appalachian region. *Ferm*, pages 645–670.
- Hudson, P. F. and Heitmuller, F. T. (2003). Local- and watershed-scale controls on the spatial variability of natural levee deposits in a large fine-grained floodplain: Lower Panuco Basin, Mexico. *Geomorphology*, 56(3-4):255–269.
- Islam, M, F. and Middelkoop, H. (2019). Controls of renewed sediment trapping in low-lying polders of the bangladesh delta. In *Land of Rivers: NCR DAYS 2019*, page 82.
- Kim, W., Dai, A., Muto, T., and Parker, G. (2009). Delta progradation driven by an advancing sediment source: Coupled theory and experiment describing the evolution of elongated deltas. *Water Resources Research*, 45(6).
- Kleinans, M. G. (2010). Sorting out river channel patterns. *Progress in Physical Geography*, 34(3):287–326.
- Kleinans, M. G., de Vries, B., Braat, L., and van Oorschot, M. (2018). Living landscapes: Muddy and vegetated floodplain effects on fluvial pattern in an incised river. *Earth surface processes and landforms*, 43(14):2948–2963.
- Latrubesse, E. M. and Franzinelli, E. (2002). The holocene alluvial plain of the middle amazon river, brazil. *Geomorphology*, 44(3-4):241–257.
- Leonardi, N., Kolker, A. S., and Fagherazzi, S. (2015). Interplay between river discharge and tides in a delta distributary. *Advances in water resources*, 80:69–78.
- Leopold, L. B. and Wolman, M. G. (1957). *River channel patterns: braided, meandering, and straight*. US Geological Survey.
- Lesser, G. R., Roelvink, J. v., Van Kester, J., and Stelling, G. (2004). Development and validation of a three-dimensional morphological model. *Coastal engineering*, 51(8-9):883–915.
- Lokhorst, I., Braat, L., Leuven, J., Baar, A., van Oorschot, M., Selakovic, S., and Kleinans, M. (2018). Morphological effects of vegetation on the fluvial-tidal transition in holocene estuaries. *Earth Surf. Dyn. Discuss*, 2018:1–28.
- Marshak, S. (2011). *Earth: Portrait of a Planet*. WW Norton & Company.
- Martinius, A. and Van den Berg, J. (2011). EAGE Houten.
- Michelazzo, G., Oumeraci, H., and Paris, E. (2018). New hypothesis for the final equilibrium stage of a river levee breach due to overflow. *Water Resources Research*.
- Mitchener, H. and Torfs, H. (1996). Erosion of mud/sand mixtures. *Coastal engineering*, 29(1-2):1–25.
- Moree, J. (2019). Reconstruction of the formation and evolution of crevasse systems in the fluvial-tidal realm of the Old Rhine. Master's thesis, Utrecht University.
- Nicholas, A. and Walling, D. (1997). Modelling flood hydraulics and overbank deposition on river floodplains. *Earth Surface Processes and Landforms: The Journal of the British Geomorphological Group*, 22(1):59–77.
- Nichols, G. (2009). *Sedimentology and stratigraphy*. John Wiley & Sons.

- Nienhuis, J. H., Törnqvist, T. E., and Esposito, C. R. (2018). Crevasse splays versus avulsions: A recipe for land building with levee breaches. *Geophysical Research Letters*, 45(9):4058–4067.
- Olariu, C. and Bhattacharya, J. P. (2006). Terminal distributary channels and delta front architecture of river-dominated delta systems. *Journal of sedimentary research*, 76(2):212–233.
- Perillo, G. M. (1995). Definitions and geomorphologic classifications of estuaries. *Geomorphology and sedimentology of estuaries. Developments in Sedimentology*, 53:17–47.
- Pierik, H., Stouthamer, E., and Cohen, K. (2017). Natural levee evolution in the Rhine-Meuse delta, the Netherlands, during the first millennium CE. *Geomorphology*, 295:215–234.
- Saucier, R. T. (1969). Geological investigation of the Mississippi River Area, Artonish to Donaldsonville, LA. *Technical Rep. No. S-69-4, US Army Engineer Waterways Experiment Station, Vicksburg, Mississippi*.
- Schumm, S. A. (1985). Patterns of alluvial rivers. *Annual Review of Earth and Planetary Sciences*, 13:5–27.
- Schuurman, F., Marra, W., and Kleinhans, M. G. (2013). Physics-based modeling of large braided sand-bed rivers: Bar pattern formation, dynamics, and sensitivity. *Journal of geophysical research: Earth Surface*, 118(4):2509–2527.
- Sellin, R. H. J. (1964). A laboratory investigation into the interaction between the flow in the channel of a river and that over its flood plain. *La Houille Blanche*, (7):793–802.
- Smith, N. D. and Pérez-Arlucea, M. (2008). Natural levee deposition during the 2005 flood of the Saskatchewan River. *Geomorphology*, 101(4):583–594.
- Stouthamer, E. (2001). Sedimentary products of avulsions in the Holocene Rhine–Meuse Delta, The Netherlands. *Sedimentary Geology*, 145(1-2):73–92.
- Stouthamer, E. (2005). Reoccupation of channel belts and its influence on alluvial architecture in the Holocene Rhine–Meuse delta, The Netherlands. *River Deltas: Concepts, Models and Examples*.
- Stouthamer, E., Cohen, K., and Gouw, M. J. (2011). Avulsion and its implications for fluvial-deltaic architecture: insights from the Holocene Rhine-Meuse delta. *SEPM Special Publication*, 97:215–232.
- Stouthamer, E., Cohen, K. M. C., and Hoek, W. Z. H. (2015). *De vorming van het land: geologie en geomorfologie*. Perspectief uitgevers.
- Stouthamer, E., Middelkoop, H., Kleinhans, M., Van der Perk, M., and Straatsma, M. (2019). *Land of Rivers: NCR DAYS 2019 Proceedings*. Netherlands Centre for River Studies.
- Syvitski, J. P. and Farrow, G. E. (1983). Structures and processes in bayhead deltas: Knight and bute inlet, british columbia. *Sedimentary geology*, 36(2-4):217–244.
- Temmerman, S., Bouma, T., Govers, G., and Lauwaet, D. (2005). Flow paths of water and sediment in a tidal marsh: Relations with marsh developmental stage and tidal inundation height. *Estuaries*, 28(3):338–352.
- Temmerman, S., Govers, G., Meire, P., and Wartel, S. (2004). Simulating the long-term development of levee–basin topography on tidal marshes. *Geomorphology*, 63(1-2):39–55.
- Törnqvist, T. E. (1993). *Fluvial sedimentary geology and chronology of the Holocene Rhine-Meuse delta, The Netherlands*. PhD thesis, Utrecht University.
- Törnqvist, T. E. and Bridge, J. S. (2002). Spatial variation of overbank aggradation rate and its influence on avulsion frequency. *Sedimentology*, 49(5):891–905.

- Törnqvist, T. E. and Dijk, G. J. V. (1993). Optimizing sampling strategy for radiocarbon dating of holocene fluvial systems in a vertically aggrading setting. *Boreas*, 22(2):129–145.
- Torres, R. and Styles, R. (2007). Effects of topographic structure on salt marsh currents. *Journal of Geophysical Research: Earth Surface*, 112(F2).
- Van Asselen, S. (2010). *Peat compaction in deltas: implications for Holocene delta evolution*. PhD thesis, Utrecht University.
- Van Asselen, S. (2011). The contribution of peat compaction to total basin subsidence: implications for the provision of accommodation space in organic-rich deltas. *Basin Research*, 23(2):239–255.
- Van der Molen, J. (2002). The influence of tides, wind and waves on the net sand transport in the North Sea. *Continental Shelf Research*, 22(18-19):2739–2762.
- van der Vegt, H. (2018). *From fluvial supply to delta deposits: Simulating sediment delivery, transport and deposition*. PhD thesis, Delft University of Technology.
- Van Dijk, W., Van De Lageweg, W., and Kleinhans, M. (2012). Experimental meandering river with chute cutoffs. *Journal of Geophysical Research: Earth Surface*, 117(F3).
- Van Dijk, W., Van De Lageweg, W., and Kleinhans, M. (2013). Formation of a cohesive floodplain in a dynamic experimental meandering river. *Earth Surface Processes and Landforms*, 38(13):1550–1565.
- Van Dinter, M. (2013). The roman limes in the netherlands: how a delta landscape determined the location of the military structures. *Netherlands Journal of Geosciences*, 92(1):11–32.
- Van Kessel, T., Spruyt-de Boer, A., Van der Werf, J., Sittoni, L., Van Pooijen, B., and Winterwerp, H. (2012). Bed module for sand-mud mixtures. Technical report, Deltares, Delft, The Netherlands.
- Van Rijn, L. C., Walstra, D., and Ormond, M. v. (2004). Description of TRANSPOR2004 and Implementation in Delft3d-ONLINE, FINAL REPORT.
- Van Rijn, L. C., Walstra, D-J, R., and Van Ormond, M. (2007). Unified view of sediment transport by currents and waves. iv: Application of morphodynamic model. *Journal of hydraulic engineering*, 133(6):649–667.
- Vink, A., Steffen, H., Reinhardt, L., and Kaufmann, G. (2007). Holocene relative sea-level change, isostatic subsidence and the radial viscosity structure of the mantle of northwest Europe (Belgium, The Netherlands, Germany, southern North Sea). *Quaternary Science Reviews*, 26(25-28):3249–3275.
- Vos, P. (2015). *Origin of the Dutch coastal landscape: long-term landscape evolution of the Netherlands during the Holocene, described and visualized in national, regional and local palaeogeographical map series*. PhD thesis, Utrecht University.
- Weerts, H. J. and Bierkens, M. F. (1993). Geostatistical analysis of overbank deposits of anastomosing and meandering fluvial systems; Rhine-Meuse delta, The Netherlands. *Sedimentary Geology*, 85(1–4):221–232.
- Wolman, M. G. and Leopold, L. B. (1957). River flood plains: some observations on their formation. Technical report, US Government Printing Office.

A | Reconstruction Old Rhine - Limes



B | Delft3D input files

MDF file

```
Ident = #Delft3D-FLOW 3.59.01.48550#
Commnt =
Filcco = #large_grid.grd#
Anglat = 0.0000000e+000
Grdang = 0.0000000e+000
Filgrd = #large_grid.enc#
MNKmax = 202 202 1
Thick = 1.0000000e+002
Commnt =
Fildep = #depth_012.dep#
Commnt =
Commnt =          no. dry points: 0
Commnt =          no. thin dams: 0
Commnt =
Itdate = #2000-01-01#
Tunit = #M#
Tstart = 0.0000000e+000
Tstop = 2.6208000e+005
Dt = 0.5
Tzone = 0
Commnt =
Sub1 = # I#
Sub2 = # C #
Namc1 = #Sediment_1      #
Namc2 = #Sediment_2      #
Namc3 = #Sediment_3      #
Namc4 = #Sediment_4      #
Namc5 = #Sediment_5      #
Namc6 = #Sediment_6      #
Commnt =
Wnsvwp = #N#
Wdint = #Y#
Commnt =
Zeta0 = 0.0000000e+000
C01 = 0.0000000e+000
C02 = 0.0000000e+000
C03 = 0.0000000e+000
C04 = 0.0000000e+000
C05 = 0.0000000e+000
C06 = 0.0000000e+000
I0 = 0.0000000e+000
Commnt =
Commnt =          no. open boundaries: 4
Filbnd = #bnd_def.bnd#
FilbcT = #timeseries.bct#
Filana = #astr_flow.bca#
FilbcC = #transport.bcc#
```

Rettis = 0.0000000e+000
0.0000000e+000
0.0000000e+000
0.0000000e+000
Rettib = 0.0000000e+000
0.0000000e+000
0.0000000e+000
0.0000000e+000
Commnt =
Ag = 9.8100000e+000
Rhow = 1.0000000e+003
Tempw = 1.5000000e+001
Salw = 3.1000000e+001
Wstres = 6.3000000e-004 0.0000000e+000 7.2300000e-003 1.0000000e+002 7.2300000e-
003 1.0000000e+002
Rhoa = 1.0000000e+000
Betac = 5.0000000e-001
Equili = #N#
Ktemp = 0
Fclou = 0.0000000e+000
Sarea = 0.0000000e+000
Temint = #Y#
Commnt =
Roumet = #C#
Ccofu = 5.0000000e+001
Ccofv = 5.0000000e+001
Xlo = 0.0000000e+000
Vicouv = 1.0000000e+000
Dicouv = 1.0000000e+001
Htur2d = #N#
Irov = 0
Filsed = #sediment.sed#
Filmor = #morph.mor#
Commnt =
Iter = 2
Dryflp = #YES#
Dpsopt = #MAX#
Dpuopt = #MOR#
Dryflc = 1.0000000e-001
Dco = -9.9900000e+002
Tlfsmo = 6.0000000e+001
ThetQH = 0.0000000e+000
Forfuv = #Y#
Forfww = #N#
Sigcor = #N#
Trasol = #Cyclic-method#
Momsol = #Cyclic#
Commnt =
Commnt = no. discharges: 0

Commnt = no. observation points: 5
Filsta = #obs.obs#
Commnt = no. drogues: 0
Commnt =
Commnt =
Commnt = no. cross sections: 2
Filcrs = #cross.crs#
Commnt =
SMhydr = #YYYYY#
SMderv = #YYYYYY#
SMproc = #YYYYYYYYYYY#
PMhydr = #YYYYYY#
PMderv = #YYY#
PMproc = #YYYYYYYYYYY#
SHhydr = #YYYY#
SHderv = #YYYYY#
SHproc = #YYYYYYYYYYY#
SHflux = #YYYY#
PHhydr = #YYYYYY#
PHderv = #YYY#
PHproc = #YYYYYYYYYYY#
PHflux = #YYYY#
Flmap = 0.0000000e+000 1000 2.6208000e+005
Flhis = 0.0000000e+000 30 2.6208000e+005
Flpp = 9.7041600e+006 0 9.7041600e+006
Flrst = 144000
Commnt =
Online = #N#
TraFrm = #vr04.tra#
Cstbnd = #yes#
Commnt =

MOR file

[MorphologyFileInformation]

FileCreatedBy = Delft3D FLOW-GUI, Version: 3.59.01.48550

FileCreationDate = Thu Jun 14 2018, 09:50:16

FileVersion = 02.00

[Morphology]

EpsPar = false Vertical mixing distribution according to van Rijn
(overrules k-epsilon model)

IopKCW = 1 Flag for determining Rc and Rw

RDC = 0.01 [m] Current related roughness height (only used if
IopKCW <> 1)

RDW = 0.02 [m] Wave related roughness height (only used if IopKCW
<> 1)

MorFac = 2.0000000e+002 [-] Morphological scale factor

MorStt = 7.2000000e+002 [min] Spin-up interval from TStart till start of
morphological changes

Thresh = 5.0000001e-002 [m] Threshold sediment thickness for transport and
erosion reduction

MorUpd = true Update bathymetry during FLOW simulation

EqmBc = true Equilibrium sand concentration profile at inflow
boundaries

DensIn = false Include effect of sediment concentration on fluid
density

AksFac = 1.0000000e+000 [-] van Rijn's reference height = AKSFAC * KS

RWave = 2.0000000e+000 [-] Wave related roughness = RWAVE * estimated
ripple height. Van Rijn Recommends range 1-3

AlfaBs = 1.0000000e+000 [-] Streamwise bed gradient factor for bed load
transport

AlfaBn = 1.5000000e+000 [-] Transverse bed gradient factor for bed load
transport

Sus = 1.0000000e+000 [-] Multiplication factor for suspended sediment
reference concentration

Bed = 1.0000000e+000 [-] Multiplication factor for bed-load transport vector
magnitude

SusW = 1.0000000e+000 [-] Wave-related suspended sed. transport factor

BedW = 1.0000000e+000 [-] Wave-related bed-load sed. transport factor

SedThr = 1.0000000e-001 [m] Minimum water depth for sediment
computations

ThetSD = 5.0000000e-001 [-] Factor for erosion of adjacent dry cells

HMaxTH = 1.5000000e+000 [m] Max depth for variable THETSD. Set <
SEDTHR to use global value only

FWFac = 1.0000000e+000 [-] Vertical mixing distribution according to van
Rijn (overrules k-epsilon model)

ISlope = 3.0000000e+000 [-] kf (Koch and Flokstra)

AShld = 0.2

BShld = 0.5

NeuBcSand = true

Espir = 1

[Underlayer]

IUnderLyR = 2
ExchLyr = false
TTLForm = 1
ThTrLyr = 0.1
NLaLyr = 0
NEuLyr = 50
ThLaLyr = 0.1
ThEuLyr = 0.1
IDiffusion = 0
Flufflyr = 0

[Output]

AverageAtEachOutputTime= true
to trim-file
BedTranspDueToCurrentsAtZeta= true

Write mean total transports at each interval

SED file

[SedimentFileInformation]

FileCreatedBy = Delft3D FLOW-GUI, Version: 3.59.01.48550

FileCreationDate = Fri Jun 22 2018, 11:39:17

FileVersion = 02.00

[SedimentOverall]

Cref = 1.6000000e+003 [kg/m3] CSoil Reference density for hindered settling calculations

IopSus = 0 If Iopsus = 1: susp. sediment size depends on local flow and wave conditions

[Sediment]

Name = #Sediment_1# Name of sediment fraction

SedTyp = sand Must be "sand", "mud" or "bedload"

RhoSol = 2.6500000e+003 [kg/m3] Specific density

SedDia = 3.0000000e-004 [m] Median sediment diameter (D50)

CDryB = 1.6000000e+003 [kg/m3] Dry bed density

IniSedThick = 2.0000000e+001 [m] Initial sediment layer thickness at bed (uniform value or filename)

FacDSS = 1.0000000e+000 [-] FacDss * SedDia = Initial suspended sediment diameter. Range [0.6 - 1.0]

[Sediment]

Name = #Sediment_2# Name of sediment fraction

SedTyp = sand Must be "sand", "mud" or "bedload"

RhoSol = 2.6500000e+003 [kg/m3] Specific density

SedDia = 2.5000000e-004 [m] Median sediment diameter (D50)

CDryB = 1.6000000e+003 [kg/m3] Dry bed density

IniSedThick = 1.5000000e+001 [m] Initial sediment layer thickness at bed (uniform value or filename)

FacDSS = 1.0000000e+000 [-] FacDss * SedDia = Initial suspended sediment diameter. Range [0.6 - 1.0]

[Sediment]

Name = #Sediment_3# Name of sediment fraction

SedTyp = sand Must be "sand", "mud" or "bedload"

RhoSol = 2.6500000e+003 [kg/m3] Specific density

SedDia = 1.2500000e-004 [m] Median sediment diameter (D50)

CDryB = 1.6000000e+003 [kg/m3] Dry bed density

IniSedThick = 1.0000000e+001 [m] Initial sediment layer thickness at bed (uniform value or filename)

FacDSS = 1.0000000e+000 [-] FacDss * SedDia = Initial suspended sediment diameter. Range [0.6 - 1.0]

[Sediment]

Name = #Sediment_4# Name of sediment fraction

SedTyp = sand Must be "sand", "mud" or "bedload"

RhoSol = 2.6500000e+003 [kg/m3] Specific density

SedDia = 7.5000000e-005 [m] Median sediment diameter (D50)

CDryB = 1.6000000e+003 [kg/m3] Dry bed density

IniSedThick = 5.0000000e+000 [m] Initial sediment layer thickness at bed (uniform value or filename)

FacDSS = 1.0000000e+000 [-] FacDss * SedDia = Initial suspended sediment
 diameter. Range [0.6 - 1.0]

[Sediment]

Name = #Sediment_5# Name of sediment fraction
 SedTyp = mud Must be "sand", "mud" or "bedload"
 RhoSol = 2.6500000e+003 [kg/m3] Specific density
 SalMax = 0.0000000e+000 [ppt] Salinity for saline settling velocity
 WS0 = 2.5000000e-004 [m/s] Settling velocity fresh water
 WSM = 2.5000000e-004 [m/s] Settling velocity saline water
 TcrSed = 1.0000000e+003 [N/m2] Critical bed shear stress for sedimentation
 (uniform value or filename)
 TcrEro = 2.0000000e-001 [N/m2] Critical bed shear stress for erosion
 (uniform value or filename)
 EroPar = 1.0000000e-004 [kg/m2/s] Erosion parameter (uniform
 value or filename)
 CDryB = 5.0000000e+002 [kg/m3] Dry bed density
 IniSedThick = 5.0000001e-002 [m] Initial sediment layer thickness at bed
 (uniform value or filename)
 FacDSS = 1.0000000e+000 [-] FacDss * SedDia = Initial suspended sediment
 diameter. Range [0.6 - 1.0]

[Sediment]

Name = #Sediment_6# Name of sediment fraction
 SedTyp = mud Must be "sand", "mud" or "bedload"
 RhoSol = 2.6500000e+003 [kg/m3] Specific density
 SalMax = 0.0000000e+000 [ppt] Salinity for saline settling velocity
 WS0 = 1.5000000e-005 [m/s] Settling velocity fresh water
 WSM = 1.5000000e-005 [m/s] Settling velocity saline water
 TcrSed = 1.0000000e+003 [N/m2] Critical bed shear stress for sedimentation
 (uniform value or filename)
 TcrEro = 2.0000000e-001 [N/m2] Critical bed shear stress for erosion
 (uniform value or filename)
 EroPar = 1.0000000e-004 [kg/m2/s] Erosion parameter (uniform
 value or filename)
 CDryB = 5.0000000e+002 [kg/m3] Dry bed density
 IniSedThick = 5.0000001e-002 [m] Initial sediment layer thickness at bed
 (uniform value or filename)
 FacDSS = 1.0000000e+000 [-] FacDss * SedDia = Initial suspended sediment
 diameter. Range [0.6 - 1.0]

C | Classification of Bakker and Schelling (1966)

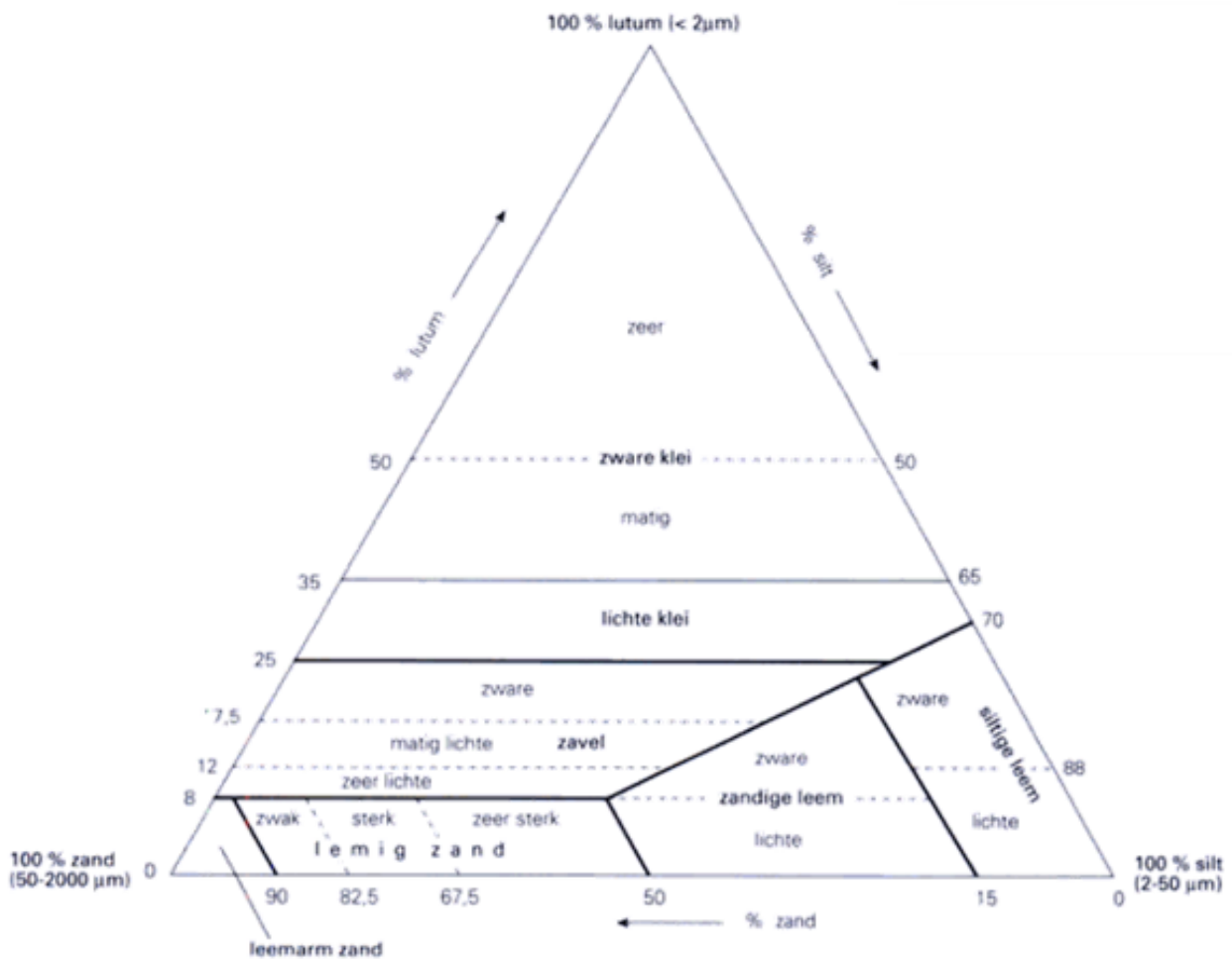
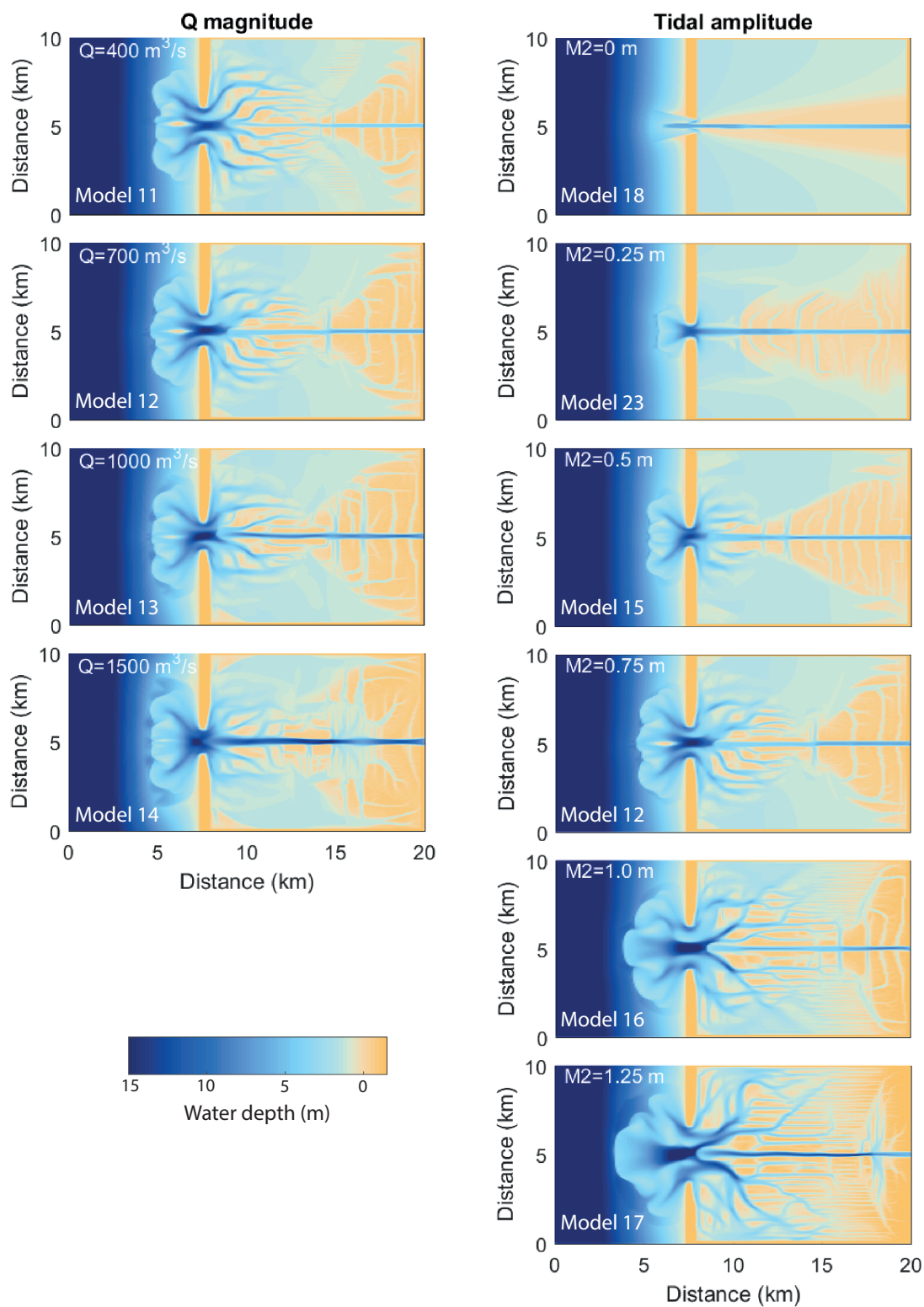


Figure C.1: Lithological classification scheme based on Bakker and Schelling (1966) adjusted by Berendsen (2005)

D | Final bathymetries



E | Levee width based on three methods for different fluvial discharge magnitudes

Figure E.1 depicts the influence of three different methods for levee width determination on the evolution of average levee width under different fluvial discharge magnitudes. Similar trends can be observed in Figure 4.10, which depicts the influence of the three methods on levee width evolution under different tidal amplitudes. The differences in Figure E.1 are however less pronounced. Indicating that the method chosen to determine levee width is especially important in cases where tidal boundary conditions changed.

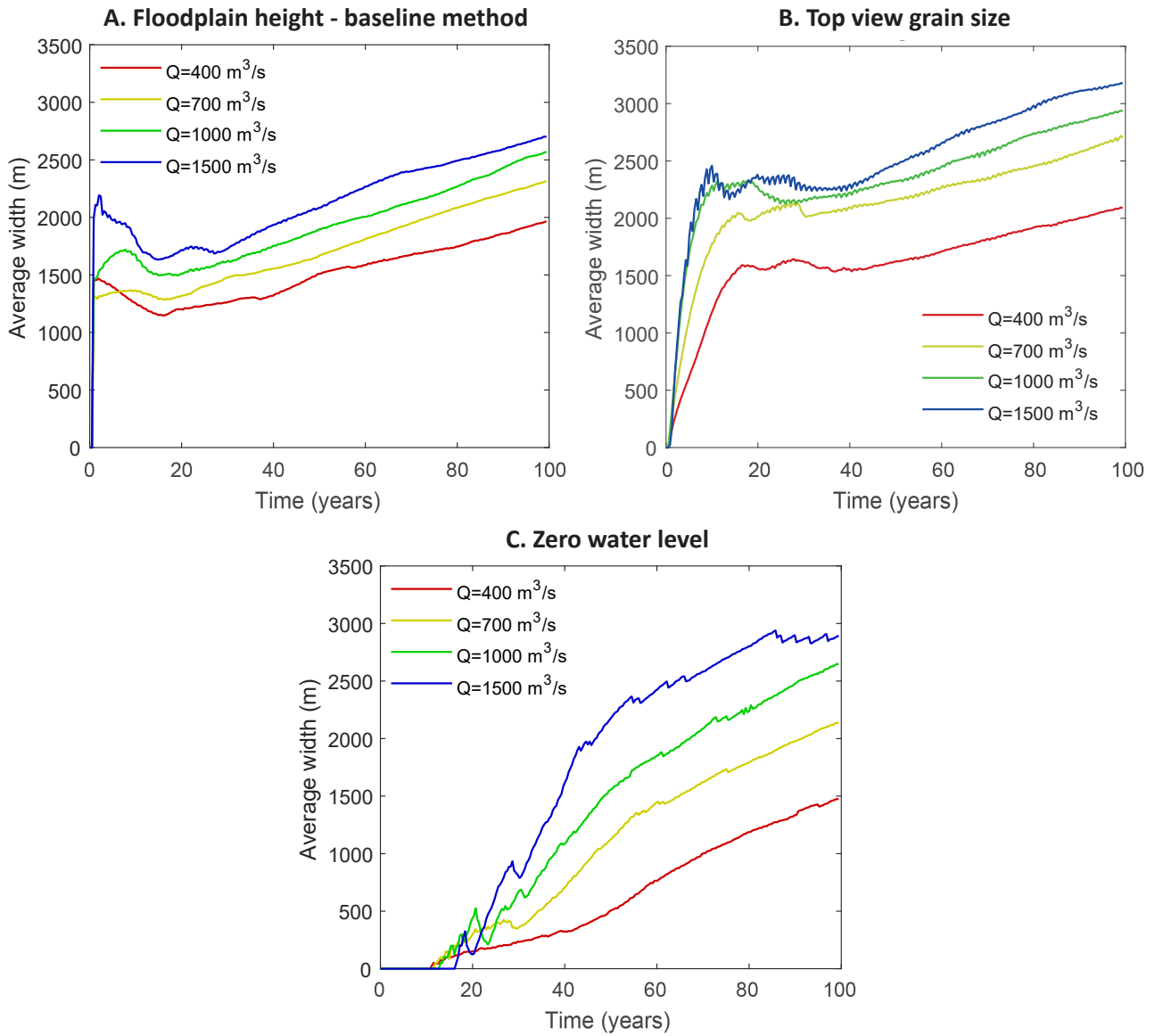
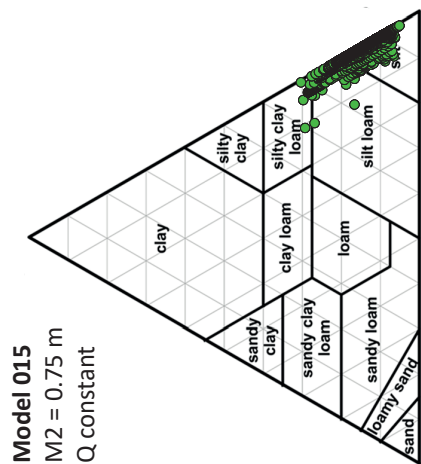
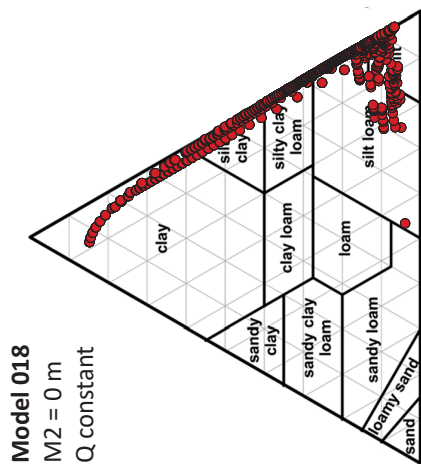
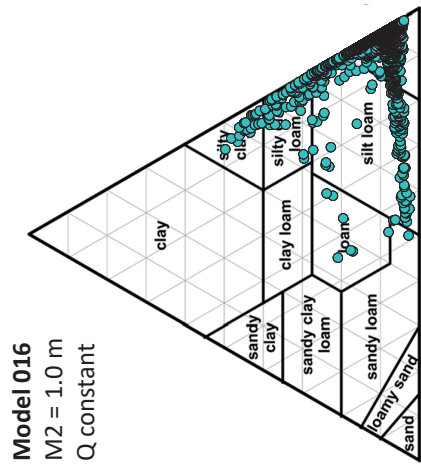
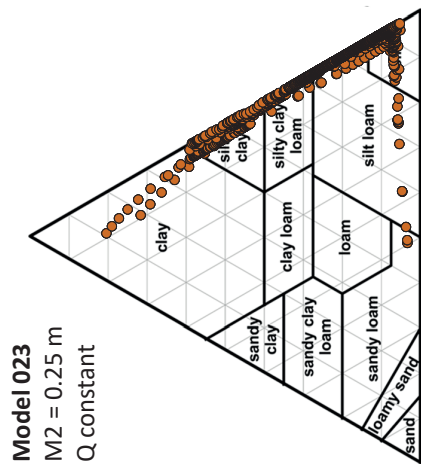
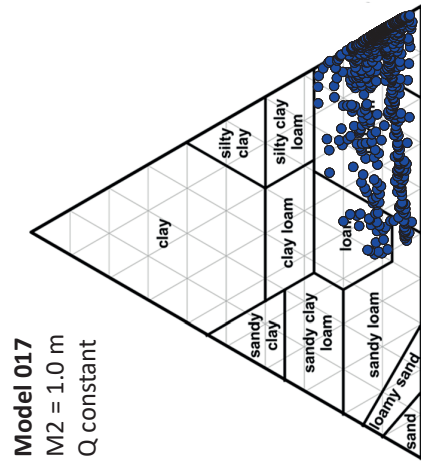
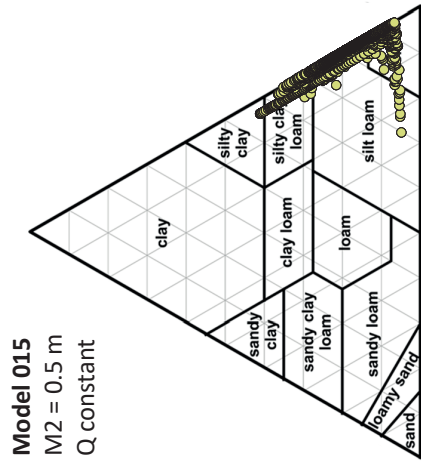


Figure E.1: Average levee width for different discharge magnitude over time calculated based on three different methods; A. floodplain height, B. top view grain size, C. zero water level.

F | Grain size analysis tidal models



G | Sensitivity analysis of the critical shear stress for erosion

G.1 Results sensitivity analysis of the critical shear stress for erosion

The presence of fines is essential for levee formation and sedimentology. In numerical modelling the presence of fines is determined by multiple modelling parameters and formulations. E.g. sediment transport formulations, implementation of multiple sediment fractions and the critical shear stress for deposition and erosion. For the formation of floodplains under tidal influence the critical shear stress for erosion (CSSE) is an important parameter. Therefore, a small sensitivity study has been conducted to test the effects of increasing the critical shear stress for erosion from 0.2 N/m^2 to 0.5 N/m^2 . An overview of the model set-ups that have been rerun with the adjusted shear stress for erosion can be found in Table 3.4. Below the results of the sensitivity analysis will be discussed in the following order; final bathymetry, sedimentology, levee dimensions and crevasse dimensions.

Final bathymetry

In Figure G.1 the final bathymetries of the models with a larger critical shear stress for erosion are displayed next to the corresponding models with a smaller CSSE. The larger CSSE value allows the levee-crevasse complex to grow in downstream direction (Figure G.1, model 39 till model 42). In addition, the width of the levee-crevasse complex seems to be larger for the models with a larger CSSE. This will be discussed in further detail below. The crevasses that breach the levee complexes have a different configuration in the case of a larger CSSE. They seem to be more oriented towards the land side of the basin and bifurcate more often (see Figure G.1, model 39 and model 40). Despite the differences, the change in final bathymetry as a result of a larger CSSE is small. The ebb deltas in the models with a larger CSSE are of equal size and shape as in the models with a CSSE and the levee complexes have similar shapes.

Sedimentology

When comparing the final top view grain size for the two CSSE values (Figure G.2) two important differences can be noticed. First, in the models with smaller tidal amplitudes more clay is present in the basin for the runs with a larger CSSE. Second, in the models with larger tidal amplitudes an increase in silt can be observed in the basin. The area where extra silt is observed corresponds to the areas where levee width increased in Figure G.1. Despite the two important differences the change in top view sedimentology as a result of a larger CSSE is small. Silt is still the main grain size in the levees, clay forms the floodplains in cases with smaller tidal amplitudes and clay is absent in the floodplain when tidal amplitude is larger than 0.5 m.

Levee dimensions

Levee height in models with a CSSE of 0.5 N/m^2 experiences the same evolution as in models with a CSSE of 0.2 N/m^2 (Figure G.3-A). Small deviations in evolution occur for the runs with variable discharge and large tidal amplitudes ($\geq 0.75 \text{ m}$). In these models the evolution is faster for models with a CSSE of 0.5 N/m^2 . Final levee heights between the two CSSE values are comparable, deviations are present on a scale of several centimetres. With most levees being slightly higher under a CSSE of 0.5 N/m^2 . The only exception is formed under the no tide condition (Figure G.3-A, red line).

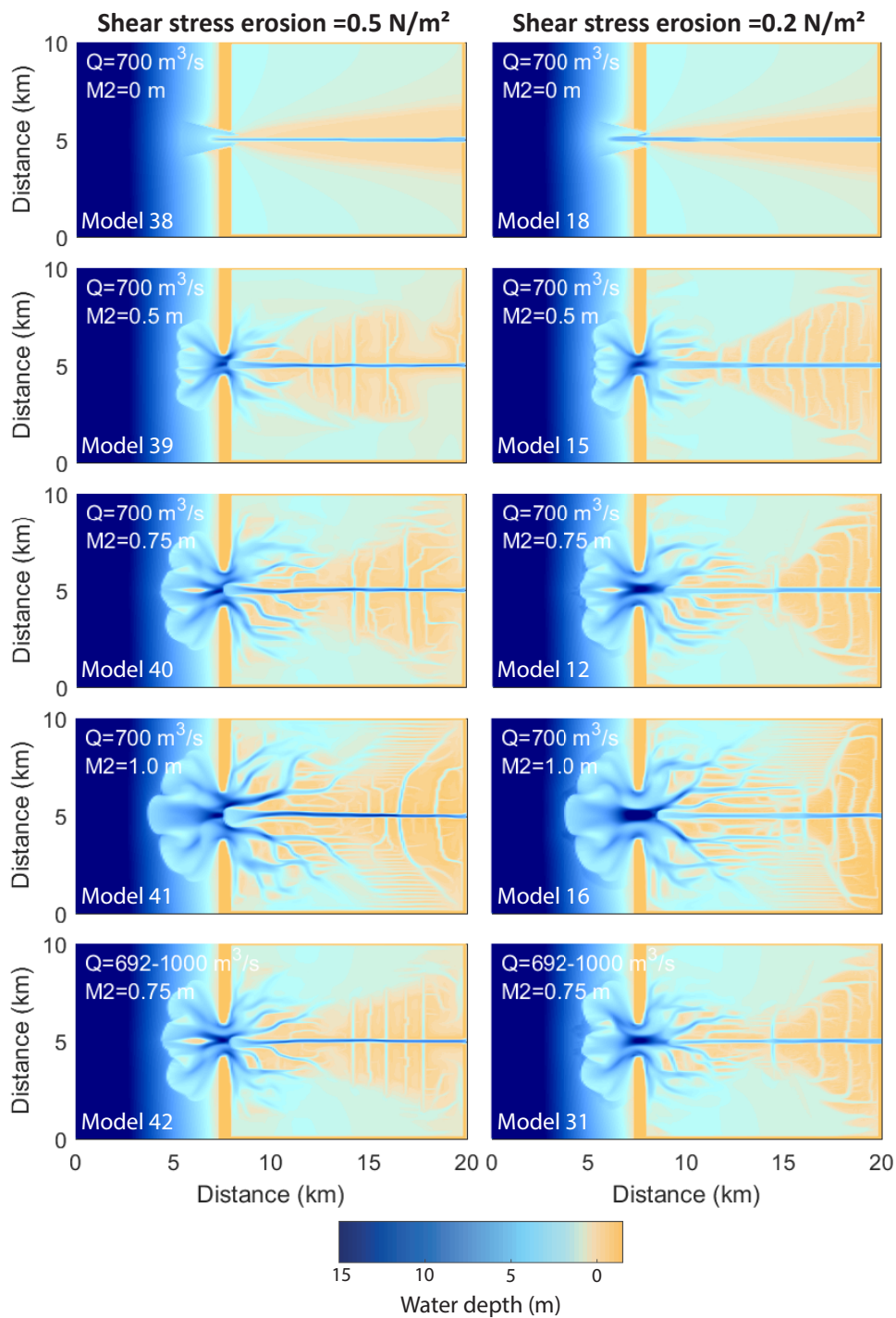


Figure G.1: Final bathymetry for chosen models to test the effects of the critical shear stress for erosion. Left column presents the bathymetries with a critical shear stress for erosion of 0.2 N/m^2 (default value in this thesis). Right column presents the bathymetries with a critical shear stress for erosion of 0.5 N/m^2 .

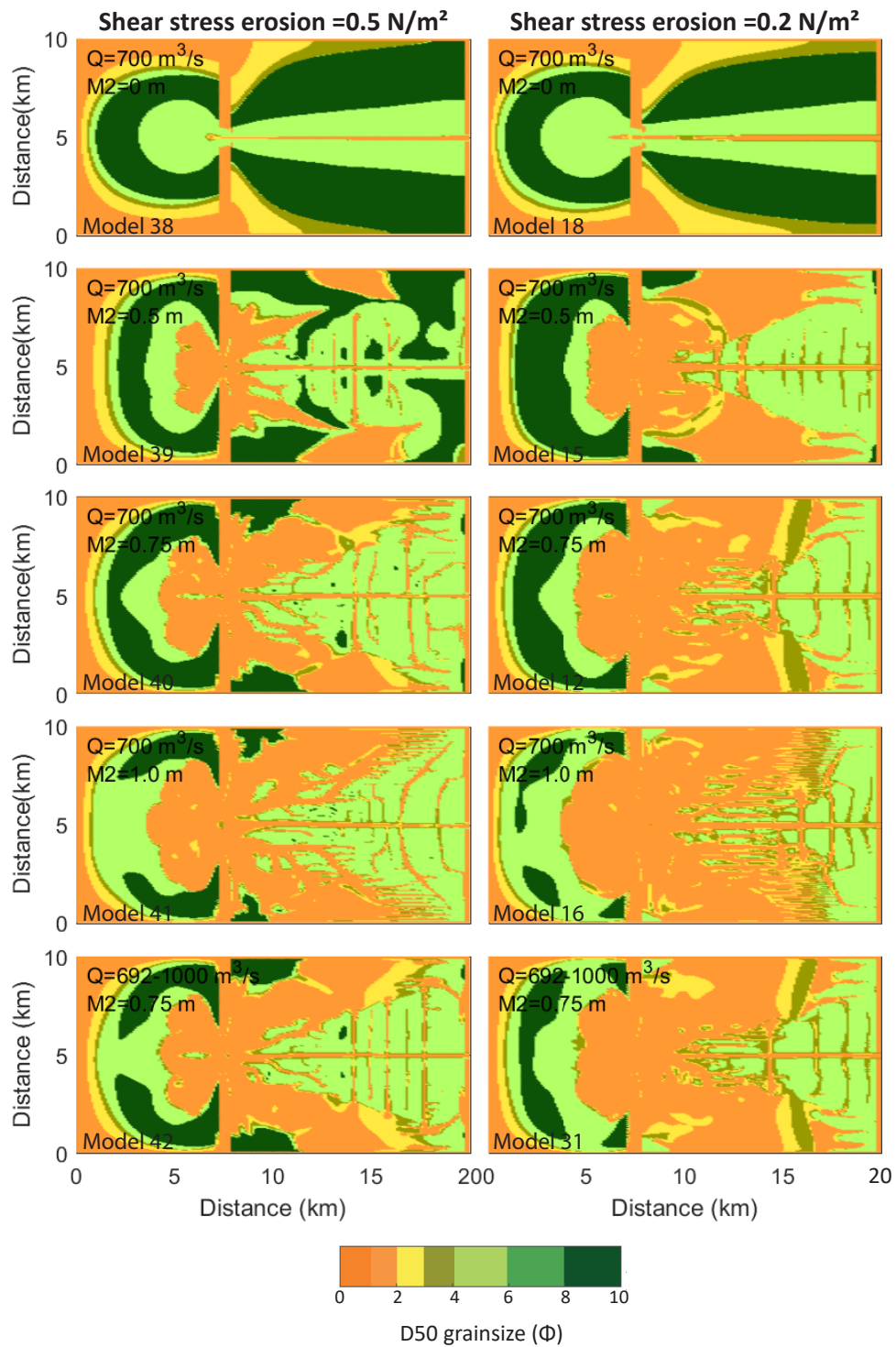


Figure G.2: Final top view D50 grainsize for chosen models to test the effects of the critical shear stress for erosion. Left column presents the top view D50 grainsizes with a critical shear stress for erosion of 0.2 N/m^2 (default value in this thesis). Right column presents the D50 grainsizes with a critical shear stress for erosion of 0.5 N/m^2 .

Hypsometric results of final cross-sections over the levee crests in the direction of the main channel are slightly different when models are run with an CSSE of 0.5 N/m^2 instead of 0.2 N/m^2 (Figure G.3-B). The hypsometric curve is elevated when a CSSE of 0.5 N/m^2 is applied for all runs with tidal amplitudes of $0.5 - 0.75 \text{ m}$ including the variable discharge case. Implying that for these runs not only the maximum levee height is higher but the entire levee is elevated. For the model without tide and with a tidal amplitude of 1 m , an CSSE of 0.5 N/m^2 results in a lower hypsometric curve.

Levee width, based on floodplain height, changes when the CSSE is increased from 0.2 N/m^2 to 0.5 N/m^2 . Increasing the CSSE results in slightly wider levees (Figure G.3-C). Except for the case with a tidal amplitude of 0.5 m . This deviation can be explained based on the final bathymetry (Figure G.1, model 39). The final bathymetry shows a very narrow levee between 16 and 20 km .

Crevasse dimensions

The cross-sectional crevasse area changes significantly when the CSSE is increased from 0.2 N/m^2 to 0.5 N/m^2 . A larger CSSE results in smaller cross-sectional crevasse area for all models over almost all time steps (Figure G.3-D). The explanation for this decrease is directly linked to the increase in the CSSE. The CSSE determines under which shear stress the bed will erode. When conditions are similar a larger CSSE thus results in less erosion and therefore less deep and wide crevasse channels.

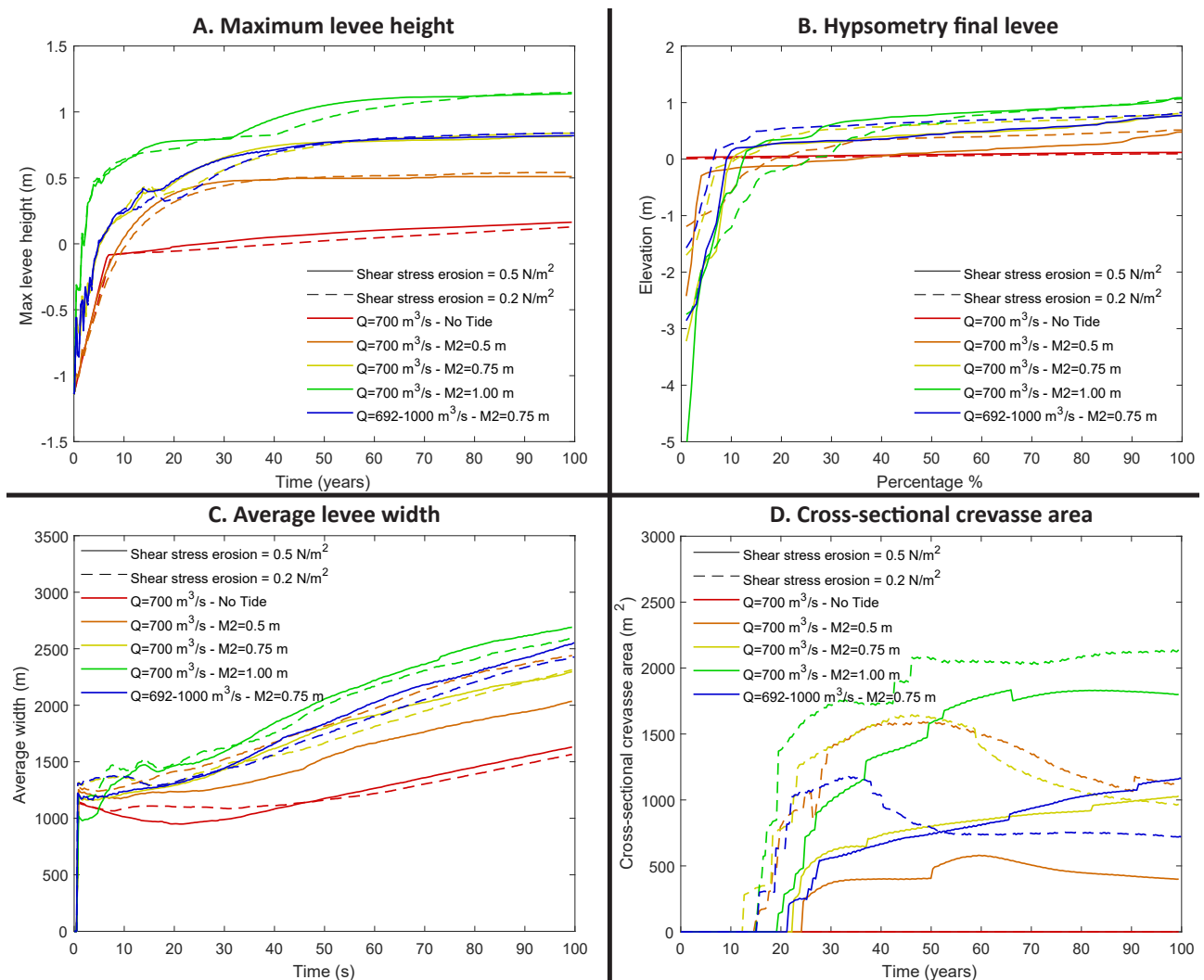


Figure G.3: Levee and crevasse dimensions for chosen models to test the effects of the critical shear stress for erosion. A. maximum levee height, B. hypsometry of final levee crest, C. average levee width, based on floodplain height (baseline method), D. cross-sectional crevasse area.

G.2 Discussion sensitivity analysis of the critical shear stress of erosion

As described above the presence of fines is essential for levee and floodplain formation and stratigraphy. Especially when tides are present and energy in the basin is larger. Due to the large effect of the CSSE parameter on the occurrence of fines, a small sensitivity study was executed in which the CSSE was increased from 0.2 N/m^2 to 0.5 N/m^2 . General morphological development of the levee-crevasse complex is similar for CSSE values of 0.2 N/m^2 and 0.5 N/m^2 (Figure G.1). The overall shape of the levee-crevasse complex remains similar. However, the planform of the crevasses seems to change under higher CSSE values, with more bifurcations and different distal directions. Further, the transition from levee to floodplain is smoother for the larger CSSE value.

Levee height is similar for the two CSSE values, with only small differences in the order of a few centimetres. This observation is not unexpected as Figure 4.8 has shown that levee height is bounded by the maximum water level. On the contrary, levee width generally increases for larger CSSE values. Which can be explained by the function of the CSSE parameter. CSSE controls the erosion of already deposited sediments. Under higher CSSE values, the shear stress must be larger for sediment to erode again, enabling the sediments on the edge of the sediments to remain in position.

To summarize, the CSSE parameter has a significant effect on the development of levee width and on the development of the floodplain area in the model. Trends in levee width under different boundary conditions however remain similar for different CSSE values. Therefore, the main findings of this thesis would not differ if all models were run with a different CSSE value. One could argue that when the development of floodplain area and the connection of floodplain to levee appear to be important for longer term morphological development of fluvial-tidal basins a CSSE value of 0.5 N/m^2 is preferable.

H | Core logs

Coördinaten		Hoogte	Diepte	KAARTEENHEID	Geomorfogenetische kaart:	
Xco	Yco	Z [m]	[cm]	Geologische kaart:	Grondwatertrap:	
107733	459219	-1.45	620	Begroeiingskaart:	Bodemkaart:	

Alphen aan den Rijn, halverwege kom (200-300 m vanaf de weg)
Kerkvaartspad 40, perceel met wandelpad

Diepte	Textuur	Org	Plr	Kleur	Redox	Grind	M50	Ca	Fe	GW	M	LKL	Strat	Bijzonderheden
10	Z-LK			br	o			0	1					ger. bijmenging zand
20	Z-LK			br	o			0	1					ger. bijmenging zand
30	Z-LK			br	o			0	1					ger. bijmenging zand
40	Z-LK			brgr	or			0	1					ger. bijmenging zand
50	Z-LK			brgr	or			0	1					
60	Z-LK		h	brgr	or			0	1	GW				
70								0	0		x			GM, kern gestoken voor
80	ZK	H2	h	brgr	r			0	0		x			overgang KR fase naar
90	ZK	H2	h	brgr	r			0	0		x			veen eronder
100	ZK	H2	h	brgr	r			0	0		x			
110		V1	h	grbr	r			0	0		x			
120		V1	h	grbr	r			0	0		x			
130		V1	h	grbr	r			0	0		x			
140		V1	h	grbr	r			0	0		x			# takje
150		V1	hr	gr	r			0	0					
160	MK		plr	gr	r			0	0					Graduele overgang naar V1
170	MK		plr	gr	r			1	0					
180	LK		rh	gr	r			1	0					
190	LK		rh	gr	r			1	0					
200	LK			lgr	r			1	0					
210								1	0					GM
220								1	0					# GM
230	LK	H0	rh	gr	r			1	0					Veel planten resten
240	LK	H0	rh	gr	r			1	0					^
250	MK		plr	gr	r			1	0					
260	MK		plr	gr	r			1	0					
270	MK		plr	gr	r			1	0					
280	MK		plr	gr	r			1	0					
290	MK		plr	gr	r			2	0					Weinig planten resten
300									0					# GM
310	ZZL		plr	gr	r			2	0					Laminatie kleur (humeus?)
320	ZZL		plr	gr	r			2	0					Slap, laminatie
330	ZZL		plr	gr	r			2	0					Laminatie kleur (humeus?)
340	ZZL		plr	gr	r			2	0					Laminatie kleur (humeus?)
350	ZZL		plr	gr	r			2	0					Takjes, laminaties
360	ZZL		plr	gr	r			2	0					laminaties kleur (humeus?)
370	ZZL		plr	gr	r			2	0					laminaties kleur (humeus?)
380	ZZL		plr	gr	r			2	0					# schelp gruis
390	ZZL		plr	dgr	r			2	0					schelp gruis
400	LK		plr	dgr	r			2	0					schelp gruis
410	ZZL		plr	dgr	r			2	0					schelp (slakje)
420	ZZL		plr	dgr	r			2	0					schelp gruis
430	ZZL		plr	dgr	r			0	0					ZZL wordt grover naar beneden
440	ZZL		plr	dgr	r			0	0					
450		V1		br	r			0	0					
460		V2		br	r			0	0					#
470		V2	r	br	r			0	0					Zegge???
480		V2	r	br	r			0	0					
490		V1	r	br	r			1	0					
500	MK	H2	r	grbr	r			2	0					Meer compact dan bovenstreams
510	MK		r	gr	r			2	0					slapper
520	LK		r	gr	r			2	0					schelp gruis
530	LK		r	lgr	r			2	0					schelp gruis
540	LK	H1	r	lgr	r			1	0					#
550	LK	H1	r	brgr	r			0	0					humeuze bandjes
560	LK	H2	r	brgr	r			1	0					
570	ZZL		r	gr	r			2	0					
580	LZ		r	gr	r			2	0					Schelp gruis, snelle overgang
590	LZ		plr	gr	r			2	0					hor. riet (event??)
600	LZ		plr	gr	r			2	0					klei bandjes

Boring: 201801009

Diepte	Textuur	Org	Plr	Kleur	Redox	Grind	M50	Ca	Fe	GW	M	LKL	Strat	Bijzonderheden
610	LZ		plr	gr	r			2	0					material wordt grover
620	LZ		plr	gr	r			2	0					roots

Einde boring: 201801009

Boorpunt: 201801010

Namen: Pierik, Moree, Roelof

Jaar: 2018

Groep: 01

Datum: 11-9-2018

Coördinaten		Hoogte	Diepte	KAARTEENHEID	Geomorfogenetische kaart:	
Xco	Yco	Z [m]	[cm]	Geologische kaart:	Grondwatertrap:	
107648	459062	-1.2	430	Begroeiingskaart:	Bodemkaart:	

Oever 1, kerkvaarderspad Alphen aan den Rijn

Boring +/- 100 m van de weg

Acc GPS = 7 m

Diepte	Textuur	Org	Plr	Kleur	Redox	Grind	M50	Ca	Fe	GW	M	LKL	Strat	Bijzonderheden
10	ZK			brgr	o			0	0					
20	ZK			brgr	o			0	0					
30	ZK			brgr	o			0	1					
40	ZK			brgr	o			0	1		x			Houtskool, sed samples
50	ZK			gr	or			1	1		x			sed samples
60	LK			gr	or			1	1		x			sed samples
70	LK			gr	or			1	1		x			sed samples, mng spots
80	LK		plr	gr	or			1	0		x			sed samples
90	LK		plr	brgr	or			1	0		x			sed samples
100	LK	H2	h	brgr	r			0	0	GW				
110	LK	H1	r	brgr	r			0	0					#
120	LK	H1	r	brgr	r			0	0					sed samples
130	ZZL	H0	plr	lbrgr	r			0	0		x			
140	ZZL	H0	r	gr	r			2	0					
150	ZZL	H0	r	gr	r			2	0					verticaal riet
160	ZZL	H0	plr	gr	r			2	0					
170	ZZL	H0	plr	gr	r			2	0					
180	ZZL	H0	plr	gr	r			2	0					
190	ZZL	H0	plr	gr	r			2	0		x			# sed samples
200	ZZL	H0	r	gr	r			2	0					#
210	ZZL	H0	r	gr	r			2	0		x			sed samples
220	ZZL	H0	h	gr	r			2	0					
230	ZZL	H0	r	gr	r			2	0					
240	LK		plr	gr	r			2	0		x			sed samples
250	ZZL		plr	gr	r			2	0		-x			begin kern
260	ZZL		plr	gr	r			0	0		x			# hout
270	ZZL	H1	h	brgr	r			0	0		x			
280	ZZL	H1	h	brgr	r			0	0		x			
290	ZZL	H1	h	brgr	r			0	0		x			
300	ZZL	H2	h	brgr	r			0	0		x			
310	ZZL	H2	h	brgr	r			0	0		x			
320		V1	r	br	r			0	0		x			/ 5 geleidelijke overgang
330		V2	h	br	r			0	0		x			
340		V2	r	br	r			0	0		x			# clay layer 1 cm
350		V1	plr	br	r			0	0		x			#
360	ZZL		plr	blgr	r			2	0					/4 geleidelijke overgang
370	ZZL			blgr	r			2	0					minder humeus
380	ZZL		r	blgr	r			2	0					^
390	ZZL		r	blgr	r			2	0					
400	ZZL			blgr	r			2	0					
410	ZZL		r	blgr	r			2	0					
420	ZZL		r	blgr	r			2	0					
430	ZZL		r	blgr	r			2	0					meer humeus

Einde boring: 201801010

Boorpunt: 201801011

Namen: Pierik,Roelofs,Boech

Jaar: 2018

Groep: 01

Datum: 12-9-2018

Coördinaten		Hoogte	Diepte	KAARTEENHEID	Geomorfogenetische kaart:	
Xco	Yco	Z [m]	[cm]	Geologische kaart:	Grondwatertrap:	
107808	459373	-1.5	470	Begroeiingskaart:	Bodemkaart:	

Kerkvaarderspad 40, Alphen aan den Rijn
 Ver het weiland in (400-600 m vanaf de weg)
 Acc. GPS = 5.9 m

Diepte	Textuur	Org	Pir	Kleur	Redox	Grind	M50	Ca	Fe	GW	M	LKL	Strat	Bijzonderheden
10	LK			brgr	o			0	1					zand. bijm.
20	LK			brgr	o			0	1					zand. bijm.
30	LK			brgr	o			0	1					
40	LK			brgr	o			0	1					
50	LK			dbgrgr	or			0	1					tikje humeus
60	MK	H2		grbr	or			0	0					
70	MK	H2		grbr	r			0	0					baksteentjes, decomposed peat
80		V2	h	br	r			0	0					
90		V2	h	br	r			0	0					
100		V2	h	br	r			0	0					
110		V2	h	br	r			0	0					
120		V2	h	br	r			0	0					
130		V2	h	br	r			0	0					
140		V2	h	br	r			0	0					
150		V2	h	br	r			0	0					#
160		V2	h	br	r			0	0					Clayey peat with a lot of wood
170		V2	h	br	r			0	0					Clayey peat with a lot of wood
180		V2	h	br	r			0	0					Clayey peat with a lot of wood
190		V1	h	grbr	r			0	0					Clayey peat with a lot of wood
200		V2	h	br	r			0	0					Clayey peat with a lot of wood
210		V2	h	br	r			0	0					Clayey peat with a lot of wood
220		V2	h	br	r			0	0					Clayey peat with a lot of wood
230		V2	h	br	r			0	0					#
240		V2	h	br	r			0	0					
250		V2	h	dbr	r			0	0					Maybe a bit of oxidation
260		V2	h	br	r			0	0					
270		V2	h	br	r			0	0					
280		V2	r	br	r			0	0					
290		V2	r	br	r			0	0					Slap, riet, sharp contact
300														GM
310														# GM
320	LK		r	blgr	r			2	0					siltig, schelp gruis, sticky
330	LK		r	blgr	r			2	0					siltig, schelp gruis, sticky
340	LK		r	blgr	r			2	0					siltig, schelp gruis, sticky
350	LK		r	blgr	r			2	0					siltig, schelp gruis, sticky
360	LK		r	blgr	r			2	0					siltig, schelp gruis, sticky
370	LK		r	blgr	r			2	0					siltig, schelp gruis, sticky
380	LK		r	blgr	r			2	0					siltig, schelp gruis, sticky
390	LK		r	blgr	r			2	0					siltig, schelp gruis, sticky
400	LK		r	blgr	r			2	0					# siltig, schelp gruis, sticky
410	LK			blgr	r			2	0					siltig, schelp gruis, sticky
420	LK			blgr	r			2	0					siltig, schelp gruis, sticky
430	LK			blgr	r			2	0					siltig, schelp gruis, sticky
440	LK			blgr	r			2	0					siltig, schelp gruis, sticky
450	LK			blgr	r			2	0					siltig, schelp gruis, sticky
460	LK			blgr	r			2	0					siltig, schelp gruis, sticky
470	LK			blgr	r			2	0					# siltig, schelp gruis, sticky

Einde boring: 201801011

Boorpunt: 201801013

Namen: Pierik,Moree,Roelofs

Jaar: 2018

Groep: 01

Datum: 12-9-2018

Coördinaten		Hoogte	Diepte	KAARTEENHEID	Geomorfogenetische kaart:	
Xco	Yco	Z [m]	[cm]	Geologische kaart:	Grondwatertrap:	
124019	457749	-0.47	370	Begroeiingskaart:	Bodemkaart:	

Houtdijk 17, Woerden

Op oever dicht bij sloot&huis (tussen boring 019&018 van Stouthamer profiel)

Acc. 3.5

Diepte	Textuur	Org	Plr	Kleur	Redox	Grind	M50	Ca	Fe	GW	M	LKL	Strat	Bijzonderheden
10	Z-MK			dbgrgr				0	0					ger
20	Z-MK			dbgrgr				0	0					ger
30	Z-MK			dbgrgr				0	1					ger
40	MK			brgr				0	1					
50	MK			brgr				0	1					
60	MK			brgr				0	1					
70	MK			brgr				1	1		x			
80	MK			brgr				0	1					
90	MK			brgr				1	1					
100	MK	H0	plr	dbgrgr				1	1					
110	ZK	H2	plr	dbgrgr				2	1					
120	ZK		r	gr				2	1					
130	ZZL		plr	gr				2	1					vert. wortel
140	ZZL		plr	gr				2	0					
150	MZL		plr	gr				2	0	GW				
160	MZL			gr				2	0					
170	MZL			gr				2	0					licht geband mm zand
180	MZL			gr				2	0					schelp gr
190	MZL		h	gr				2	0					zand laagje
200	LK			gr				2	0					
210	ZZL			gr				2	0					#
220	ZZL			gr				2	0					Zandband cm
230	LZ			gr				2	0		x			UFZ
240	MZL			gr				2	0		x			
250	MZL			gr				2	0					zeer sterk geband zand mm
260	MZL			gr				2	0					zeer sterk geband zand mm
270	MZL			gr				2	0					detritus bandje, zand band mm
280	ZZL		plr	gr				2	0					detritus bandje, verslagen r/h
290	LK		plr	gr				2	0					#
300	ZZL		plr	gr				2	0					detritus
310	ZZL		h	gr				2	0					houtje, sterk geband
320	LK		plr	gr				2	0					sterk geband
330	MK	H1	plr	gr				1	0		x			r&h, h bandje, schelp gr
340	MK	H1	plr	gr				1	0					H bandje zwart, r, schelp gr
350	MK	H1	plr	gr				1	0					
360		V1	plr	grbr				0	0					geleidelijke overgang naar 360
370		V1	plr	grbr				0	0					#

Einde boring: 201801013

Coördinaten		Hoogte	Diepte	KAARTEENHEID	Geomorfogenetische kaart:	
Xco	Yco	Z [m]	[cm]	Geologische kaart:	Grondwatertrap:	
124011	457810	-0.78	560	Begroeiingskaart:	Bodemkaart:	

Houtdijk 17, Woerden
 Boring 18 uit profiel Stouthamer
 Op de hoek van het bosje

Diepte	Textuur	Org	Plr	Kleur	Redox	Grind	M50	Ca	Fe	GW	M	LKL	Strat	Bijzonderheden
10	ZK			gr	o			0	1					
20	ZK			gr	o			0	1					
30	ZK			gr	o			0	1					
40	MK			gr	o			0	1					
50	MK		r	gr	o			0	1					
60	MK		plr	gr	or			0	2					
70	MK		plr	gr	or			0	2					
80	MK	H2	plr	grbr	r			0	0					geleidelijke overgang
90	MK	H2	plr	grbr	r			0	0					riet, takjes
100	MK	H2	hr	grbr	r			0	0					verkoold hout, takjes
110		V1	hr	br	r			0	0					hout stuk
120		V1	hr	br	r			0	0					
130		V1	hr	br	r			0	0					#
140	MK		plr	gr	r			2	0					stuk hout
150	MK		plr	gr	r			2	0					versp riet
160	MK		plr	gr	r			2	0					versp riet
170	LK	H0	plr	gr	r			2	0					hum, detri. bandjes (mm)
180	LK		plr	gr	r			2	0					sch. gr
190	LK		plr	gr	r			2	0					slap
200														# GM
210	LK		plr	gr	r			2	0					# Slap detr. bandje
220	LK		plr	gr	r			2	0					detr. band, schgr, versp h r
230	LK		plr	gr	r			2	0					detr. band, schgr, versp h r
240	LK		plr	gr	r			2	0					detr. band, schgr, versp h r
250	LK		plr	gr	r			2	0					dikker detr. bandjes, schgr
260	LK		plr	gr	r			2	0					versp h, schgr
270	LK		plr	gr	r			2	0					dikker detr. bandjes, schgr
280	LK		plr	gr	r			2	0					#
290	LK	H1	plr	br	r			0	0					#schgr, versp plr, gel. overga
300		V2	hr	br	r			0	0					bosveen houtriet, compact
310		V2	hr	br	r			0	0					
320	LK	H2	hr	grbr	r			0	0					stevig
330	LK	H1	hr	grbr	r			0	0					
340	LK	H1	hr	grbr	r			0	0					
350	LK	H1	hr	grbr	r			0	0					
360		V2	plr	br	r			0	0					# hout, compact
370		V2	plr	br	r			0	0					#
380		V2	plr	br	r			0	0					
390		V2	plr	br	r			0	0					
400		V2	plr	br	r			0	0					
410		V3	plr	br	r			0	0					Hout
420		V3	plr	br	r			0	0					Hout
430		V3	plr	br	r			0	0					Hout
440		V3	plr	br	r			0	0					#Hout
450		V3	plr	br	r			0	0					#Hout
460		V3	plr	br	r			0	0					Hout
470		V3	plr	br	r			0	0					Hout
480		V3	plr	br	r			0	0					Hout
490		V3	plr	br	r			0	0					Hout
500		V3	plr	br	r			0	0					Hout
510		V3	plr	br	r			0	0					Riet
520		V3	plr	br	r			0	0					Riet
530		V3	plr	br	r			0	0					#Riet
540		V3	plr	br	r			0	0					#Riet
550		V3	plr	br	r			0	0					Riet
560		V3	plr	br	r			0	0					Riet

Boorpunt: 201801016

Namen: Roelofs,BoechatAlber

Jaar: 2018

Groep: 01

Datum: 13-9-2018

Coördinaten		Hoogte	Diepte	KAARTEENHEID	Geomorfogenetische kaart:	
Xco	Yco	Z [m]	[cm]	Geologische kaart:	Grondwatertrap:	
97480	460864	-1.1	370	Begroeiingskaart:	Bodemkaart:	

Hazerswoude, Houtdijk 5a, Trees
 Naast grote sloot voor perceel Heineken (meest distale boring)
 Acc. GPS=3.7 m

Diepte	Textuur	Org	Plr	Kleur	Redox	Grind	M50	Ca	Fe	GW	M	LKL	Strat	Bijzonderheden
10	ZZL		plr	brgr	o			0	1					ger, zandige bijmeng
20	ZZL		plr	brgr	o			0	1					
30	LK		plr	brgr	o			0	1					
40	LK		plr	brgr	o			0	1					
50	LK		plr	brgr	or			0	1					
60	LK		plr	brgr	or			0	1					
70	LK		plr	brgr	r			0	0	GW				
80	LK	H1	r	brgr	r			0	0					
90	LK	H1	r	brgr	r			0	0					
100	LK	H0	r	brgr	r			0	0					
110	LK	H0	r	brgr	r			0	0					
120	LK	H0	plr	brgr	r			0	0					
130	LK	H1	h	brgr	r			0	0					
140	LK	H1	h	brgr	r			0	0					#
150	ZK	H1	h	grbr	r			0	0					grad. overgang /5
160		V1	hr	br	r			0	0					
170		V1	r	br	r			0	0					
180		V2	h	br	r			0	0					
190		V2	r	br	r			0	0					klei bandjes tussen het pure v
200		V2	r	br	r			0	0					klei bandjes tussen het pure v
210		V1	r	br	r			0	0					
220		V1	r	br	r			0	0					# bandjes, hor r
230	LK	H2	r	br	r			1	0					
240	MK		r	blgr	r			1	0					
250	MK		r	blgr	r			1	0					Zandlaagje 0.4 mm
260	MK		r	blgr	r			2	0					
270	MK		r	blgr	r			2	0					
280	LK		r	blgr	r			2	0					Sticky, stiffer
290	ZZL		r	blgr	r			2	0					Schelp gr
300	ZZL		r	blgr	r			2	0					#Schelp gr
310	ZZL		r	blgr	r			2	0					
320	MZL		r	blgr	r			2	0					
330	LZL		r	blgr	r			2	0					
340	LZ		r	blgr	r			2	0					
350	LZ		r	blgr	r			2	0					Humic band
360	UFZ		r	blgr	r		50-105	2	0					
370	LZ		r	blgr	r			2	0					# klei bandje

Einde boring: 201801016

Boorpunt: 201801017

Namen: Pierik,Moree,McMahon

Jaar: 2018

Groep: 01

Datum: 13-9-2018

Coördinaten		Hoogte	Diepte	KAARTEENHEID	Geomorfogenetische kaart:	
Xco	Yco	Z [m]	[cm]	Geologische kaart:	Grondwatertrap:	
97496	460891	-1.15	460	Begroeiingskaart:	Bodemkaart:	

Hazerswoude, Houtdijk 5a, bij Trees
 Oeverwal dicht bij limesweg (meer proximaal dan 20180116)
 Acc. GPS = 7.9 m

Diepte	Textuur	Org	Plr	Kleur	Redox	Grind	M50	Ca	Fe	GW	M	LKL	Strat	Bijzonderheden
10	ZZL			dbgr	o			0						geroerd
20	ZZL			dbgr	o			0						
30	LK			gr	or			0	1					
40	LK			gr	or			0	1					
50	LK			gr	or			0	1					
60	LK			gr	or			0	1	GW				
70				gr	or			0	1					# GM
80	LK		plr	gr	or			0	1					
90	LK		plr	gr	r			0	0					
100	LK		plr	gr	r			0	0					takjes
110	LK		r	gr	r			0	0					takjes
120	LK		r	gr	r			0	0					takjes
130	LK		plr	gr	r			0	0					
140	LK		plr	gr	r			0	0					#
150	LK		plr	gr	r			0	0					#
160	ZK	H1	plr	dgr	r			0	0					
170	ZK	H1	plr	dgr	r			0	0					
180	ZK	H1	h	dgr	r			0	0					hout stuk
190		V1	h	grbr	r			0	0					riet & hout stuk
200		V2	r	grbr	r			0	0					riet
210		V1	r	grbr	r			0	0					riet
220		V1	r	grbr	r			0	0					# riet
230		V1	r	dbr	r			0	0					#
240		V1	r	dbr	r			0	0					
250	LK		r	zw	r			0	0					
260	LK		r	blgr	r			2	0					
270	LK		r	blgr	r			2	0					mm z band H0
280	LK		r	blgr	r			2	0					
290	LK		r	blgr	r			2	0					
300	LK		r	blgr	r			2	0					#
310	ZZL		r	blgr	r			2	0					#
320	ZZL		r	blgr	r			2	0					
330	ZZL		r	blgr	r			2	0					
340	ZZL		r	blgr	r			2	0					
350	MZL		r	blgr	r			2	0					
360	LZ		r	blgr	r			2	0					
370	LZ		r	blgr	r			2	0					
380	LZ		r	blgr	r			2	0					#
390	LZ		r	blgr	r			2	0					#
400	LZ		r	gr	r			2	0					
410	LZ		r	gr	r			2	0					
420	MZL		r	gr	r			2	0					
430	MZL		r	gr	r			2	0					
440	MZL		r	gr	r			2	0					
450	ZZL		r	gr	r			2	0					
460	LK		r	gr	r			2	0					#

Einde boring: 201801017

Boorpunt: 201801018

Namen: Pierik,Moree,McMahon

Jaar: 2018

Groep: 01

Datum: 13-9-2018

Coördinaten	Hoogte	Diepte	KAARTEENHEID	Geomorfogenetische kaart:	
Xco	Yco	Z [m]	Geologische kaart:	Grondwatertrap:	
97536	460935	-1.3	Begroeiingskaart:	Bodemkaart:	

Hazerswoude, Houtdijk 5a, bij Trees
 Op 50 cm op iets wat Limeseg lijkt (?)
 Acc. GPS = 3.4 m

Diepte	Textuur	Org	Plr	Kleur	Redox	Grind	M50	Ca	Fe	GW	M	LKL	Strat	Bijzonderheden
10	MZL			dbrgr										Geroerd
20	MZL			dbrgr										
30	MZL			dbrgr										
40	MZL			dbrgr										Grindje, LIMES???
50	MZL			dbrgr										

Einde boring: 201801018

Boorpunt: 201801019

Namen: Moree,Pierik,McMahon

Jaar: 2018

Groep: 01

Datum: 13-9-2018

Coördinaten		Hoogte	Diepte	KAARTEENHEID	Geomorfogenetische kaart:	
Xco	Yco	Z [m]	[cm]	Geologische kaart:	Grondwatertrap:	
97542	460947	-1.26	330	Begroeiingskaart:	Bodemkaart:	

Hazerswoude, Houtdijk 5a, bij Trees
 In zandige oeverwal, net ten Noorden van Limes
 Acc GPS = ? m

Diepte	Textuur	Org	Plr	Kleur	Redox	Grind	M50	Ca	Fe	GW	M	LKL	Strat	Bijzonderheden
10	MZL			dbgrgr	or			1	2					ger
20	MZL			dbgrgr	or			1	2					ger
30	MZL			gr	or			2	2			Sed		
40	MZL			gr	or			2	2					
50	MZL			gr	or			2	2					
60	MZL			gr	or			2	2					
70	MZL			gr	or			2	2					
80	MZL			gr	or			2	2					
90	MZL			gr	or			2	2					
100	MZL			gr	r			2	0	GW		Sed		
110	MZL		plr	gr	r			2	0					# zeer gelaagd, met zand mm/cm
120	MZL		plr	gr	r			2	0					zeer gelaagd met zand mm/cm
130	MZL		plr	gr	r			2	0					zeer gelaagd met zand mm/cm
140	MZL		plr	gr	r			2	0					zeer gelaagd met zand mm/cm
150	LZL		plr	gr	r			2	0					zeer gelaagd met zand mm/cm
160	LZL			gr	r			2	0			Sed		zeer gelaagd met zand mm/cm
170	LZL			gr	r			2	0					# zeer gelaagd met zand mm/cm
180	LZL			gr	r			2	0					#
190	LZL			gr	r			2	0					
200	LZL			gr	r			2	0					
210	LZL			gr	r			2	0					
220	LZ			gr	r			2	0					Z=MZ210-300, bed/kronkelwaard?
230	LZ			gr	r			2	0					detr. band
240	LZ			gr	r			2	0					
250	LZ			gr	r			2	0					#
260														# GM
270														GM, zand gevoeld
280														GM, zand gevoeld
290														GM, zand gevoeld
300														GM, zand gevoeld
310														GM, zand gevoeld
320														GM, zand gevoeld
330														GM, zand gevoeld

Einde boring: 201801019

Boorpunt: 201801020

Namen: Roelofs,BoechatAlber

Jaar: 2018

Groep: 01

Datum: 13-9-2018

Coördinaten	Hoogte	Diepte	KAARTEENHEID	Geomorfogenetische kaart:	
Xco	Yco	Z [m]	Geologische kaart:	Grondwatertrap:	
97566	460973	-1.1	Begroeiingskaart:	Bodemkaart:	
		140			

Hazerswoude, Houtdijk 5a, bij Trees,
Meest proximale locatie, op de stroomrug?
Acc GPS = 8.7 m

Diepte	Textuur	Org	Plr	Kleur	Redox	Grind	M50	Ca	Fe	GW	M	LKL	Strat	Bijzonderheden
10	LK			brgr	o			2	1					ger
20	LK			brgr	o			2	1					minder zandig
30	ZZL			brgr	o			2	1					
40	ZZL			gr	o			2	1					
50	ZZL			gr	o			2	1					
60	MZL			gr	o			2	1					meer zandig
70								2	1					# GM
80	MZL			gr	or			2	1					
90	MZL			gr	or			2	1					klei laagje
100	MZL			gr	or			2	1					
110	FZ			gr	or		150-210	2	0					
120	LZL			gr	or			2	0					
130	ZZL			gr	or			2	0					
140	LZL			gr	or			2	0					#

Einde boring: 201801020

I | Statistics of grain size analysis field samples

Table I.1: Summary of statistics of grain size analysis of levee sediments at three field locations for two levee phases. Pos., Neg., sort. and Skew. are abbreviations for positively, negatively, sorted and skewed respectively.

Sample name	Borehole nr.	Elevation NAP (cm)	Sand (%)	Silt (%)	Clay (%)	D50 (%)	Sorting	Skewness	Kurtosis	Lithology class Dutch	Grain size Wentworth
Location 1											
<i>Phase 2, proximal</i>											
HWA-I	20180113	221-234	50.2	41.8	8.0	4.0	Poorly sort.	Very Pos. Skew.	Very Leptokurtic	zeer sterk lemig zand	Very fine sand
HWA-II	20180113	234-240	32.3	52.4	15.3	4.5	Poorly sort.	Very Pos. Skew.	Platykurtic	zware zandige leem	Coarse silt
HWA-III	20180113	330-336	0.5	50.8	48.6	7.9	Poorly sort.	Very Neg. Skew.	Platykurtic	matig zware klei	Very fine silt
HWA-IV	20180113	127-137	4.7	70.5	24.8	6.1	Poorly sort.	Pos. Skew.	Very Platykurtic	zware siltige leem	Fine silt
<i>Phase 2, Distal</i>											
HWB-I	20180115	200	0.3	71.4	28.3	6.8	Poorly sort.	Symmetrical	Platykurtic	zware siltige leem	Fine silt
<i>Phase 3, Proximal</i>											
HWA-V	20180113	70	1.9	26.1	72.0	8.3	Mod. sort.	Very Neg. Skew.	Leptokurtic	zeer zware klei	Coarse clay
Location 2											
<i>Phase 2, Proximal</i>											
KPA-VI	20180110	130-140	3.7	66.8	29.6	6.7	Poorly sort.	Symmetrical	Platykurtic	lichte klei	Fine silt
KPA-VII	20180110	180-190	12.9	64.5	22.6	5.6	Poorly sort.	Pos. Skew.	Very Platykurtic	zware siltige leem	Medium silt
KPA-VIII	20180110	210	18.3	59.8	21.9	5.6	Poorly sort.	Pos. Skew.	Very Platykurtic	zware zavel	Medium silt
KPA-X	20180110	240	12.4	67.3	20.3	6.0	Poorly sort.	Symmetrical	Platykurtic	zware siltige leem	Medium silt
<i>Phase 3, Proximal</i>											
KPA-I	20180110	40-50	0.3	53.4	46.3	7.7	Poorly sort.	Very Neg. Skew.	Platykurtic	matig zware klei	Very fine silt
KPA-II	20180110	50-60	0.4	29.7	69.9	8.3	Mod. sort.	Very Neg. Skew.	Leptokurtic	zeer zware klei	Coarse clay
KPA-III	20180110	60-70	0.3	53.3	46.4	7.8	Poorly sort.	Very Neg. Skew.	Platykurtic	matig zware klei	Very fine silt
KPA-IV	20180110	70-80	0.6	57.5	41.9	7.5	Poorly sort.	Very Neg. Skew.	Platykurtic	matig zware klei	Very fine silt
KPA-V	20180110	80-90	0.2	49.3	50.5	8.0	Poorly sort.	Very Neg. Skew.	Platykurtic	zeer zware klei	Coarse clay
Location 3											
<i>Phase 2, Proximal</i>											
HZB-I	20180119	30	1.7	67.5	30.8	7.0	Poorly sort.	Symmetrical	Platykurtic	lichte klei	Fine silt
HZB-II	20180119	105	15.5	69.7	14.9	5.2	Poorly sort.	Very Pos. Skew.	Platykurtic	zware siltige leem	Medium silt
HZB-III	20180119	165	23.1	63.9	13.0	4.8	Poorly sort.	Very Pos. Skew.	Leptokurtic	zware zandige leem	Coarse silt
<i>Phase 2, Medial</i>											
HZA-III	20180117	30	14.3	61.2	24.5	5.9	Poorly sort.	Symmetrical	Platykurtic	zware zavel	Medium silt
HZA-IV	20180117	80	3.3	70.4	26.3	6.6	Poorly sort.	Symmetrical	Platykurtic	zware siltige leem	Fine silt
HZA-V	20180117	140	21.6	62.3	16.1	4.9	Poorly sort.	Very Pos. Skew.	Platykurtic	zware zandige leem	Coarse silt